Advanced Polymeric Membranes and Multi-Layered Films for Gas Separation and Capacitors

By
Andrew Thomas Shaver

Dissertation submitted to the faculty of the Virginia Polytechnic Institute and State University in partial fulfillment of the requirements for the degree of

Doctor of Philosophy
In
Macromolecular Science and Engineering

James E. McGrath, Chair
Judy S. Riffle, Co-Chair
S. Richard Turner
Richey M. Davis
E. Bruce Orler
John Lesko

(04/26/2016)
Blacksburg, VA

Fluorinated Dielectric Materials, Microlayer Coextrusion, Poly(Arylene Ether Ketone)s, Gas Separation, PPO, Poly(dimethyl phenylene oxide)

Advanced Polymeric Membranes and Multi-Layered Films for Gas Separation and Capacitors

Andrew Thomas Shaver

ABSTRACT

The following studies describe the synthesis and properties of a family of poly(arylene ether ketone)s which are well known to have good thermal stability, mechanical durability, and other film properties. These poly(arylene ether ketone)s were functionalized with fluorine, oxidized, blended, and crosslinked to increase performance with focus on materials for polymeric capacitors and gas separation membranes.

There is a need for polymeric capacitors with improved energy storage density and thermal stability. In this work, the affect of polymer molecular structure and symmetry on Tg, breakdown strength, and relative permittivity was investigated. A systematic series of four amorphous poly(arylene ether ketone)s was compared. Two of the polymers had symmetric bisphenols while the remaining two had asymmetric bisphenols. Two contained trifluoromethyl groups while the other two had methyl groups. The symmetric polymers had Tg's of approximately 160 °C while the asymmetric polymers showed higher Tg's near 180 °C. The symmetric polymers had breakdown strengths near 380 kV/mm at 150 °C. The asymmetric counterparts had breakdown strengths near 520 kV/mm even at 175 °C, with the fluorinated polymers performing slightly better in both cases. The non-fluorinated polymers had higher relative

permittivities than the fluorinated materials, with the asymmetric polymers being better in both cases.

Two amorphous, high glass transition, crosslinkable poly(arylene ether)s for gas purification membranes have been studied. The polymers were polymerized via step growth and contained tetramethyl bisphenol F and either 4,4'-difluorobenzophenone or 4,4'-dichlorodiphenylsulfone. The benzylic methylene group in tetramethyl bisphenol F can undergo oxidation reactions and crosslinking with UV light. The polymers were oxidized under two different conditions, one by chemical treatment using oxone and KBr and one by elevated thermal treatment in air. Thermogravimetric analysis, ^{1}H-NMR and attenuated total reflectance Fourier transform infrared spectroscopy revealed the progress of the thermal oxidation reactions. Both polymers produced tough, ductile films and gas transport properties of the non-crosslinked linear polymers and crosslinked polymer was compared. Crosslinking was performed by irradiating polymer films for one hour on each side in air under a 100W high intensity, long-wave UV lamp equipped with a 365-nm light filter. The O_2 permeability of tetramethyl bisphenol F containing non-crosslinked poly(arylene ether ketone) was 2.8 Barrer, with an O_2/N_2 selectivity of 5.4. Following UV crosslinking, the O_2 permeability decreased to 1.8 Barrer, and the O_2/N_2 selectivity increased to 6.2.

Poly(2,6-dimethyl-1,4-phenylene oxide) (PPO) is a commercial polymer that is utilized for gas separation membranes. It has a relatively high free volume with high gas permeabilities but suffers from low gas selectivities. In this study, PPO polymers with number average molecular weights of 2000, 6000, 17,000, 19,000 and 22,000 were synthesized and blended with a poly(arylene ether ketone) synthesized from bisphenol A

and difluorobenzophenone (BPA-PAEK) to make UV-crosslinkable films. The ketone and benzylic methylene groups on the BPA-PAEK and the PPO polymers respectively formed crosslinks upon exposure to broad wavelength UV light. The crosslinked blends had increased selectivities over their linear counterparts. DSC thermograms showed that the blends with all but the lowest molecular weight PPO had two T_g's, thus suggesting that two phases were present, one high in PBA-PAEK and the other high in PPO composition. The PBA-PAEK blend with the 2000 Mn PPO showed only one T_g between the two control polymers. Despite the immiscibility of these films, the gel fractions after UV exposure were high. Gel fractions as a function of the amount of the 22,000 Mn PPO were explored and did not show any significant change. UV spectroscopy of the individual components and the blends showed that more broad wavelength light was transmitted through the PPO component, so it was reasoned that films that was high in PPO composition crosslinked to deeper depths. The O_2/N_2 permeabilities and selectivities were measured for the linear and crosslinked films. Between the 33/67, 67/33, and 90/10 22k PPO/BPA PAEK crosslinked blended films, the 90/10 PPO/BPA PAEK gained the most selectivity and maintained a larger amount of its permeability. In comparison to commercial gas separation polymers, the non-crosslinked 33/67 22,000 Mn PPO/BPA PAEK blend outperformed polysulfone and cellulose acetate with a 2.45 degree of acetylation. Overall, we were able to blend a small amount of BPA PAEK with the commercially used PPO to create a mechanically robust crosslinked polymer film.

Advanced Polymeric Membranes and Multi-Layered Films for Gas Separation and Capacitors

Andrew Thomas Shaver

GENERAL AUDIENCE ABSTRACT

The following studies describe the synthesis and properties of a family of engineering polymers which are well known to have good thermal stability, mechanical durability, and other film properties. The two main areas of application are high temperature capacitors and gas separation membranes.

Today's electronics are involved in many vital functions of everyday life and capacitors serve key roles in these devices. Because of miniaturization and increased energy consumption in such applications, new materials for capacitors must be developed that can store more energy. In this study, four different polymers were synthesized and compared to isolate the most beneficial structural differences in relation to energy storage. Two of the polymers had symmetric functional groups while the remaining two had asymmetric functional groups. Two contained fluorine while the other two did not contain any fluorine. This study showed that the asymmetric fluorine containing polymer had more potential to store energy than the symmetric counterpart.

Gas separations via membranes have grown over the past approximately 50 years due to reduced energy consumption, equipment size, and waste generation. Currently, membrane based gas separation is used to separate various gas pairs in applications

including nitrogen enrichment, acid gas treatment, ammonia purge gas recovery, refinery gas purification, and dehydration. There are issues that need to be addressed within these areas such as gas purity, polymer softening over time due to CO_2 adsorption (plasticization), physical aging, and chemical and thermal stability of the membranes. To address these issues, this paper explored the benefits of crosslinkable polymers as gas separation membranes. The first gas separation study utilized a polymer that contained a group that can undergo an oxidation reaction. This reaction was done via a chemical treatment as well as via elevated thermal treatment in air. This oxidation reaction created a group that would interact with UV light which would then react with another group within the polymer to create a crosslinked polymer. A crosslinked polymer is when the polymers within the system are connected to each other via chemical or other bonds. Once the polymers were crosslinked via UV light, gas separation selectivity was increased over the non-crosslinked films.

The next system used a blend of two polymers to create a crosslinked polymer. One polymer in the blend is a commercial polymer that is utilized for gas separation membranes which would be beneficial for commercialization. Gas can move through the commercial polymer at relatively high rates but suffers from low gas selectivities. The other polymer contains a group that will interact with UV light and then react with the commercial polymer to form crosslinks to connect the two chains. The crosslinked blends were tested and had increased selectivities over their non-crosslinked counterparts. Overall, we were able to blend a small amount of an engineering polymer with the commercial polymer to create a mechanically robust crosslinked polymer film.

Acknowledgment

I would like to express my deepest gratitude to my late advisor, Dr. James E. McGrath. His presence as a great man, scientist, and friend will always be remembered and has guided me through graduate school and will guide me into the future. I am truly happy that he brought me in as his student and the opportunity to work with a legend like him is a gift.

It is hard to express how thankful I am to Dr. Judy Riffle for her guidance and kindness. I am very grateful that she took on the responsibility of seeing me and the other McGrath students to the end of our graduate degrees. However, I am most grateful for the immense amount of knowledge, advice, and professionalism that she has given me. I am truly blessed to have her as an advisor.

I would also like to thank Dr. Mecham and Dr. Turner for their assistance after the passing of Dr. McGrath and throughout my graduate journey. I learned so much about polymer instrumentation from Dr. Mecham and I look forward to using it in the future. Dr. Turner's industrial class gave insight into the world outside academia and it has been very useful during the job hunt and I am sure it will be useful once I am a part of the industry world. Over the past few years it has been a pleasure working with Dr. Bruce Orler and his teachings and advice about instrumentation are most appreciated. I will always make sure to take proper care of any instruments that I use. Over the years, I enjoyed the lectures and knowledge that I gained from Dr. Davis about dynamic light scattering, self-assembling structures, and nanoparticles. In the last year, I am thankful for the greater understanding of mechanical properties from Dr. Lesko and how to properly measure and present them.

I would also like to like to thank my fellow labmates from both the McGrath and Riffle groups for their research suggestions and discussions. Specifically, I would like to thank Dr. Jarrett Rowlett, Greg Miller, Dr. Hailun Borjigin, Dr. Ben Sundell, Matt Joseph, Gurtej Narang, Ran Lui, and Amin Daryaei for their help and friendship over the years. I would also like to thank the administrative assistants in the Macromolecules and Interface Institute and Chemistry Department, specifically Laurie Good and Tammy Jo Hiner.

Lastly I would like to thank my family and friends whose help and encouragement has been essential over these past years. I would first like to thank my parents who gave me my sense of curiosity and then guided me into to science and engineering. I would not be where I am today without them. I would also like to acknowledge my late great uncle Jack. He was truly a great man and the best barber. I cannot count the amount of ears that I have lost to his scissors.

Attribution

Chapter 2: Fluorinated Poly(Arylene Ether Ketone)s for High Temperature Dielectrics – Bulk and Multilayered Films.

Chapter 2.1 was accepted and published in Polymer.

Fluorinated Poly(Arylene Ether Ketone)s for High Temperature Dielectrics.

Kezhen Yin, B.S. (Macromolecular Science and Engineering Program) is currently a Ph.D. candidate at the Case Western Reserve University. Mr. Yin was a co-author on this paper and performed the refractive index, breakdown strength, and dielectric thermal analysis.

Hailun Borjigin, Ph.D. (Macromolecular Science and Engineering Program) graduated with his Ph.D from Virginia Tech. Dr. Borjigin was a co-author on this paper and performed the NMR testing and analysis.

Wenrui Zhang, B.S. (Macromolecular Science and Engineering Program) is currently a Ph.D. candidate at Virginia Tech. Mr. Zhang was a co-author on this paper and synthesized the 1,1-bis(4-hydroxyphenyl)-1-phenyl-2,2,2-trifluoroethane monomer.

Shreya Roy Choudhury, B.S. (Macromolecular Science and Engineering Program) is currently a Ph.D. candidate at Virginia Tech. Ms. Roy Choudhury was a co-author on this paper and synthesized the 1,1-bis(4-hydroxyphenyl)-1-phenyl-2,2,2-trifluoroethane monomer.

Eric Baer, Ph.D. (Department of Macromolecular Science and Engineering, CWRU) is a professor at Case Western Reserve University. Dr. Baer was a co-author on this paper and principal investigator for the grant supporting this research.

Sue J. Mecham, Ph.D. (Department of Chemistry) is currently a research scientist at the University of North Carolina at Chapel Hill. Dr. Mecham was a co-author on this paper supplied her expertise in SEC and contributed revisions to the final document.

Judy S. Riffle, Ph.D. (Department of Chemistry) is a professor at Virginia Tech. Dr. Riffle was a co-author on this paper, contributed revisions to the final document, and oversaw completion of the project.

James E. McGrath, Ph.D. (Department of Chemistry) was a professor at Virginia Tech. Dr. McGrath was a co-author on this paper and oversaw early stages of this project.

Chapter 2.2

Microlayered Fluorinated Poly(Arylene Ether Ketone)s with PVDF for High Temperature Dielectrics

Matthew Mackey, Ph.D. (Department of Macromolecular Science and Engineering, CWRU) graduated with his Ph.D from Case Western Reserve University. Dr. Mackey performed the breakdown strength, dielectric hysteresis measurements, and dielectric thermal analysis.

Yu Chen, Ph.D. (Macromolecular Science and Engineering Program) graduated with his Ph.D from Virginia Tech. Dr. Chen was a performed the early synthesis of the polymers used for this study.

Chapter 3: Synthesis, Oxidation, Crosslinking and Characterization of Tetramethyl Bisphenol F (TMBPF)-Based Polymers for Oxygen/Nitrogen Gas Separations

Chapter 3.1 was accepted and published in Polymer

Synthesis, Oxidation and Crosslinking of Tetramethyl Bisphenol F (TMBPF)-Based Polymers for Oxygen/Nitrogen Gas Separations

Benjamin J Sundell, Ph.D. (Macromolecular Science and Engineering Program) graduated with his Ph.D from Virginia Tech. Dr. Sundell was the principal author on this paper and performed the synthesis, chemical oxidation, and gel fractions.

Qiang Liu, Ph.D. (Department of Chemical Engineering) graduated with his Ph.D from University of Texas at Austin. Dr. Liu was a co-author on this paper and contributed to the gas transport testing of the polymer films.

Ali Nebipasagil, Ph.D. (Macromolecular Science and Engineering Program) graduated with his Ph.D from Virginia Tech. Dr. Nebipasagil was a co-author on this paper and performed the NMR analysis on one of the polymer samples.

Priya Pisipati, Ph.D. (Macromolecular Science and Engineering Program) graduated with his Ph.D from Virginia Tech. Dr. Pisipati was a co-author on this paper and contributed to the IR spectroscopy performed on the polymers.

Sue J. Mecham, Ph.D. (Department of Chemistry) is currently a research scientist at the University of North Carolina at Chapel Hill. Dr. Mecham was a co-author on this paper and contributed to the SEC analysis of the polymers.

Benny D. Freeman, Ph.D. (Department of Chemical Engineering) is currently a professor at the University of Texas at Austin. Dr. Freeman was a co-author on this paper, co-principal investigator for one of the grants supporting this research and assisted in revisions of the final document.

Judy S. Riffle, Ph.D. (Department of Chemistry) is a professor at Virginia Tech. Dr. Riffle was a co-author on this paper and contributed revisions to the final document.

James E. McGrath, Ph.D. (Department of Chemistry) was a professor at Virginia Tech. Dr. McGrath was a co-author on this paper and co-principal investigator for one of the grants supporting this research.

Chapter 3: Poly(2,6-dimethyl-1,4-phenylene oxide) and Bisphenol A Poly(arylene ether ketone) Blends for Gas Separation Membranes

Josh Moon, B.S. (Department of Chemical Engineering) is currently a Ph.D candidate at the University of Texas at Austin. Mr. Moon performed to the gas transport testing of the polymer films.

Donald Savacool (Department of Chemical Engineering) is currently a undergraduate at Virginia Tech. Mr. Savacool assisted with the film casting, UV crosslinking, gel fractions, and the tensile properties.

Wenrui Zhang, B.S. (Macromolecular Science and Engineering Program) is currently a Ph.D. candidate at Virginia Tech. Mr. Zhang synthesized the 6k, 17k and 22k PPO.

Gurtej Narang, B.S. (Macromolecular Science and Engineering Program) is currently a Ph.D. candidate at Virginia Tech. Mr. Narang assisted with UV spectroscopy.

Greg Miller, B.S. (Macromolecular Science and Engineering Program) is currently a Ph.D. candidate at Virginia Tech. Mr. Miller assisted in the initial film casting and overall setup of the project.

Britannia Vondrasek, M.S. (Macromolecular Science and Engineering Program) is currently a Ph.D. candidate at Virginia Tech. Ms. Vondrasek assisted in the tensile testing.

John Lesko, Ph.D. the Associate Dean for Research and Graduate Studies at Virginia Tech. Dr. Lesko has overseen the mechanical analysis of this system.

Benny D. Freeman, Ph.D. (Department of Chemical Engineering) is currently a professor at the University of Texas at Austin. Dr. Freeman is co-principal investigator for one of the grants supporting this research and overseen the gas transport analysis.

Judy S. Riffle, Ph.D. (Department of Chemistry) is a professor at Virginia Tech. Dr. Riffle has overseen the whole project.

James E. McGrath, Ph.D. (Department of Chemistry) was a professor at Virginia Tech. Dr. McGrath co-principal investigator for one of the grants supporting this research.

Table of Contents

List of Figures

Chapter 1

Chapter 2

Chapter 3

Chapter 4

List of Tables

Chapter 1

Chapter 2

Chapter 3

Chapter 4

Chapter 1: Polymeric Microlayered Dielectrics via Forced Assembly Coextrusion

1.1 Introduction

Electronics today are involved in many vital functions of everyday life, with capacitors being essential components of these devices. The nature and function of a capacitor in an electronic device can drastically change depending on the type of dielectric material and the type of current used in the capacitor. Because of this, capacitors can be used for energy storage, filtering (controlling the flow of current), tuning (frequency bypassing), blocking (filtering AC from DC or vice versa), bypass (frequency separation), and many more applications.[1, 2] The main focus of this section will be on the types of dielectric materials, specifically polymers, and how the industrial and the academic community have advanced capacitor performance using polymeric materials.

1.1.1 Discovery of Capacitors

The first capacitor was created by Pieter van Musschenbrock in 1746 in an attempt to electrify water.[1] At the time little was known about the nature of electricity, with the theory on electricity still undefined. For the experiment he lined the inside and the outside of a jar with copper foil. The inside foil was attached to the negative terminal and the outside was attached to a positive terminal, and when Musschenbrock applied a voltage from the battery nothing happened to the water. However, while discarding the water and disconnecting the battery, Musschenbrock touched one of the electrodes and

was shocked from the built up charge. This first experiment was named a Leyden jar due to the location of invention at the University of Leiden.[1]

1.1.2 Principles of Capacitors

From the Leyden jar, capacitors have advanced in shape, materials, and construction but the principles remain the same. One electrode is positively charged while the other is negatively charged, and both must be separated by a dielectric material. In the Leyden jar the dielectric material was glass, but the dielectric layer can be as simple as air or as complicated as multi-layered polymeric materials.[2] For this discussion, we refer to the separating layer as the dielectric material.

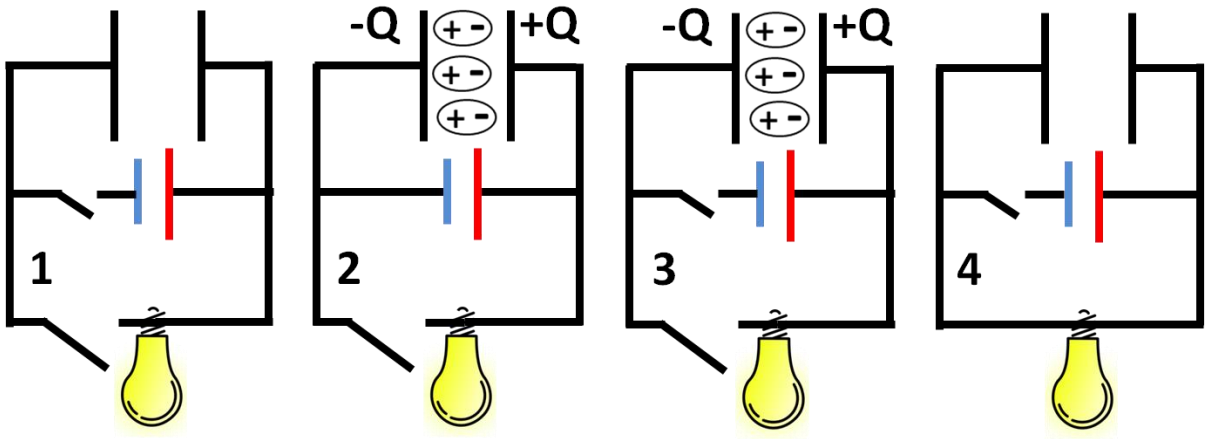

Figure 1.1 Depiction of four stages of capacitor operation. The power source is represented by the blue (negative electrode) and red (positive electrode). The capacitor is represented by the two black lines with a space in between which represents the two electrodes that can be either negatively or positively charged.

In Figure 1.1, there are four example circuits which include a capacitor, power source, and light bulb to help give a basic idea of how a capacitor functions. In the first circuit, the direct current (DC) power source and light bulb is disconnected from the

capacitor so there is no capacitance being produced. Once the connection is established between the power source and the capacitor in the second circuit, the electrons will flow from the anode of the DC power source to the left electrode of the capacitor. The electrons quickly accumulate, creating a negative charge on the left side of the capacitor. Consequently, the right electrode begins to build up a positive charge. An electric field is created within the dielectric material, which is the mechanism of energy storage within the capacitor. In the third figure, the connection is broken between the power source and the capacitor. Even though the capacitor has no power source, the energy level is maintained between the two electrodes and within the dielectric layer. If too much time passes before the stored energy is used, the negative charge will dissipate to the positive electrode, reducing the electric field and therefore the stored energy. However if the stored energy is used within a short time of charging, it can power electrical devices, such as a light bulb which can be seen in the fourth circuit.

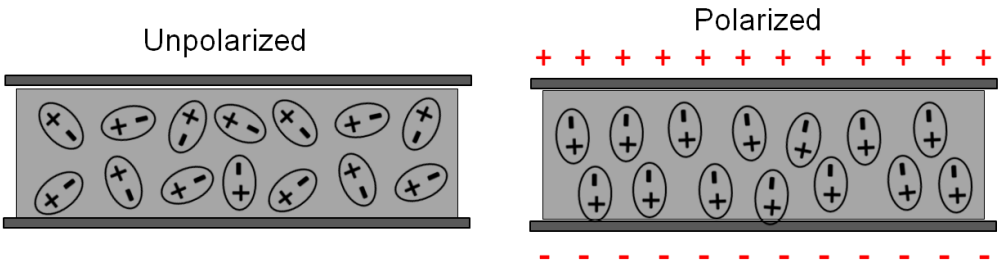

Figure 1.2 The un-polarized versus the polarized state of a dielectric material.

When an electric field is applied between the electrodes, the dielectric material becomes polarized. This polarization is depicted in Figure 1.2 where the material initially shows a completely random distribution of polar groups with no electric field, but the polar groups align with the electrodes once the field is applied. When the electric field is removed, the polar groups within the material return to their original random orientation

with an overall neutral charge. There are a few cases (ferroelectric materials) where the polar groups do not return to the random orientation, but this will be discussed later.

1.1.3 Permittivity and Dielectric Constant

The performance of a capacitor depends heavily on the material chosen as the dielectric. The absolute permittivity is the measure of how an applied electric field interacts with a dielectric material; it measures the electric field that is generated from any polarizable aspects within that material. Therefore, if the material has a high capacity to be polarized, it will be able to sustain a greater electric field and have a larger absolute permittivity. [3]

The relative permittivity is the absolute permittivity of the material divided by the vacuum permittivity as shown in Equation 1.1

$$\varepsilon_r(\omega) = \frac{\varepsilon(\omega)}{\varepsilon_0} \tag{1.1}$$

where $\varepsilon_r(\omega)$ is the frequency dependent relative permittivity, $\varepsilon(\omega)$ is the absolute permittivity of the material, and ε_0 is the vacuum permittivity. Historically, the value of the relative permittivity was called the dielectric constant but in recent years the term relative permittivity is preferred over dielectric constant. This is because dielectric constant has been used to describe several different concepts over the years, clouding its definition when used today. Furthermore, the term dielectric constant implies that it is a constant number, but it is frequency-dependent. This is because the relative permittivity (or dielectric constant) is a complex value and has real and imaginary components as shown in Equation 1.2.[3]

$$\varepsilon_r(\omega) = \varepsilon'_r(\omega) + i\varepsilon''_r(\omega) \tag{1.2}$$

Some examples for relative permittivity values are listed in Table 1.1.

Table 1.1 Relative permittivity values for materials currently and previously used as dielectrics.4, 5

Material	Relative Permittivity
Vacuum	1
Air	1.02
Teflon	2.1
Polyethylene	2.3 – 2.7
Bi-axially Oriented Polypropylene (BOPP)	2.4
Polystyrene	2.5 – 2.9
Fluorinated Polyimide	2.5 – 2.9
Polycarbonate (PC)	2.8
Poly Arylene Ether	2.8 – 2.9
Polyimide	2.8 – 3.2
Fluorosilicate Glass	3.2 – 4.0
Polyester (PET)	3.3
SiO_2	3.9 – 4.5
Paper (Kraft)	4
Poly(vinylidene fluoride) (PVDF)	6 – 12
Porcelain	6.2
Mica	7.5
Glass	7.6
Neoprene	9.8
H_2O	78
TiO_2	100

Vacuum permittivity has an assigned value of one and this is used as the standard.[3] Most polymers fall in the range from 2 to 4, except ferroelectric materials such as PVDF, which will be discussed in greater detail in a later section. Mica was one of the first materials used as a dielectric because it naturally breaks into flat, thin layers, which may then be coated and used as dielectrics.[2] Mica is still used today for applications in extreme environments because of its stable properties over a wide range of temperatures.

However, due to the expensive processing and material cost, clay (porcelain) replaced mica. Clay (porcelain) is still a market leader due to decreased cost with adequate performance.[2] Paper also became popular, and was used because it was much more mechanically stable in comparison to the other materials, but it also must be specially processed for use as a dielectric material. Finally, plastics have become popular because of superior mechanical properties, low material cost, processability, and in some cases self-healing properties.[2]

1.2 Dielectric Testing and Characterization Techniques

1.2.1 Dielectric Spectroscopy

Dielectric Spectroscopy is used to explore the dielectric properties of a material and takes advantage of the complex nature of permittivity. The permittivity of a dielectric material is split into ε' (storage or real permittivity) and ε'' (loss or imaginary permittivity). The relationship between storage and loss permittivity is shown in Equation 1.3 and is displayed graphically in Figure 1.3.[6]

$$\varepsilon^*(\omega) = \varepsilon'(\omega) + i\varepsilon''(\omega) \tag{1.3}$$

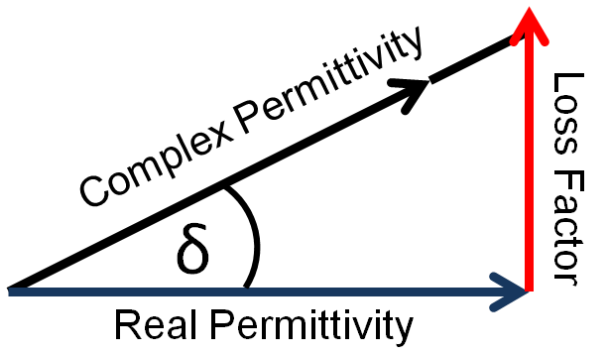

Figure 1.3 Graphical representation of the relationship between complex, real, and loss permittivity.

The storage permittivity represents the component of complex permittivity that is able to release all of the energy used to polarize the material. The loss permittivity is the component representing energy lost due to friction, inelastic scattering (i.e. permanent dipole switching and charge migration), and displacement current. The angle between the storage permittivity and the complex permittivity is referred to as δ, and tan δ is the ratio between ε' and ε''. In Equation 3, each permittivity is dependent on frequency, which indicates that the values of ε*, ε', and ε'' will change with applied frequency. [6, 7]

In most polymeric dielectric materials, there are four main contributors to the polarization of a material: electronic, atomic, orientation, and ionic. Electronic polarization is the alignment of the electron cloud with the applied electric field. This movement of the electron cloud is in respect to the atom's nucleus which creates an overall polarization.[7, 8] Atomic polarization is the movement of two covalently bonded, non-polar atoms with respect to the electric field. This movement induces an overall polar moment in the non-polar atoms that would not naturally exist.

Similar to atomic polarization, orientation polarization is the alignment of covalently bonded atoms with the electric field. However, orientation polarization occurs only in polar domains. The origin of the name, orientation, is because it is the orientation of polar atoms and molecules with the electric field whereas atomic polarization is the creation of polarization. An example of the difference between atomic and orientation polarization would be with CO_2 versus H_2O. Carbon dioxide is non-polar and when an electric field is applied, the CO_2 would have an induced polarization. Water already has an existing polar moment but when an electric field is applied the polar moment will

orient with the electric field. Orientation polarization can also be referred to as dipolar polarization. [7]

Ionic polarization is when displacement occurs between two ionically charged atoms that are not covalently bonded such as NaCl. Orientation and ionic polarization are similar, in that, both types of polarization are related to two atoms moving with respect to each other. However, the elastic force bringing the two atoms back to the original position (after the electric field is removed) is starkly different. The elastic force in atomic polarization results from a covalent bond and ionic polarization results from ionic bonds. Since the covalent bond brings the two atoms back to their original position very quickly, the two types of polarization occur on different time scales.[9]

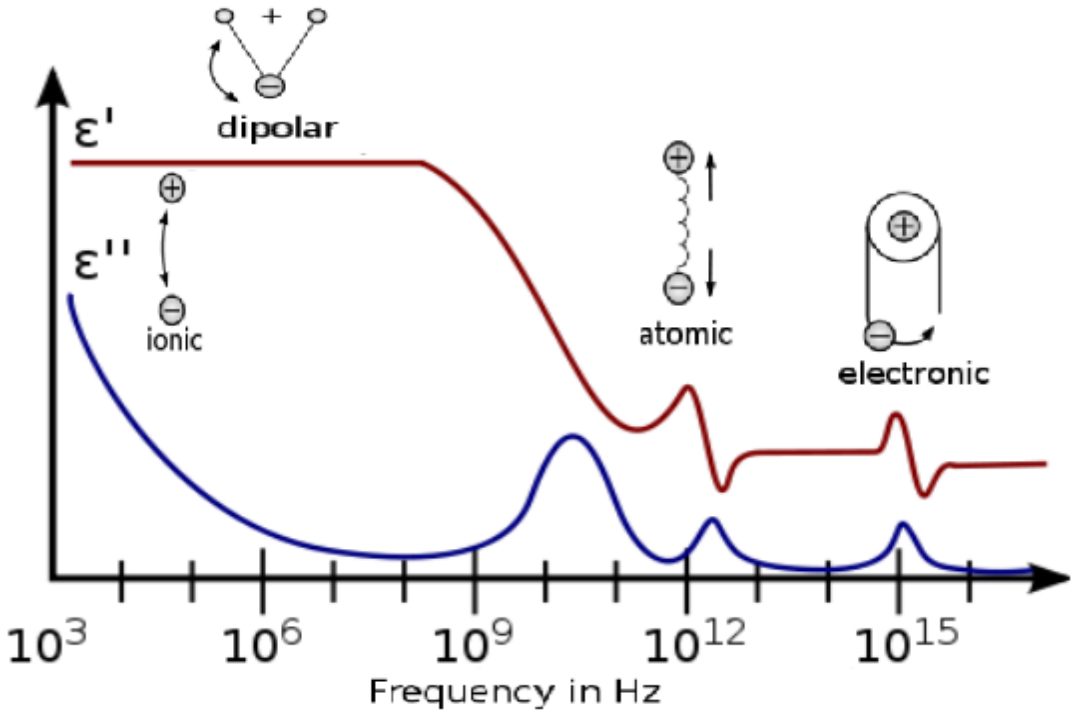

Figure 1.4 The frequency ranges for the four common relaxations. The y-axis is unit-less. 5 https://en.wikipedia.org/wiki/Dielectric_spectroscopy, Public Domain.

The time scale of the polarization mechanism has a significant impact on the properties of dielectrics. This time scale can be measured via dielectric spectroscopy and an example is shown in Figure 1.4. The top graph is the storage permittivity (molar polarization) and the bottom is the loss permittivity (dissipation). The two peaks in the 10^{16} and 10^{13} frequency range correspond to electronic and atomic polarizations respectively.[7] This is because these two types of polarization involve motions that recover very quickly once the electric field is removed. Also, electronic and atomic polarization involve low loss permittivity and therefore release more of the stored energy. This is advantageous because electronic and atomic polarizations can quickly store and release energy, while ensuring that the energy loss is insignificant.

At lower frequencies the relaxations due to larger motions such as orientation and ionic polarizations appear in the spectra. These polarizations are at lower frequencies because the associated movements take longer to align with the electric field. They cannot contribute to the high frequency range because the time in between the applied alternating current does not give the dipole or ionic groups enough time to align with the electric field. However, since the orientation and ionic moieties are larger, they are able to contribute a greater amount to the permittivity of the material.

1.2.2 Breakdown Strength or Dielectric Strength

Breakdown strength measurements are simple in nature and the needle-plane method is depicted in Figure 1.5. The film is coated with the plane electrode (the negative electrode in Figure 1.5) and a charged needle is applied to the other surface. The charges can be reversed so the needle can be either negative or positive. The applied voltage is then increased incrementally until the film catastrophically breaks.[10]

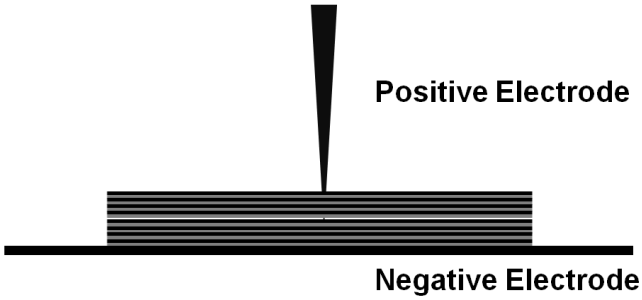

Figure 1.5 Depiction of the needle-plane electrode apparatus for measuring breakdown strength.

1.2.3 Polarization Hysteresis

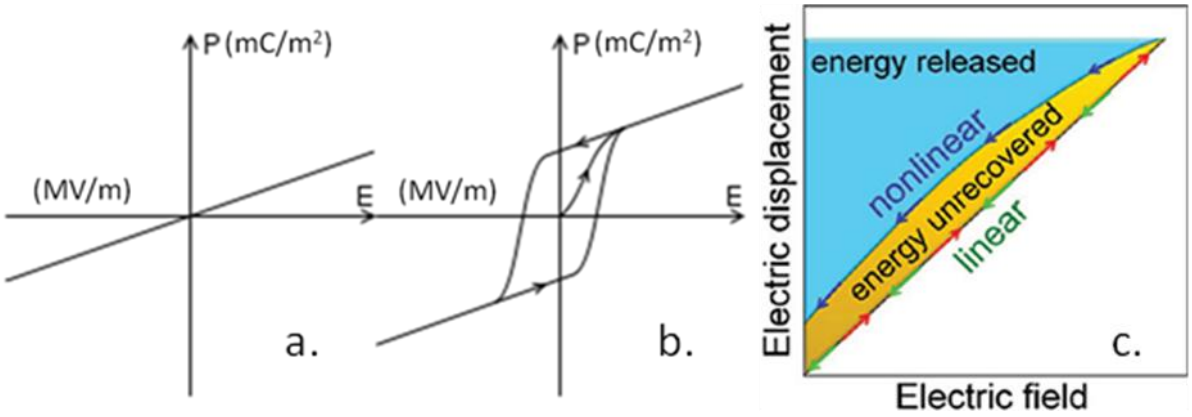

Figure 1.6 Polarization curves for a linear dielectric (A) and ferroelectric (B) material. https://en.wikipedia.org/wiki/Ferroelectricity, Public Domain. Graph C shows where the energy is lost when using a ferroelectric material.9 "Zhu, L.; Wang, Q., *Macromolecules* 2012, *45* (7), 2937-2954." Reprinted with permission of American Chemical Society, 2016, Copyright "2012" American Chemical Society.

A polarization curve (Figure 1.6) is used to characterize the effect of an electric field on a dielectric material. A voltage is applied to the capacitor, which creates an electric field and the amount of electric displacement is measured. Electric displacement measures the extent of polarization with units of Coulomb/area (mC/m^2). A coulomb (C) is a unit of charge and is defined as amperes (current) per second. Current is the flow of

electrons, therefore electric displacement describes how many electrons flow and stay in the capacitor over time and in a specific area of the capacitor.

The plots of both a linear dielectric and a ferroelectric material are shown in Figure 1.6. The dielectric plot shows a linear polarization process, from complete polarization while the electric field is being applied, to zero polarization without an electric field. The ferroelectric material shows a more complex process including a hysteresis loop. In a hysteresis loop, energy is lost to the process which may be quantified by the area of the loop. The energy loss is due to friction and irreversible polarized ions and polar groups. This can be seen in the last image of Figure 1.6. The hysteresis loop is diagrammed further in Figure 1.7 and more detail on ferroelectric materials will be discussed in the materials section.[7]

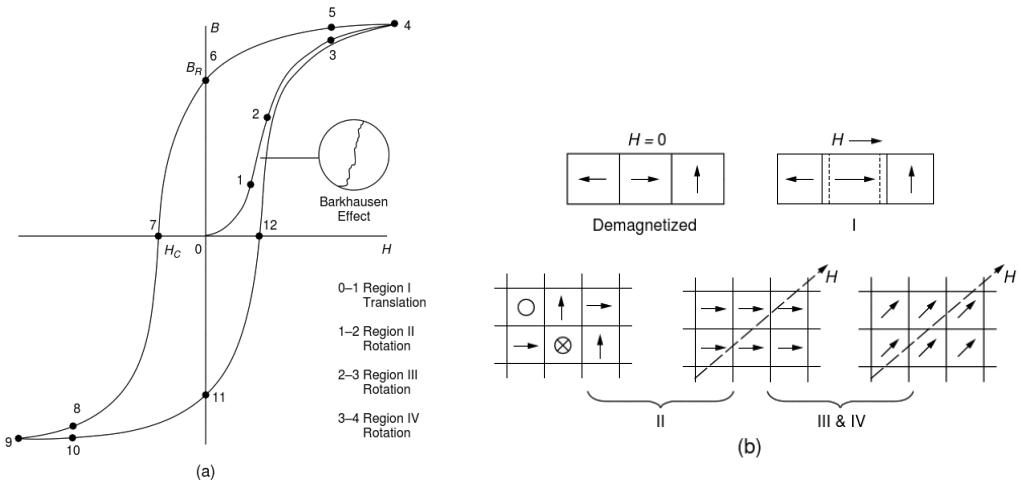

Figure 1.7 (a) An in-depth graph of the polarization hysteresis loop for a ferroelectric material. (b) Corresponding depiction of the polarization process of Regions I, II, III, and IV.[7] From "Kao, K.-C., *Dielectric phenomena in solids : with emphasis on physical concepts of electronic processes*. Academic Press: Amsterdam; Boston, 2004." Reprinted with permission of Elsevier, 2016, Copyright "2004" Elsevier.

The curve in Figure 1.7 (a) is numbered to help identify the sections and each of the listed regions has a corresponding depiction in Figure 1.7 (b). The first region, denoted H, is the beginning of any orientation in the direction of the applied field. Once the electric field is increased to region II, the polar domains begin orienting in the "easy" direction. In the "easy" direction, the polar domains are much more susceptible to orientation and a weaker electric field is needed to align the polar regions. During region III, the remaining un-oriented polar domains are aligned in the "easy" direction. The final section, region IV, is the orientation of the polar domains in a final, more difficult, direction. This final polarization requires an increased applied electric field.[7, 11]

Once the ferroelectric material is completely polarized, removal of the electric field results in a different path on the hysteresis curve. To return on the same path, the polar domains would have to be randomly oriented but from this point on, the polar domains will be partially oriented. The return to zero polarization requires an electric field in the opposite direction, which requires the use of additional electrical energy. This indicates that part of the process is irreversible. Since this is an irreversible process, energy is lost which may be calculated by taking the area of the curve. The polarization hysteresis is one of the main challenges with the use of ferroelectric materials as a dielectric layer, but new techniques are being investigated to circumvent these problems. **[7, 11]**

1.3. Polymeric Material for Capacitors

1.3.1 Polyester

Polyesters were one of the first polymers to be used as the dielectric layer within a capacitor[1]. Interest began at Dupont in the 1950's using Mylar polyester.[12] Poly(ethylene

terephthalate) (PET) is synthesized through step growth polymerization of ethylene glycol and terephthalic acid.[13]

DuPont reported good dielectric properties throughout a range of frequencies and temperatures.[12, 14] The reported temperature range for utilizing Mylar films is between -55 ^{o}C and 85^{o}C. The maximum use temperature is limited to 85 ^{o}C as beyond that point, Mylar will be reach its glass transition temperature and the properties will decline quickly.

1.3.2 Polypropylene

Polypropylene (PP) has been one of the most popular polymeric materials for use as a dielectric film, especially if it is bi-axially oriented (BOPP).[15-17] Polypropylene is synthesized through chain growth polymerization using a Ziegler-Natta catalyst to control the stereochemistry.[13] The advantages of using PP are that it is produced on a large scale, inexpensive, and that once oriented, the PP film gains beneficial thermal, mechanical, and electrical properties.[18-20] The capacitors that are produced from these films have reported large energy densities and breakdown strengths which is what originally brought interest to PP as a dielectric material.[17]

1.3.3 Polycarbonate

For high temperature applications, polycarbonate (PC) capacitors are one of the best options[21]. It is produced via step growth polymerization between bisphenol A and phosgene in the presence of base.[13] The patent to use polycarbonate as a capacitor was filed by General Electric in 1965.[22] These capacitors were of interest for many aerospace, military, and other specialty applications because the polycarbonate operating temperature range spans from -55 ^{o}C to 125^{o}C. Also the dielectric properties are stable

across this temperature range, allowing for consistent performance in many different environments.[21]

1.3.4 Polyimides

Polyimides gained interest as a dielectric material because of their excellent thermal properties, such as high Tg, and good mechanical properties.[23] Some commercial polyimides are Kapton and Matrimid.[23, 24] Polyimides are synthesized through a reaction between dianhydrides and diamines. The classic polyimide polymerization proceeds via a two step process involving a poly(amic acid) which then forms the polyimide.[13] Polyimides are oxidatively stable and show good organic solvent resistance which is beneficial in harsher environments. Some of them can be used continuously at high temperatures such as 300-350^{o}C.[23-26] Polyimides have reported dielectric constants near 3 to 3.5, which does not change significantly beyond 100^{o}C.[24] There is a significant range of dielectric constant values because various substituents and structure changes can affect the value. Current research into polyimides as dielectric materials includes blending with nanoparticles, creating composite materials, and synthesizing polyimides with asymmetric structures.[27-30]

1.3.5 Ferroelectric Materials – PVDF

Ferroelectricity refers to the ability of some materials to be permanently polarized or un-polarized through the use of an electric field.[11] Most materials will become unpolarized with the removal of an electric field. However, ferroelectric materials will maintain their polarization after the electric field is removed but their polarization can be reversed by applying an electric field in the opposite direction.[11] The polarization can produce interesting changes to the material's physical dimensions and temperature,

referred to as piezoelectric and pyroelectric materials respectively. These materials are very useful in many sensor applications.[31]

Because of the unique nature of ferroelectric materials and their high relative permittivity, much research has been published on these materials as dielectrics.[32-37] One polymer of interest is poly(vinylidene fluoride) (PVDF). With relative permittivity values reaching 12 (this number can change depending on the crystallinity), PVDF could be used to produce an inexpensive and efficient capacitor. However, the performance of these materials is strongly dependent on its polarization curve.[9, 38]

1.4. Forced Assembly Multilayer Coextrusion Process

Many techniques have been developed to increase the performance of polymer systems through the use of polymer blending, block copolymerization, and additives. One technique of interest is forced assembly microlayer coextrusion, which creates a film with alternating layers of two or more polymers. Each film can vary from 32 to 4096 layers that afford individual layer thicknesses down to the nanometer scale, in some cases approaching the radius of gyration of the individual molecules. This polymer architecture enables novel polymer systems that provide unique information and performance. Finally, microlayering can produce this unique structure at a large scale using an economically viable processing method.[39]

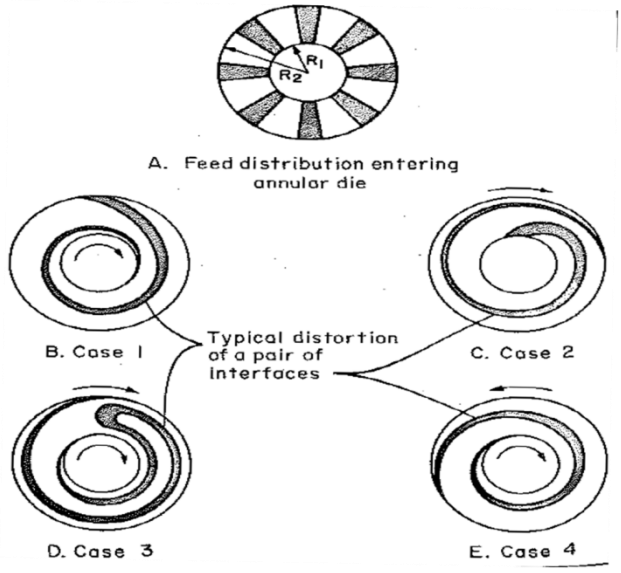

Figure 1.8 The initial technique created at Dow for microlayered films of two different materials.[40] Schrenk, W. J., *SPE J.* 1973, 29 (6), 38. SPE Journal is out of print. Mr. Allen Lee at Dow was contacted regarding this image.

The forced assembly microlayer film technique was developed during the 1970's at Dow Chemical Company and was headed by Water Schrenk, Douglas Chisholm, Kenneth Cleereman, and Turner Alfrey Jr. Schrenk and Alfrey initially developed and published a coextrusion multilayer blown film system that could create layered films through a rotating die.[41-45] In this process, two polymers of similar viscosities are coextruded and processed though a die, as shown in A of Figure 1.8 The two polymer flows are then rotated by either the inner mandrel or outer ring that creates the desired multilayered flow. Figure 1.8 also depicts the four different layer patterns that can arise from the different modes of die rotation.[40] This process affords the desired layered films.

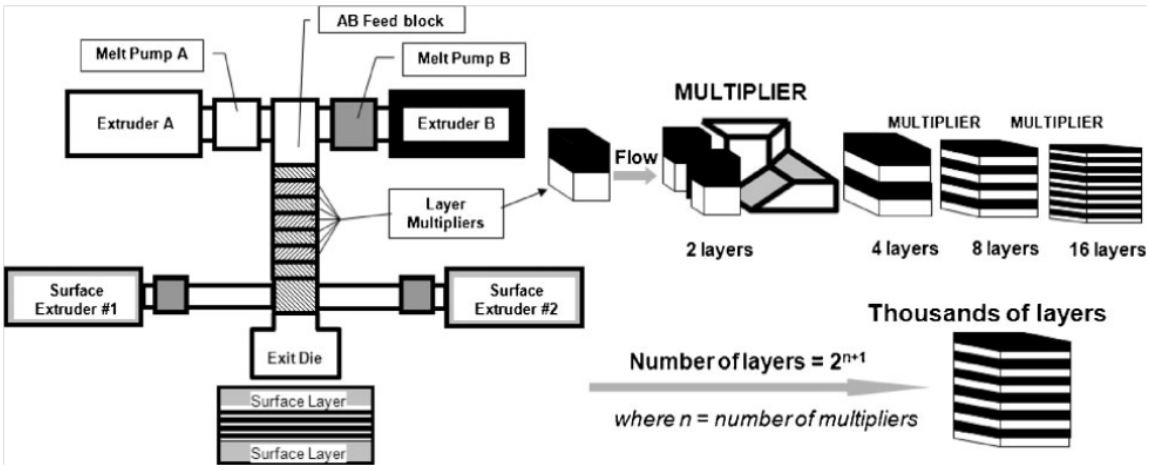

Figure 1.9 A depiction of how the forced assembly microlayer coextruder produces multi-layer films.[39] "Ponting, M.; Hiltner, A.; Baer, E., *Macromolecular Symposia* 2010, *294* (1), 19-32." Reprinted with permission of John Wiley and Sons, 2016, Copyright "2010" John Wiley and Sons.

At Case Western Reserve University (CWRU), a forced assembly microlayer coextruder has been developed within the National Science Foundation Center for Layered Polymeric Systems (CLiPS).[46-53] Figure 1.9 depicts the microlayer coextruder at CWRU and the function of the layer multipliers.[39] Initially the two extruders melt and thrust polymer forward into a feed block, where the two polymers are stacked to create a bi-layered polymer flow. Once stacked the layer multipliers split, compress, and spread the polymer flow to be stacked again. The number of layers in the flow is again doubled, and continues to be doubled with each multiplier added in series. Before reaching the die, an additional polymer can be added to both sides of the flow in order to improve the final quality. This additional layer is able to reduce the force of drag on the key microlayered flow while being compressed by the die into film form. A cooling roll can be used after the die to slowly or quickly cool the film and can control the extent of drawing, which influences the final thickness of the film.[39, 54, 55]

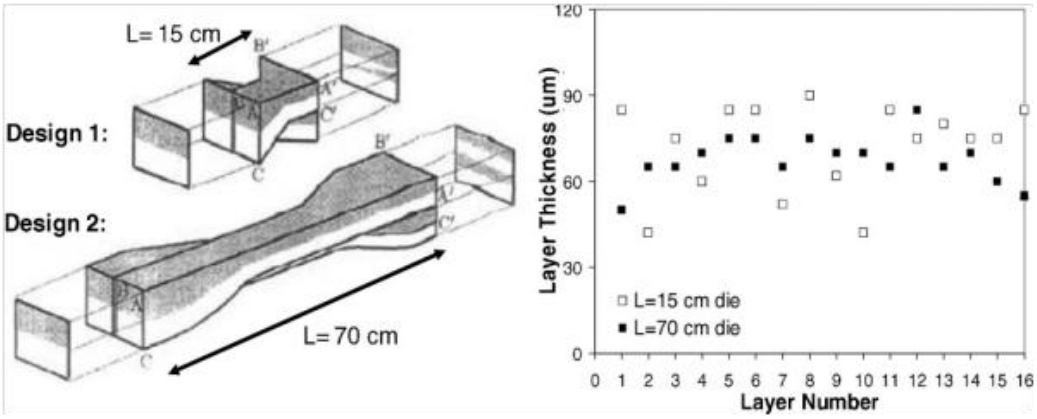

Figure 1.10 The two different layer multiplier designs and corresponding layer thickness consistency verses layer number.[39] "Ponting, M.; Hiltner, A.; Baer, E., *Macromolecular Symposia* 2010, *294* (1), 19-32." Reprinted with permission of John Wiley and Sons, 2016, Copyright "2010" John Wiley and Sons.

Experimentation with the layer multipliers has produced additional layer uniformity of the microlayered system along with asymmetric layering capabilities. Each multiplier has a pathlength, variable L, which affects its layering ability. In Figure 1.10, two different pathlengths are labeled with the corresponding lengths and the graph compares the consistency of the two designs. The Design 2 layer multipliers showed greater uniformity over a range of layer numbers and superior average layer thickness, with Design 2 being 69 ± 8μm and Design 1 being 71 ± 17μm.[39, 54]

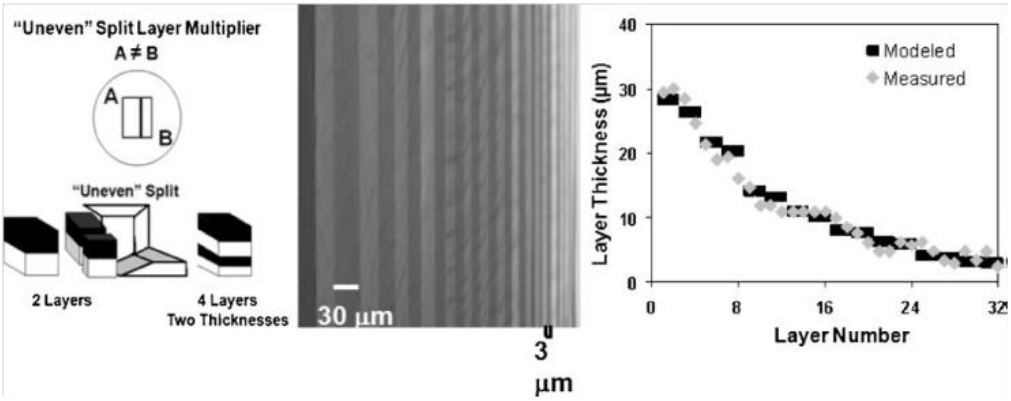

Figure 1.11 A depiction of how the forced assembly microlayer coextruder can produce asymmetric layered films.[39] "Ponting, M.; Hiltner, A.; Baer, E., *Macromolecular Symposia* 2010, *294* (1), 19-32." Reprinted with permission of John Wiley and Sons, 2016, Copyright "2010" John Wiley and Sons.

Further complexity was added to the multipliers by introducing an uneven split of the bi-layered polymer flow (Figure 1.11). This causes an asymmetric distribution of layer thickness throughout the film, which is useful for specific applications such as polymeric lenses. The asymmetric layers were imaged using AFM as shown in Figure 1.11, with the experimental and modeled values displayed to the right. For further control of the asymmetric layer thicknesses, many "uneven" multipliers can be placed in series followed by "even" multipliers. Detailed work and control has gone into asymmetric microlayered materials, but the focus of this work will be on the symmetrical layering technique. [39, 54, 55]

1.5. Microlayered Films as Dielectric Materials

Prior research has shown that barriers to electric breakdown channels can augment the performance through dielectric strength, also known as breakdown strength.[56, 57] Essentially, the layers or fillers in the polymer film impede the voltage breakdown

pathway and allow for the material to be operated at higher voltages and therefore higher capacitance. The architecture of the forced assembly microlayer films would take advantage of this behavior and bring about further investigation into the electrical benefits of this unique structure.

To take advantage of the microlayered system, the initial study by Wolak et al. utilized a polymer with a high dielectric constant and microlayered it with a polymer that had a high breakdown strength.[58] A common choice for a polymer with a high dielectric constant is poly(vinylidene fluoride) copolymerized with hexafluoropropylene (PVDF-HFP Grade: Solef 21508), which has a dielectric constant ranging from 10 – 15. The optimal polymer for high breakdown strength is polycarbonate (PC) which withstands voltages up to 600 kV/mm and has a dielectric constant around 3. These two polymers were processed into films with 32 and 256 layers, and the composition was systematically varied which allowed them to explore the effect of each polymer on the overall system. [58]

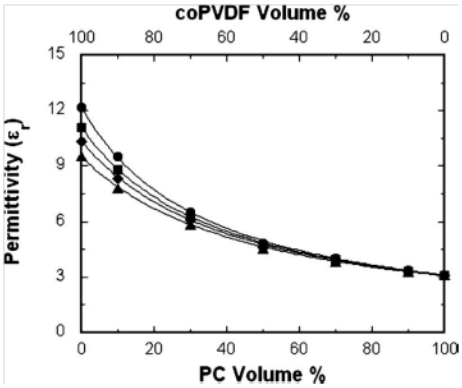

Figure 1.12 The relationship of permittivity performance with the change in PC and PVDF composition.[58] "Wolak, M. A.; Pan, M.-J.; Wan, A.; Shirk, J. S.; Mackey, M.; Hiltner, A.; Baer, E.; Flandin, L., *Applied Physics Letters* 2008, *92* (11), 113301." Reprinted with permission of AIP Publishing LLC, 2016, Copyright "2008" AIP Publishing LLC.

Figure 1.12 shows the permittivity or dielectric constant with changing composition at 100 Hz. The films with larger percentages of PVDF-HFP had the highest permittivity, which decreased with increasing PC content. This trend follows Equation 1.4 for permittivity with changing volume fractions of two different dielectric materials.

$$\frac{1}{\varepsilon_r} = \frac{\varphi_1}{\varepsilon_{r1}} + \frac{\varphi_2}{\varepsilon_{r2}} \tag{1.4}$$

The variable ε_r is the overall permittivity while ε_{r1} and ε_{r2} are the permittivities of each individual material and ϕ_1 and ϕ_2 are the respective volume fractions. The experimental values were within 3% of the predicted values from Equation 1.4.[58]

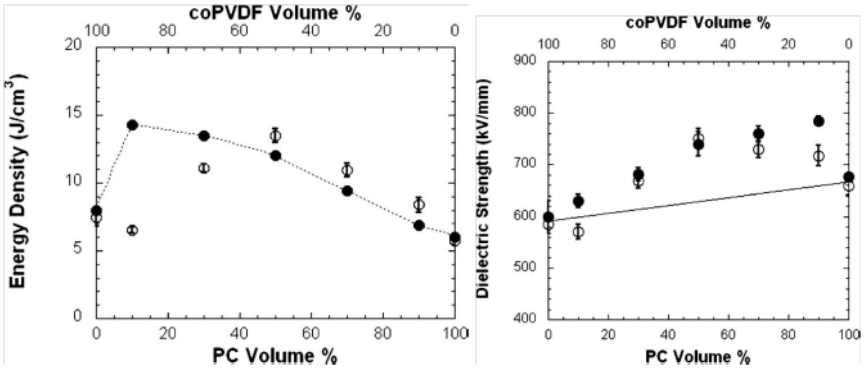

Figure 1.13 The relationship of energy density and dielectric strength (breakdown strength) performance with the change in PC and PVDF.[58] "Wolak, M. A.; Pan, M.-J.; Wan, A.; Shirk, J. S.; Mackey, M.; Hiltner, A.; Baer, E.; Flandin, L., ***Applied Physics Letters*** **2008,** ***92*** **(11), 113301." Reprinted with permission of AIP Publishing LLC, 2016, Copyright "2008" AIP Publishing LLC.**

The microlayering technique increased the performance by as much as 20% and 60% in dielectric strength and energy density respectively (Figure 1.13 where solid circles represent 32 layers and open circles correspond to materials with 256 layers). The highest performance with regards to dielectric strength (breakdown strength) was with 10 wt% of PVDF-HFP and 90% PC, which is expected because PC is a high breakdown

strength polymer. Once the energy density of the dielectric is considered the trend reverses and higher weight percentages of the PVDF-HFP within the films are preferred. This correlates to the high dielectric constant of PVDF-HFP which allows for more energy to be stored within the electric field.[58]

1.5.1 Effect of Polarization Hysteresis on the Microlayer Structure

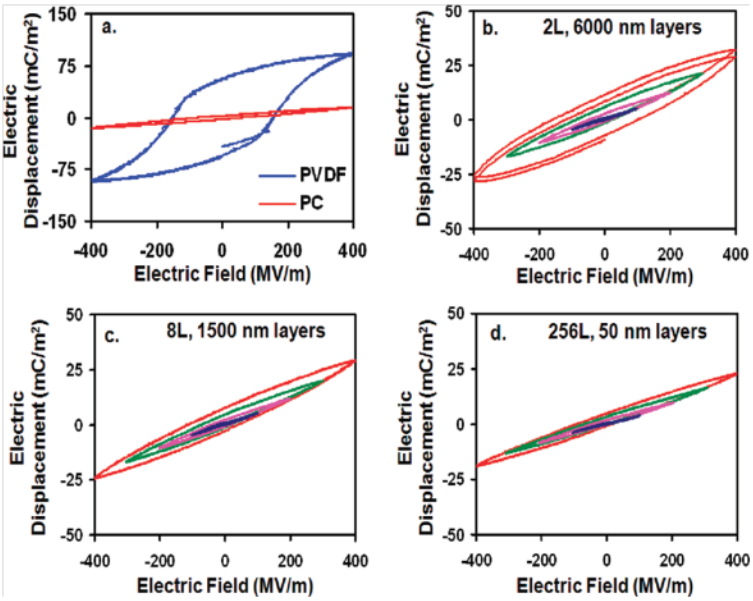

Figure 1.14 Hysteresis loops for PVDF and PC controls along with the microlayered systems.[59] "Mackey, M.; Schuele, D. E.; Zhu, L.; Flandin, L.; Wolak, M. A.; Shirk, J. S.; Hiltner, A.; Baer, E., *Macromolecules* 2012, *45* (4), 1954-1962." Reprinted with permission of American Chemical Society, 2016, Copyright "2012" American Chemical Society.

In Figure 1.14 (a.), the polarization hysteresis loops of PVDF and PC are compared. The PVDF curve has a large area which indicates that the electric field permanently polarizes PVDF. Upon further examination, PVDF maintains electric displacement even though the applied electric field is 0. This indicates that the electric field has permanently oriented a portion of the PVDF's polar groups. Permanent

polarization or orientation will reduce the performance of the capacitor and therefore should be reduced in any ideal dielectric material. An example of minimal hysteresis is the PC curve seen in Figure 1.14 (a.).[59]

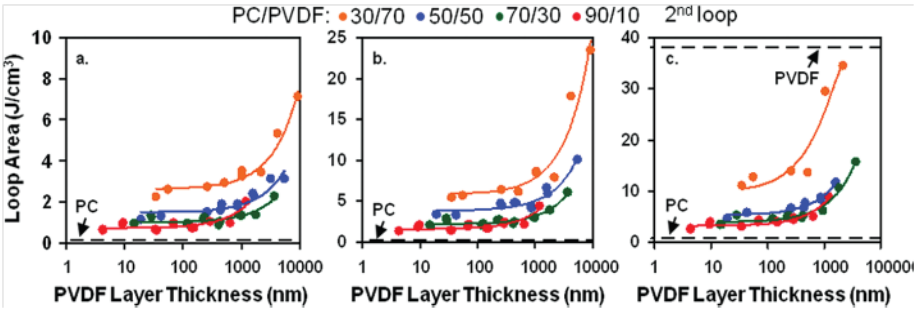

Figure 1.15 Hysteresis loop area plotted against PVDF layer thickness with various applied voltages: (a) 300 MV/m (b) 400 MV/m and (c) 500 MV/m[59] "Mackey, M.; Schuele, D. E.; Zhu, L.; Flandin, L.; Wolak, M. A.; Shirk, J. S.; Hiltner, A.; Baer, E., *Macromolecules* 2012, *45* (4), 1954-1962." Reprinted with permission of American Chemical Society, 2016, Copyright "2012" American Chemical Society.

Even though the hysteresis for the PVDF polarization curve is larger, the amount of electric displacement is higher, indicating that it can store more energy. By microlayering PVDF and PC, Mackey *et al.* showed in Figure 1.14 (B, C, and D) that the combination of the two polymers provides a film with a low hysteresis loop and higher electric displacement.[59] Furthermore, the amount of layers was increased, causing the individual layer thickness to decrease which showed the effect of the individual layer thickness on the hysteresis loop. It was found that the smaller the individual layer thickness became, the smaller the hysteresis loop area. In Figure 15, this is shown by measuring the loop area and subsequently plotting it against the individual PVDF layer thickness. When comparing the PC to PVDF ratio, the area of the hysteresis loop increased with increasing PVDF content. In another experiment, the electric field was

increased in Figure 1.15 from 300 MV/m to 400 MV/m to 500 MV/m. Increasing the electric field also increased the hysteresis loop. This trend corresponds to the enhanced electrical displacement that occurs with an increase in electrical field (Figure 1.15).[59]

1.5.1.1 Charge Migration

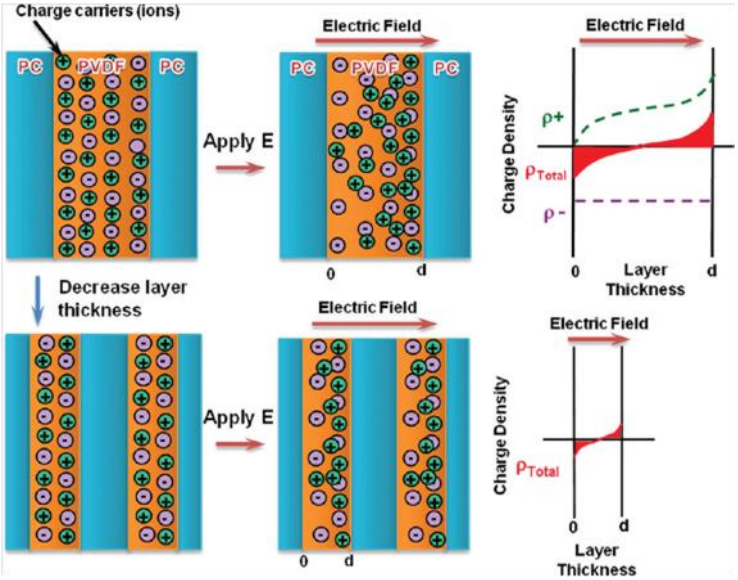

Figure 1.16 A schematic of how charge migration can be reduced in layered polymeric films.[59] "Mackey, M.; Schuele, D. E.; Zhu, L.; Flandin, L.; Wolak, M. A.; Shirk, J. S.; Hiltner, A.; Baer, E., *Macromolecules* 2012, *45* (4), 1954-1962." Reprinted with permission of American Chemical Society, 2016, Copyright "2012" American Chemical Society.

Mackey *et al* proposed that charge migration, which is the movement of ions within an applied electric field, could possibly be causing the changes in hysteresis with layer thickness.[59] This can best be imagined through the top row of images in Figure 1.16 where two materials (PVDF and PC) are coextruded into the nano-confined microlayer architecture. The ideal situation occurs when the ions remain associated with oppositely charged ions and do not move from their original position.[60] Thus, one way to maintain capacitor performance over time is to confine the ion movement.[59, 61]

Mackey *et al*. proposed the images in Figure 1.16 to explain the benefits of microlayered systems and their ability to reduce charge migration.[59] Essentially, the smaller the individual material layer becomes, the more ion confinement occurs which reduces the effects of charge migration. By reducing charge migration, the microlayered architecture maintains the desired ion proximity discussed earlier.[59] Sawada *et al*. attributed the ions in the PVDF to surfactant residue originating from the suspension polymerization with a concentration of <1 ppm by weight.[60]

Another aspect associated with charge migration is the difference in permittivity of the two coextruded materials. In this coextruded system PVDF has a high permittivity where PC has a lower permittivity. The difference in permittivity causes each interface to act as a barrier to ions and therefore impedes the movement of ions into the next layer.[56, 61] This is especially important to increase the breakdown strength because the buildup of ions on the electrode surface will produce heat and cause catastrophic failure.[62-64]

1.5.2 Dielectric Spectroscopy of Microlayer Films

Dielectric spectroscopy is used to examine the ionic and dipolar relaxations of multilayer films which occur at low frequencies. One such example was investigated in the work by Mackey *et al*. in which varying multilayer systems where made with PVDF and PC. Figure 1.17 shows the tan δ over a frequency range for this multilayered system. The high frequency peak showed relatively little change with the different layer thicknesses while the low frequency peak showed a drastic reduction in the tan δ as the layer thickness decreased. The high frequency peak was identified as the α crystallinity peak of the PVDF and is not associated with charge migration. The authors associated the change in

the lower frequency peaks as a reduction in the charge migration as the layer thickness decreased.[59, 61]

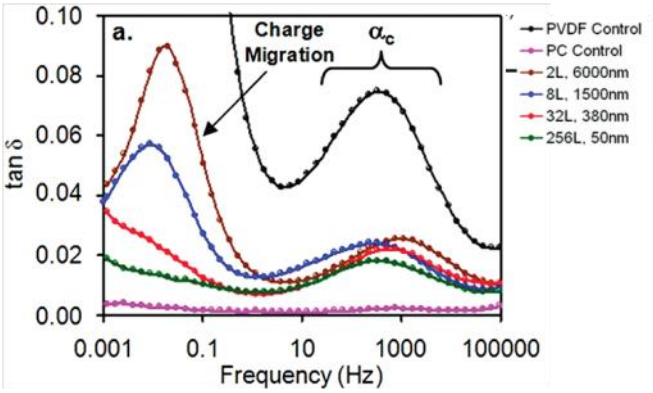

Figure 1.17 The tan δ plotted against the frequency for the PVDF and PC control and the microlayered films[59] "Mackey, M.; Schuele, D. E.; Zhu, L.; Flandin, L.; Wolak, M. A.; Shirk, J. S.; Hiltner, A.; Baer, E., *Macromolecules* 2012, *45* (4), 1954-1962." Reprinted with permission of American Chemical Society, 2016, Copyright "2012" American Chemical Society.

Ion motion requires energy, which cannot be recaptured because ion migration is inelastic. Therefore, charge migration contributes to the PDVF hysteresis loss. To examine this loss, the output energy density and unrecovered energy of each material is graphed against the applied electric field in Figure 1.18. For this test, energy was applied to the capacitor and the output energy density was recorded. The output energy density was subtracted from the input energy density and was then divided by the input energy density to get the percent unrecovered energy.[59]

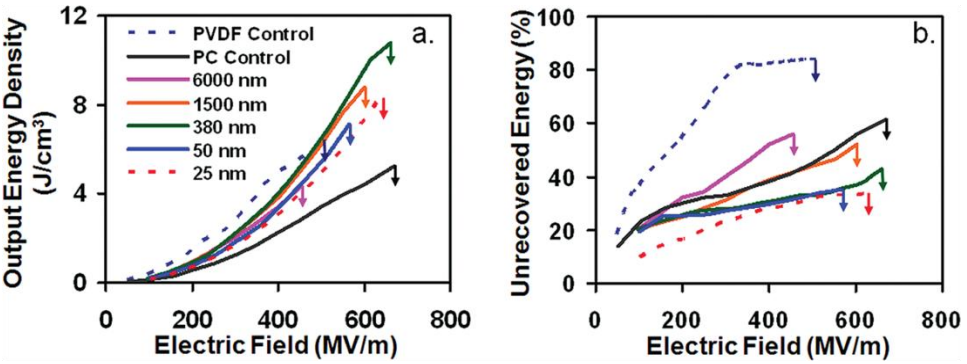

Figure 1.18 The output energy density and percent unrecovered energy plotted against electric field for the PVDF and PC control and the microlayered films[59] "Mackey, M.; Schuele, D. E.; Zhu, L.; Flandin, L.; Wolak, M. A.; Shirk, J. S.; Hiltner, A.; Baer, E., *Macromolecules* 2012, *45* (4), 1954-1962." Reprinted with permission of American Chemical Society, 2016, Copyright "2012" American Chemical Society.

Figure 1.18 (a) shows how much output energy was recovered versus the applied electric field. The optimal dielectric material will have a higher output energy density along with a low amount of unrecovered energy. PVDF does show high output densities, but the unrecovered energy is high as well. Furthermore, it does not reach high electric field values. The PC control shows low output energy but has low unrecovered energy and can go to higher electric fields. The microlayered material performs well in both of the areas as shown in Figure 1.19, where the output energy density and unrecovered energy are plotted against the PVDF layer thickness. Through the microlayering process the output energy density was increased in comparison to the PC control. The unrecovered energy did show a clear downward trend with lowered PVDF layer thickness. Overall, the microlayering process was able to lower the unrecovered energy while maintaining a high output energy density.[59]

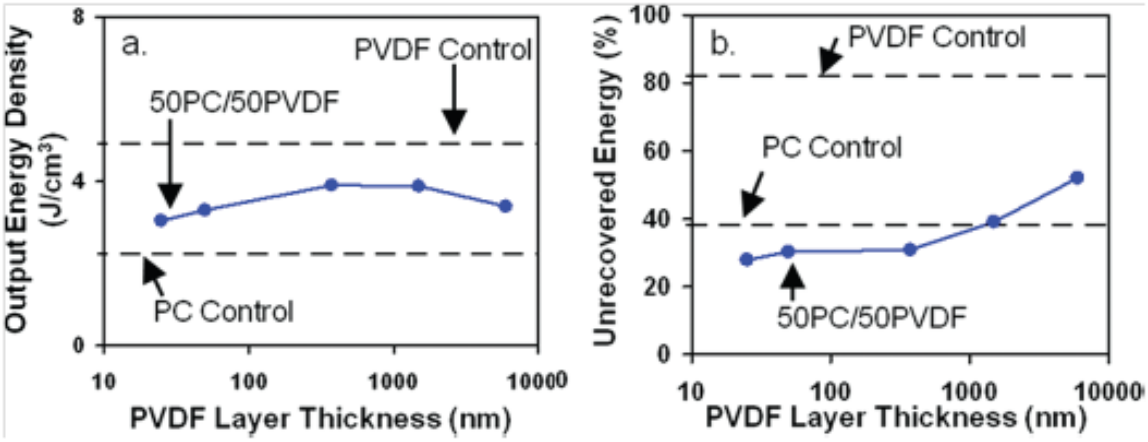

Figure 1.19 The output energy density and percent unrecovered energy plotted against PVDF layer thickness for the PVDF and PC control and the microlayered films at 400 MV/m applied voltage[59] "Mackey, M.; Schuele, D. E.; Zhu, L.; Flandin, L.; Wolak, M. A.; Shirk, J. S.; Hiltner, A.; Baer, E., *Macromolecules* 2012, *45* (4), 1954-1962." Reprinted with permission of American Chemical Society, 2016, Copyright "2012" American Chemical Society.

1.5.3 Breakdown Strength and Imaging of the Breakdown Site

Mackey *et al*. explored the breakdown process and what aspects impede and enhance performance using PVDF-HFP and PC. The first test compared the microlayered system to a melt blended system. To blend the PVDF-HFP and PC, an extruder melts and combines the two materials into a single flow. The flow is pushed through a flat die which creates the dielectric film. Figure 1.20 shows that the blended film produced a decrease in breakdown strength with respect to the weighted average of the two polymers. This drop is due to the immiscible nature of the PVDF-HFP/PC system, which creates heterogeneous interfaces within the film. By multilayering the two immiscible polymers, the breakdown strength is increased significantly above the control polymers. The interfaces between the two heterogeneous polymers can be parallel to the applied

electric field and therefore act as breakdown pathways for the current. The results in Figure 1.20 show that the multilayer architecture enhances the breakdown strength. The increased performance can be attributed to several reasons which will be discussed later, but Figure 1.20 points to the layered structure. Through the microlayering process a film is produced with perpendicular interfaces to any applied electric field which impedes the breakdown process.[10]

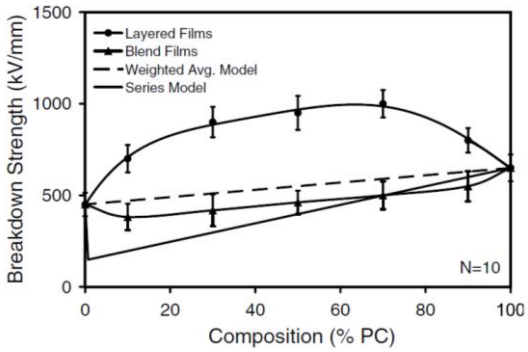

Figure 1.20 Comparison of the layered (32 Layer, 12 µm, PC/PVDF-HFP) and blended films (PC/PVDF-HFP) as a function of polycarbonate content.[10] "Mackey, M.; Hiltner, A.; Baer, E.; Flandin, L.; Wolak, M. A.; Shirk, J. S., *Journal of Physics D: Applied Physics* 2009, *42* (17), 175304." Reprinted with permission of IOP Publishing, 2016, Copyright "2009" IOP Publishing.

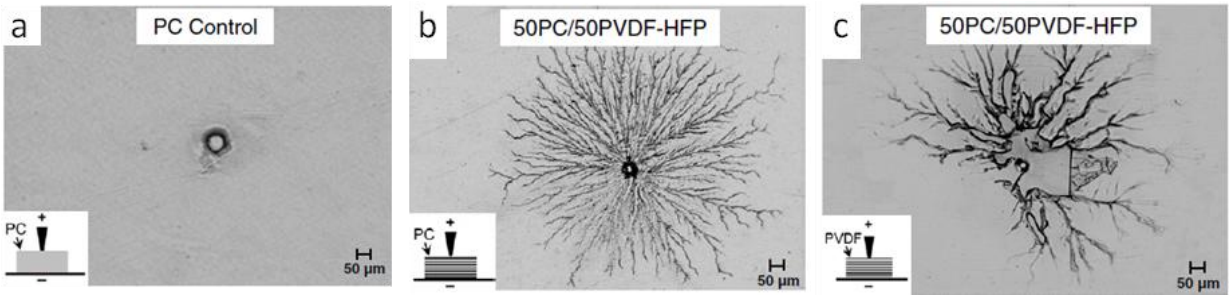

Figure 1.21 Comparison of the optical micrographed damage sites for three dielectric films (a) PC control (b) 32 Layer, 12µm, PC/PVDF-HFP with PC closest to the positive needle electrode (c) 32 Layer, 12µm, PC/PVDF-HFP with PVDF-HFP closest to the positive needle

electrode[10] "Mackey, M.; Hiltner, A.; Baer, E.; Flandin, L.; Wolak, M. A.; Shirk, J. S., *Journal of Physics D: Applied Physics* 2009, *42* (17), 175304." Reprinted with permission of IOP Publishing, 2016, Copyright "2009" IOP Publishing.

Traditional breakdown sites of monolithic polymer films (using a positive needle electrode) produce a simple hole in the film as shown in Figure 1.21 (a). However the optical micrograph of the multilayered PVDF-HFP/PC shows a distinct tree-like pattern surrounding the breakdown hole (Figure 1.21 (b)). This phenomenon is further changed depending on which material is facing the surface and adjacent to the positive electrode (Figure 1.21 (b) and (c)). When the PC layer (the higher breakdown strength material) is near the electrode the pinhole is encircled by the tree patterns.[10] When the PVDF-HFP layer (higher dielectric constant material) is touching the electrode the treelike behavior was produced but also resulted in delamination of one or more layers. The difference in the two breaking patterns is due to the high breakdown strength of PC versus PVDF-HFP. The PC layer that is nearest to the positive electrode is able to reach higher electric fields. The PVDF-HFP layer is not able to reach higher electric field values, but the microlayered film does have this ability. Therefore, the PVDF-HFP top layer delaminates, creating the breakdown pattern seen above.[10]

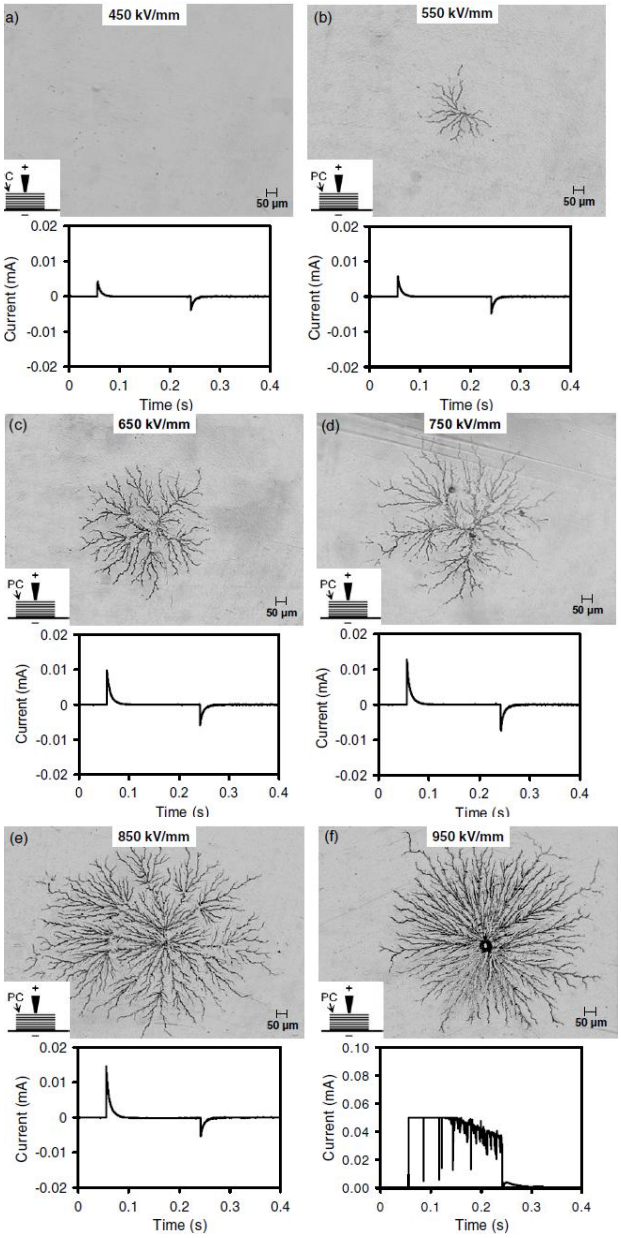

Figure 1.22 Comparison of optical micrographed damage sites resulting from applied electric fields from 450 kV/mm to 950 kV/mm at intervals of 100 kV/mm for 32 Layers, 12 µm, PC/PVDF-HFP with PC closest to the positive needle electrode[10] "Mackey, M.; Hiltner, A.; Baer, E.; Flandin, L.; Wolak, M. A.; Shirk, J. S., *Journal of Physics D: Applied Physics* 2009, *42* (17), 175304." Reprinted with permission of IOP Publishing, 2016, Copyright "2009" IOP Publishing.

Investigation into the two different damage patterns was continued by gradually increasing breakdown strength from 450 to 950kV/mm (at intervals of 50 kV/mm), once for PC touching the needle and again with PVDF-HFP touching the needle. The optical micrograph and the corresponding current profile of the 450 to 950 kV/mm (at intervals of 100 kV/mm) for PC nearest the positive needle is shown in Figure 1.22 (the optical micrographs of the PVDF-HFP nearest to the positive electrode can be seen in reference 7). The current profile below the corresponding micrograph is the graph of the current over time which includes the input current (how much current is stored in the capacitor's electric field) and the output current (how much current was retained after time passed or in this case how much current was remaining after the treeing or delamination). As the applied electric field increases, the amount of treeing increases in diameter. The increased electric field also correlates to a higher input current which was observed in the Figure 1.22 current profiles.[10]

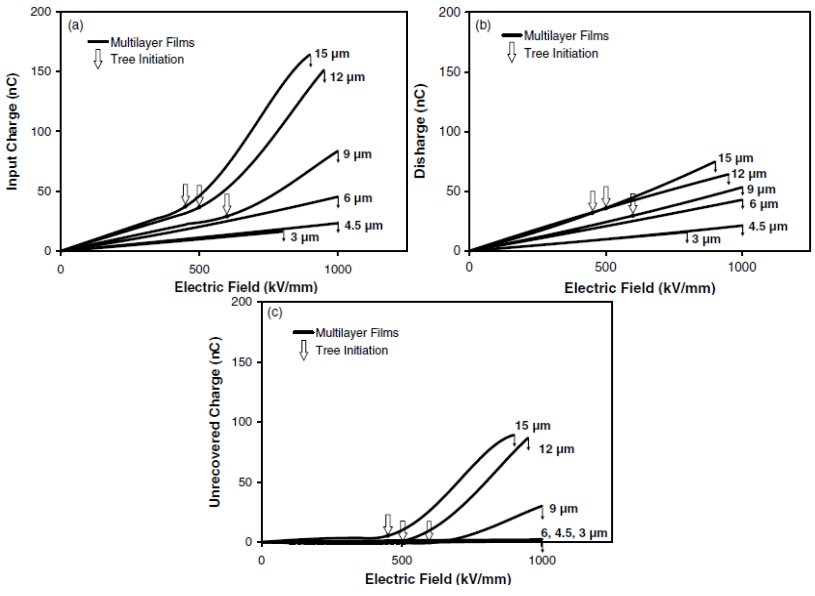

Figure 1.23 Input charge, discharge, and unrecovered charge plotted against electric field for 15, 12, 9, 6, 4.5, and 3 µm overall film thicknesses of the 32 Layer, PC/PVDF-HFP film

with PC layer closest to the positive needle electrode[10] "Mackey, M.; Hiltner, A.; Baer, E.; Flandin, L.; Wolak, M. A.; Shirk, J. S., *Journal of Physics D: Applied Physics* 2009, *42* (17), 175304." Reprinted with permission of IOP Publishing, 2016, Copyright "2009" IOP Publishing.

In Figure 1.23 the input, output (discharge), and unrecovered charge of the 50PC/50PVDF-HFP, 32 layers, at various overall film thicknesses is plotted against electric field. The large arrow signifies the electric field value for the onset of the tree-like breaking. As the overall film thickness is decreased, the point at which the treeing occurs moves to higher applied electric fields. This is why there are no arrows for films below 6 μm. This behavior can be explained by the units for electric field which is kV per mm of thickness. The thicker films reach higher values of electric field, but dielectric thickness must also be taken into consideration. This indicates that a large overall electric field is required to cause the local charge build up within the layered structure to cause the tree like patterns around the breakdown sites.[10]

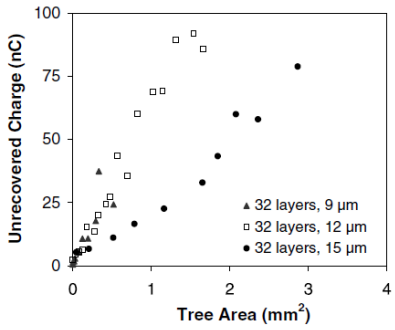

Figure 1.24 Unrecovered charge plotted against tree area for 15, 12, and 9 μm overall film thicknesses of the 32 Layer, PC/PVDF-HFP film with PC layer closest to the positive needle electrode.[10] "Mackey, M.; Hiltner, A.; Baer, E.; Flandin, L.; Wolak, M. A.; Shirk, J. S., *Journal of Physics D: Applied Physics* 2009, *42* (17), 175304." Reprinted with permission of IOP Publishing, 2016, Copyright "2009" IOP Publishing.

After the films begin to tree in Figure 1.23 (a), the amount of input charge begins to increase. However, Figure 1.23 (b) does not show an increase in the output which indicates that energy is being lost in the treeing process. This is confirmed in Figure 1.23 (c) which shows the loss of energy in the multilayered films beginning at the tree initiation. Therefore, the tree pattern absorbs the electric energy but cannot give it back. In Figure 1.24, this is further shown by plotting the unrecovered charge against the tree area (found by outlining the tree pattern and taking the area). It shows that as the thickness of the film becomes larger the tree area becomes larger and with more tree area there is an increase in unrecovered charge. However, the treeing breakdown pattern can be avoided by reducing the thickness of the film and the benefits of the multilayer structure will be maintained. Each of the layer interfaces will still build up local charge and the effects of defects and impurities will still be reduced.[10]

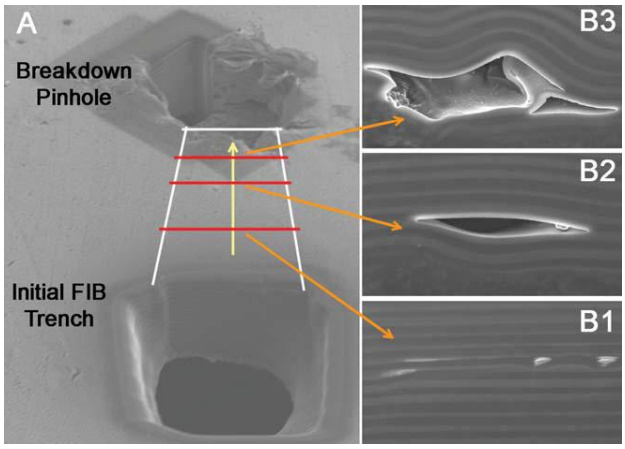

Figure 1.25 SEM images of focused ion beam milling process and the delamination of the layers caused by the breakdown process[65] "Wolak, M. A.; Wan, A. S.; Shirk, J. S.; Mackey, M.; Hiltner, A.; Baer, E., ***Journal of Applied Polymer Science*** **2012,** ***123*** **(4), 2548-2557." Reprinted with permission of John Wiley and Sons, 2016, Copyright "2012" John Wiley and Sons.**

Wolak *et al*. characterized the breakdown in layers towards the center of the film, rather than just on the surface. In order to do this, a film that already had a breakdown pin hole was cut using focused ion beams in a systematic manner. After each cut was made the surface of the hole was imaged using SEM. An example of the technique and results can be seen in Figure 1.25. From this technique, the layer delamination within the film indicates the effectiveness of the layered structure to act as barriers to the electric breakdown pathway. [65]

1.5.4 Dielectric Lifetime of Multilayer Films

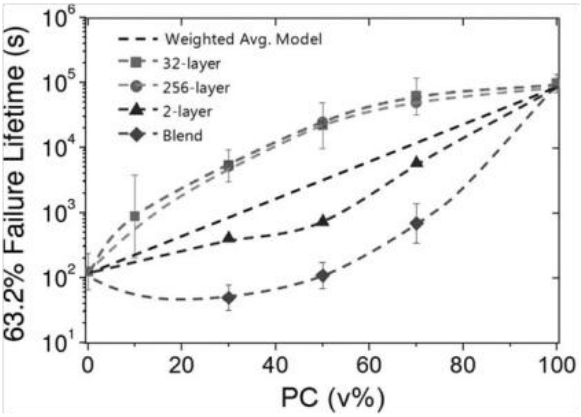

Figure 1.26 The relationship of 63.2% failure lifetime with the change in PC and PVDF. The layered films were compared by the amount of layers within the film. Additionally the results were compared to a blended film and a weighted average.[62] "Zhou, Z.; Mackey, M.; Carr, J.; Zhu, L.; Flandin, L.; Baer, E., *Journal of Polymer Science Part B: Polymer Physics* 2012, *50* (14), 993-1003." Reprinted with permission of John Wiley and Sons, 2016, Copyright "2012" John Wiley and Sons.

Zhou *et al*. investigated the long term stability of the microlayered polymer system in comparison to control and blended films. The results of the study can be seen in Figure 1.26 and it is clear that the multilayered architecture is superior to the blended system.

The two layer system does not do as well but once the layers are increased to at least 32 the lifetime performance is significantly increased. The polycarbonate shows the best lifetime but the PVDF has superior dielectric performance so the layered structure has merged polycarbonate superior lifetime performance and PVDF's superior energy storage performance.[62]

Zhou *et al*. proposed reasoning for this increased performance based on the data and prior research. Mainly it is due to the deceased amount of charge migration which has been proven in the layered structure.[59, 61] The charge migration traditionally affects the dielectric properties but in the case of lifetime performance charge build up actually increases the heat on the dielectric surface which eventually leads to catastrophic failure. By introducing more layers the multilayer structure inhibits the excessive built up of charge on the surface and allows for enhanced lifetime.[62]

1.6 Summary

In summary, polymers have become a popular choice as a dielectric material because of superior mechanical properties, low material cost, processability, and in some cases self-healing properties.[2] Force assembly microlayer coextrusion has been utilized to increase dielectric film performance.[10,58,59,61-65] In this process, two polymers are multilayered in a film to create a structure with many parallel alternating layers.[39] This is advantageous for capacitors because the properties of two different materials can be combined and each interface of the two polymers works to bolster the overall dielectric properties.[10,58] One of the polymers, the insulating layer with low dielectric constant, is chosen to have high breakdown strength and low loss, e.g. poly(ethylene terephthalate)[63] or polycarbonate[10,58,59,61,62,64,65]. The other polymer has a high dielectric constant such as

poly(vinylidene fluoride)[10,61] or its copolymers[58,59,62-65] that can increase the energy density.

Mackey *et al.* fount that the multilayer structure would reduce the hysteresis loop area when compared to PVDF. The hysteresis was further reduced when the individual layer thickness was reduced. Mackey *et al.* proposed that this could be attributed to the reduction of charge migration within the layered system.[59] Mackey et al. found that multilayer architecture also enhances the breakdown strength with respect to the linear wt% PC composition. This was attributed to the many perpendicular interfaces which impedes the breakdown process.[10] Zhou *et al.* found that introducing more layers the multilayer structure inhibits the excessive built up of charge on the surface and allows for enhanced lifetime.[62]

References

1. Mullin, W. F., ABC's of capacitors. H.W. Sams: Indianapolis, **1978**.
2. Nalwa, H. S., Handbook of low and high dielectric constant materials and their applications. Academic Press: San Diego, **1999**.
3. Riande, E. D.-C. R., Electrical properties of polymers. Marcel Dekker: New York, **2004**.
4. Shihai, Z.; Chen, Z.; Xin, Z.; Anderson, D.; Zellers, B.; Qiming, Z. In Polymer film capacitors with high dielectric constant, high capacitance density, and high energy density, IEEE International Power Modulator and High Voltage Conference (IPMHVC) 2010, 23-27 **2010**; pp 221-224.
5. Zulkifli, A., Polymer Dielectric Materials. **2012**.
6. Elliott, R. S., Electromagnetics. McGraw-Hill: New York, **1966**.
7. Kao, K.-C., Dielectric phenomena in solids : with emphasis on physical concepts of electronic processes. Academic Press: Amsterdam; Boston, **2004**.
8. Simpson, J. O.; St.Clair, A. K., Thin Solid Films 1997, 308–309 (0), 480-485.
9. Zhu, L.; Wang, Q., *Macromolecules* **2012**, 45 (7), 2937-2954.
10. Mackey, M.; Hiltner, A.; Baer, E.; Flandin, L.; Wolak, M. A.; Shirk, J. S., *J. Phys. D Appl. Phys.* **2009**, 42 (17), 175304.
11. Dubois, J.-C., *Adv. Mater.* **1996**, 8 (6), 542-542.
12. Films, D. T., Mylar Polyester Film Dielectric Properties. **2003**.
13. Odian, G. G., Principles of polymerization. Wiley-Interscience: Hoboken, N.J., **2004**.

14. Inc, N. E., Mylar/Polyester Film Capacitor Specifications. nteinc.com.

15. Asakura, M.; Hirano, T.; Nagai, I.; Tanaka, S. Biaxially oriented polypropylene film and a capacitor made thereof. US5724222, **1998**.

16. Sugata, M.; Okamoto, K.; Asano, T. Biaxially oriented polypropylene film, metallized film, and film capacitor. US5724222, **2013**.

17. Barshaw, E. J.; White, J.; Chait, M. J.; Cornette, J. B.; Bustamante, J.; Folli, F.; Biltchick, D.; Borelli, G.; Picci, G.; Rabuffi, M., *IEEE Trans. Magn.* **2007**, 43 (1), 223-225.

18. Umemura, T.; Akiyama, K.; Couderc, D., *IEEE Trans. Electr. Insul.* **1986**, EI-21 (2), 137-144.

19. Dervos, C. T.; Tarantili, P. A.; Athanassopoulou, M. D., *J. Phys. D Appl. Phys.* **2009**, 42 (13), 135409.

20. Nash, J. L., *Polym Eng Sci* **1988**, 28 (13), 862-870.

21. Cieloszyk, G. S.; Cruz, M. T.; Salinger, G. L., *Cryogenics* **1973**, 13 (12), 718-721.

22. Wilson, J. D. Capacitor with a polycarbonate dielectric. US3328654 A, 1967.

23. Sugimoto, E., *IEEE Electr. Insul. Mag.* **1989**, 5 (1), 15-23.

24. Yen, S. P. S.; Lewis, C. R.; Jow, T. R.; Cygan, P. J. In Development of high temperature polyimide dielectric film for leaded and surface mount capacitor application, *IEEE 35th International Power Sources Symposium*, **1992**; pp 363-366.

25. Chern, Y.-T.; Twu, J.-T.; Chen, J.-C., *Eur. Polym. J.* **2009**, 45 (4), 1127-1138.

26. Liu, J.-G.; Zhao, X.-J.; Yang, H.-X.; Li, H.-S.; Fan, L.; Yang, S.-Y., *Macromol. Chem. Phys.* **2006**, 207 (14), 1272-1277.

27. Yang, F.; Li, Y.; Ma, T.; Bu, Q.; Zhang, S., *J. Fluorine Chem.* **2010**, 131 (7), 767-775.

28. Shi, C.-Y.; Hao, X.-J.; Zha, J.-W., *J. Adv. Phys.* **2012**, 1 (1), 78-83.

29. Naima, B.-S.; Edmondson, C. A.; Wintersgill, M. C.; Fontanella, J. J.; Todd, A., *Smart Mater. Struct.* **2011**, 20 (9), 094001.

30. Chi, Q.; Sun, J.; Zhang, C.; Liu, G.; Lin, J.; Wang, Y.; Wang, X.; Lei, Q., J. *Mater. Chem. C* **2014**, 2 (1), 172-177.

31. Wang, The Applications of Ferroelectric Polymers. Blackie: 1988; pp 387-pp.

32. Glossmann, J.; Hoischen, A.; Roder, T.; Kitzerow, H.-s., *Ferroelectrics* **2000**, 243 (1), 95-106.

33. Guan, F.; Pan, J.; Wang, J.; Wang, Q.; Zhu, L., *Macromolecules* **2009**, 43 (1), 384-392.

34. Chu, B.; Zhou, X.; Ren, K.; Neese, B.; Lin, M.; Wang, Q.; Bauer, F.; Zhang, Q. M., *Science* **2006**, 313 (5785), 334-336.

35. Su, R.; Tseng, J.-K.; Lu, M.-S.; Lin, M.; Fu, Q.; Zhu, L., *Polymer* **2012**, 53 (3), 728-739.

36. Tomer, V.; Manias, E.; Randall, C. A., *J. Appl. Phys.* **2011**, 110 (4), 044107-044107-10.

37. Hao, X., J. *Adv. Dielectr.* **2013**, 03 (01), 1330001.

38. Lovinger, A. J., *Science* **1983**, 220 (4602), 1115-1121.

39. Ponting, M.; Hiltner, A.; Baer, E., *Macromolecular Symposia* **2010**, 294 (1), 19-32.

40. Schrenk, W. J., *SPE J.* **1973**, 29 (6), 38.

41. Schrenk, W. J. Apparatus for multilayer coextrusion of sheet or film. US 3884606 A, **1975**.

42. Schrenk, W. J.; Chisholm, D. S.; Cleereman, K. J.; Alfrey, T. Method of preparing multilayer plastic articles. US3565985 A, **1971**.

43. Schrenk, W. J.; Chisholm, D. S.; Cleereman, K. J.; Alfrey, T. Multilayered iridescent plastic articles. US3576707, **1971**.

44. Radford, J. A.; Alfrey, T.; Schrenk, W. *J., Polym. Eng. Sci.* **1973**, 13 (3), 216-221.

45. Schrenk, W. J.; Alfrey, T., *Polym. Eng. Sci.* **1969,** 9 (6), 393-399.

46. Ramanathan, R.; Schrenk, W. J.; Wheatley, J. A. Coextrusion of multilayer articles using protective boundary layers and apparatus therefor. US5269995, **1993**.

47. Ayres, R. F.; Gosen, D. J.; Schrenk, W. J.; Shastri, R. K. Interfacial surface generator. US 5094788, **1992**.

48. Lewis, R. A.; Ramanathan, R.; Schrenk, W. J.; Wisniewski, D. M. Layer thickness gradient control in multilayer polymeric bodies. US 5389324, **1995**.

49. Hebrink, T. J.; Liu, Y. J.; Merrill, W. W.; Nerad, B. A.; Wheatley, J. A. Method for making coPEN/PMMA multilayer optical films. US6830713, **2004**.

50. Gregory, B. L.; Siegmann, A.; Im, J.; Hiltner, A.; Baer, E., *J. Mater. Sci.* **1987**, 22 (2), 532-538.

51. Kazmierczak, T.; Song, H.; Hiltner, A.; Baer, E., *Macromol. Rapid Commun.* **2007**, 28 (23), 2210-2216.

52. Baer, E.; Hiltner, A.; Jarus, D., *Macromolecular Symposia* **1999**, 147 (1), 37-61.

53. Ma, M.; Vijayan, K.; Hiltner, A.; Baer, E.; Im, J., *J Mater Sci* **1990**, 25 (4), 2039-2046.

54. Carr, J. M.; Langhe, D. S.; Ponting, M. T.; Hiltner, A.; Baer, E., *J. Mater. Res.* **2012**, 27 (10), 1326-1350.

55. Hiltner, A.; Liu, R. Y. F.; Hu, Y. S.; Baer, E., J. *Polym. Sci. B: Polym. Phys.* **2005**, 43 (9), 1047-1063.

56. Agoris, D. P.; Vitellas, I.; Gefle, O. S.; Lebedev, S. M.; Yu, P. P., *J Phys D Appl Phys* **2001**, 34 (24), 3485.

57. Gefle, O. S.; Lebedev, S. M.; Pokholkov, Y. P.; Gockenbach, E.; Borsi, H., *J. Phys. D Appl. Phys.* **2004**, 37 (16), 2318.

58. Wolak, M. A.; Pan, M.-J.; Wan, A.; Shirk, J. S.; Mackey, M.; Hiltner, A.; Baer, E.; Flandin, L., *Appl. Phys. Lett.* **2008**, 92 (11), 113301.

59. Mackey, M.; Schuele, D. E.; Zhu, L.; Flandin, L.; Wolak, M. A.; Shirk, J. S.; Hiltner, A.; Baer, E., *Macromolecules* **2012**, 45 (4), 1954-1962.

60. Sawada, A., *Jpn. J. Appl. Phys. 2*, **1999**, 38 (part 1, no. 3a), 1418-1422.

61. Mackey, M.; Schuele, D. E.; Zhu, L.; Baer, E., *J. Appl. Phys.* **2012**, 111 (11), 113702-113702-9.

62. Zhou, Z.; Mackey, M.; Carr, J.; Zhu, L.; Flandin, L.; Baer, E., *J. Polym. Sci. B Polym. Phys.* **2012**, 50 (14), 993-1003.

63. Carr, J. M.; Mackey, M.; Flandin, L.; Schuele, D.; Zhu, L.; Baer, E., *J. Polym. Sci. B Polym. Phys.* **2013**, 51 (11), 882-896.

64. Zhou, Z.; Carr, J.; Mackey, M.; Yin, K.; Schuele, D.; Zhu, L.; Baer, E., *J. Polym. Sci. B Polym. Phys.* **2013**, 51 (12), 978-991.

65. Wolak, M. A.; Wan, A. S.; Shirk, J. S.; Mackey, M.; Hiltner, A.; Baer, E., *J. Appl. Polym. Sci.* **2012**, 123 (4), 2548-2557.

Chapter 2: Fluorinated Poly(Arylene Ether Ketone)s for High Temperature Dielectrics

Andrew T. Shaver,[1] Kezhen Yin,[2] Hailun Borjigin,[1] Wenrui Zhang,[1] Shreya Roy Choudhury,[1] Eric Baer,[2] Sue J. Mecham,[1] J. S. Riffle,[1] James E. McGrath[1]*

[1]Macromolecules and Interfaces Institute, Virginia Tech, Blacksburg, VA

[2]Center for Layered Polymeric Systems, Department of Macromolecular Science and Engineering, Case Western Reserve University, Cleveland, OH

Shaver, A. T.' Yin, K.; Borjigin, B.; Zhang, W.; Roy Choudhury, S.; Baer, E.; Mecham, S. J.; Riffle, J. S.; McGrath, J. E., Polymer Volume 83, 28 January 2016, Pages 199–204

2.1. Introduction

Today's electronics are involved in many vital functions of everyday life and capacitors serve key roles in these devices.[1-4] Because of miniaturization and increased energy consumption in such applications, new dielectric materials must be developed with higher energy density while maintaining low loss of that energy.[1, 4] Considerable research has been devoted to polymeric dielectric materials due to their ease of manufacturing, high breakdown strength, low loss, and self-clearing capabilities.[1, 5, 6] Biaxially oriented polypropylene is widely regarded as the current state-of-the-art material and it is well known that many of its properties originate from the biaxial orientation process.[7-9] However, the use of biaxially oriented polypropylene is limited due to its poor performance above ~85 $^{\circ}$C and low energy density.[7, 9, 10]

A processing technique under investigation to increase dielectric film performance has been termed forced assembly microlayer coextrusion.[11-19] In this

process, two polymers are multilayered in a film to create a structure with many parallel alternating layers.[20] This is advantageous for capacitors because the properties of two different materials can be combined and each interface of the two polymers works to bolster the overall dielectric properties.[11, 12] One of the polymers, the insulating layer with low dielectric constant, is chosen to have high breakdown strength and low loss, e.g. poly(ethylene terephthalate)[18], polycarbonate[11-17], or polysulfone[19]. The other polymer has a high dielectric constant such as poly(vinylidene fluoride)[12, 15, 19] or it's copolymers[11, 13, 14, 16-18] that can increase the energy density. The layered structure leads to build-up of Maxwell-Wagner-Sillars interfacial polarization at the interfaces. The charge buildup at these interfaces allows the films to discharge along the interfaces and thus results in higher breakdown strengths[18].

In this work, four different poly(arylene ether)s were synthesized to compare symmetric and asymmetric fluorine-containing structures versus their non-fluorinated counterparts. Prior work on low dielectric polymers as insulators showed that asymmetric versus symmetric fluorination could affect a material's overall polarization[21]. Therefore, this paper describes poly(arylene ether ketone)s (PAEKs) with systematic fluorine- and non-fluorine containing geometries that could be melt processed for use in capacitors (Fig. 2.1). In the future, they could be layered with poly(vinylidene fluoride) to explore the effect that fluorination and symmetry have on the interfaces of the microlayer film architecture. Literature shows that increasing the strength of the interface can increase the breakdown strength of layered dielectric films[22]. It was reasoned that added fluorine structures in the polymers may improve interactions with fluorinated high dielectric constant materials such as PVDF.

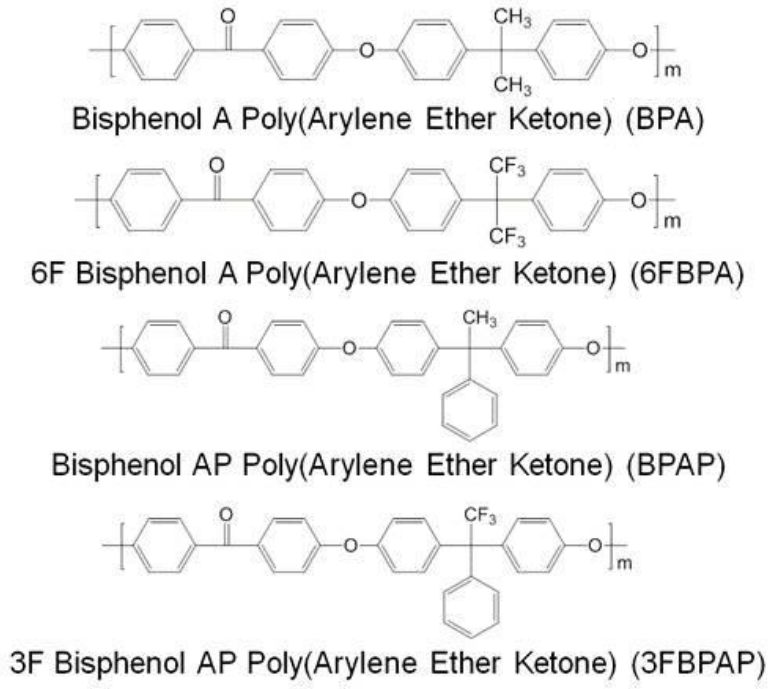

Figure 2. 1 The polymer chemical structures

2.2. Experimental

Materials

N,N-Dimethylacetamide (DMAc), dichloromethane, triflic acid, toluene, 4,4'-(1-phenylethylidene)bisphenol, 2,2,2-trifluoroacetophenone, and phenol were purchased from Sigma Aldrich. DMAc was vacuum distilled from calcium hydride. Triflic acid, toluene, dichloromethane, 2,2,2-trifluoroacetophenone and phenol were used as received. 4,4'-(1-Phenylethylidene)bisphenol was dried at 110 °C under vacuum. 4,4'-Difluorobenzophenone and bisphenol A were kindly donated by Solvay and recrystallized from 2-propanol and toluene, respectively. 4,4'-Hexafluoroisopropylidenediphenol was obtained from Ciba and purified by sublimation, followed by recrystallization from toluene. Potassium carbonate was purchased from Fisher Scientific and dried at 150 °C under vacuum.

Synthesis of 1,1-bis(4-hydroxyphenyl)-1-phenyl-2,2,2-trifluoroethane (the bisphenol monomer for 3FBPAP)

Phenol (41.32 g, 440 mmol) and 2,2,2-trifluoroacetophenone (19.32 g, 110 mmol) were charged to a 250-mL, three-neck, round bottom flask equipped with a magnetic stir bar, N_2 inlet, and an addition funnel fitted with a drying tube and heated to 45 °C. Once a homogeneous solution was achieved, triflic acid (3.8 mL, 42 mmol) was introduced dropwise while maintaining the temperature at 45 °C. After 1 h, the slurry was treated with 200 mL of hot deionized water and the product was isolated by filtration. The pink solid was stirred in 200 mL of hot deionized water for 30 min, vacuum filtered, and washed with hot water, then dichloromethane. The product was dried at 80 °C under vacuum for 24 h. Yield was ~90%. The mp was 215 °C, consistent with literature[23].

Synthesis of BPA, 6FBPA, 3FBPAP and BPAP poly(arylene ether ketone)s

The procedure for all four polymers was the same. A representative synthesis of the BPA polymer was adapted from previous literature[24-28]. For example, bisphenol A (67.713 g, 296.6 mmol), 4,4'-difluorobenzophenone (65.643 g, 306.4 mmol), and DMAc (600 mL) were charged to a three-neck flask equipped with a N_2 inlet, mechanical stirrer, and Deane Stark trap. Toluene (300 mL) and K_2CO_3 (48.352 g, 349.8 mmol) were added to the flask and the Deane Stark trap was filled with toluene. The apparatus was placed in a silicone oil bath that was heated to 155 °C to begin azeotropic removal of water. After 4 h the toluene and water were removed from the Dean Stark trap. The oil bath was maintained at 150 °C for 12 h, then the reaction was allowed to cool to room temperature. The polymer solution was filtered to remove any excess K_2CO_3 or by-product salts. The polymer solution was precipitated into deionized water, then the polymer was stirred in

deionized water at 80 °C to further assist the removal of salts and solvents. The white polymer was filtered and dried at 110 °C under vacuum. Yield was 81%.

The values for the remaining three reactions were as follows. For the 6FBPA polymer the amounts of the materials were: 4,40- hexafluoroisopropylidenediphenol (2.733 g, 8.128 mmol), 4,4'-difluorobenzophenone (1.814 g, 8.468 mmol), DMAc (24 mL), toluene (12 mL), and K2CO3 (1.3800 g, 9.985 mmol). Yield was 92%. For the 3FBPAP polymer the amounts of the materials were: 1,1-bis(4-hydroxyphenyl)-1-phenyl-2,2,2-trifluoroethane (9.960 g, 28.93 mmol), 4,4'-difluorobenzophenone (6.481 g, 30.25 mmol), DMAc (24 mL), toluene (12 mL), and K2CO3 (6.4370 g, 46.57 mmol). Yield was 82%. For the BPAP polymer the amounts of the materials were: 4,4'-(1-phenylethylidene)bisphenol (2.081 g, 7.167 mmol), 4,4'-difluorobenzophenone (1.600 g, 7.469 mmol), DMAc (24 mL), toluene (12 mL), and K_2CO_3 (1.2300 g, 8.899 mmol). Yield was 89%.

Proton nuclear magnetic resonance (NMR) spectroscopy

^{1}H NMR analysis was performed on a Varian Inova spectrometer operating at 400 MHz. All spectra were obtained from 15% (w/v) 1 mL solutions in chloroform-d.

Film-casting

The polymer (0.4 g) was weighed into a small glass vial with a magnetic stir bar. Chloroform (11 mL) was added to the vial to obtain a 2.5 wt% solution. The solution was filtered using a 1-mm syringe filter into a clean glass vial. A 5 x 5 glass plate was placed in a base bath for 30 min for surface treatment. The glass plate was rinsed and dried, then placed on a level surface for casting. The solution was poured onto the plate and the solution was spread to the edges of the plate until it covered the whole glass plate. A

glass dome with 2 outlets was used to cover the plate. One outlet was fitted with a syringe filter and the otherwas connected to the house air stream running at 2 SCFH. The plate was left undisturbed for a minimum of 30 min, then transferred to an oven at 110 °C for an additional 30 min. The filmwas removed from the glass plate using a razor blade by slowly lifting the edges until the film came off.

Size exclusion chromatography (SEC)

SEC was conducted to measure molecular weights and distributions. The mobile phase was DMAc distilled from CaH_2 containing dry LiCl (0.1 M). The column set consisted of 3 Agilent PLgel 10-μm Mixed B-LS columns 300 x 7.5 mm (polystyrene/divinylbenzene) connected in series with a guard column having the same stationary phase. The columns and detectors were maintained at 50 °C. An isocratic pump (Agilent 1260 infinity, Agilent Technologies) with an online degasser (Agilent 1260), autosampler and column oven was used for mobile phase delivery and sample injection. A system of multiple detectors connected in series was used for the analyses. A multi-angle laser light scattering detector (DAWN-HELEOS II, Wyatt Technology Corp.), operating at a wavelength of 658 nm, a viscometer detector (Viscostar, Wyatt Technology Corp.), and a refractive index detector operating at a wavelength of 658 nm (Optilab T-rEX, Wyatt Technology Corp.) provided online results. The system was corrected for interdetector delay and band broadening using a 21,000 g/mole polystyrene standard. Data acquisition and analysis were conducted using Astra 6 software from Wyatt Technology Corp. Validation of the system was performed by monitoring the molar mass of a known molecular weight polystyrene sample by light scattering. The accepted variance of the 21,000 g/mole polystyrene standard was defined as 2 standard

deviations (11.5% for M_n and 9% for M_w) derived from a set of 34 runs. Specific refractive index values were calculated based on the assumption of 100% recovery.

Thermogravimetric analysis (TGA)

Thermal stabilities of the polymers were investigated using a TA Instruments TGA Q5000 under a N_2 atmosphere with the N_2 running at 25 mL/min. The heating rate was 10 °C/min from room temperature to 700 °C.

Differential scanning calorimetry (DSC)

The thermal properties were investigated with a TA Instruments DSC Q200. The polymers were heated under N_2 to ensure an inert atmosphere at 60 mL/min. The heating rate was 10 ^{o}C/min to 350 °C, then the sample was cooled to 0 °C at 10 °C/min. It was heated once more to 350 °C at 10 °C/min and the reported DSC thermograms are from the second scans.

Refractive indices

The refractive indices of PAEK films were characterized using a 2010 Metricon instrument with a 633 nm laser at room temperature. The PAEK films were brought into contact with the base of a prism with a known refractive index. The laser beam began horizontal (90°) to the prism/polymer interface so all light was totally reflected, and then it rotated until it was normal to the prism/polymer interface (0°). At some angle between 90° and 0° the reflected laser light intensity decreased which indicated the critical angle. The refractive indices of the films were calculated by Snell's Law (equation (2.1))

$$n_p sin\theta_p = n_f sin\theta_f \qquad (2.1)$$

where n_p and n_f are the refractive indices of the prism and the film, respectively, θ_p is the critical angle and θ_f equaled 90° [29].

Breakdown strength

Breakdown strengths of the PAEK films were measured with a needle-plane electrode. The needle electrode was the positive side and the diameter of the needle tip was 40 mm. The negative electrode was a 3 x 10 cm rectangular aluminum plate. A Quadtech (Marlborough, MA) Guardian 20-kV HiPot tester was used as the voltage source and the voltage ramp speed was 500 V/s. The breakdown strength measurements were carried out in an oil bath at 25, 75, 125, 150, and 175 °C with twenty repetitions for each film at each temperature.

Dielectric thermal analysis (DETA)

Dielectric spectroscopy was measured with a frequency sweep from 0.01 Hz to 10000 Hz at 25 °C at a constant voltage of 1 V using a Novocontrol (Hundsangen, Germany) spectrometer. Electrodes on each side of the film were sputtered-coated with gold using an EMS Q300 T sputter coater (Electron Microscopy Science, Quantum Technologies, Ashford, Kent, England). The diameter of the gold electrode was 1 cm. Prior to testing, the films were dried for 24 h at 120 °C. The frequency sweep measurements were carried out at room temperature and the temperature sweep heating rate was 5 °C/min.

2.3. Results and discussion

The structures, molecular weights and thermal properties of the poly(arylene ether ketone)s were characterized by proton NMR, SEC and DSC. The ^{1}H NMR spectra shown

in Fig. 2.2 confirmed the expected chemical structures. The integral values were consistent with the expected structures and no extraneous peaks were observed.

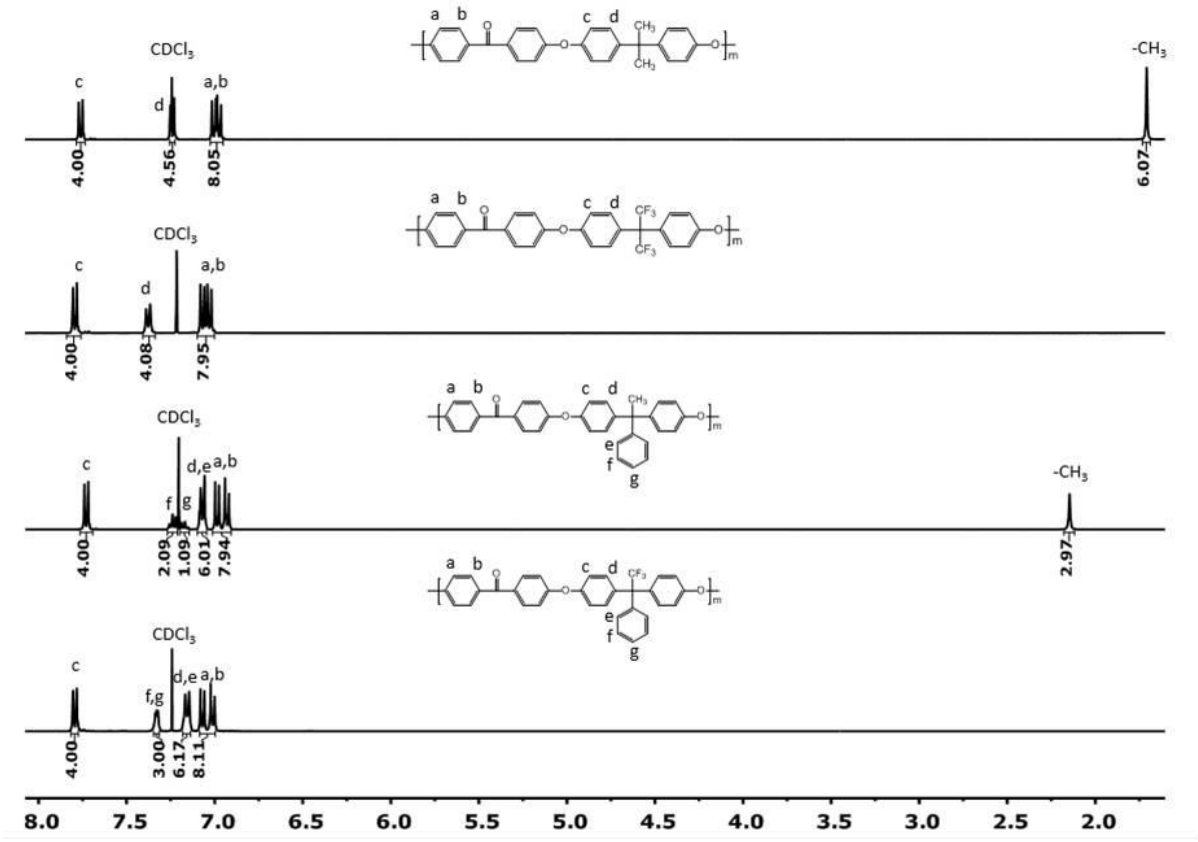

Figure 2. 2 Confirmation of structure via proton NMR

The SEC results showed that the polymer M_w's were within close range of each other and that high molecular weights had been achieved (Table 2.1 and Fig. 2.3). The PDI's were all symmetric and comparable to each other. Step growth polymerization PDI values should ideally be two. The lower values may be due to lower molecular weight chains being lost during precipitation as well as the fact that light scattering calculations of broad molecular weight polymers tend to overestimate the Mn and thereby reduce the PDI.

Table 2. 1 Molecular weights in DMAc with 0.1 M LiCl at 50 °C

	M_w (kDa)	PDI
BPA PAEK	78	1.5
6FBPA PAEK	67	1.4
BPAP PAEK	67	1.5
3FBPAP PAEK	62	1.4

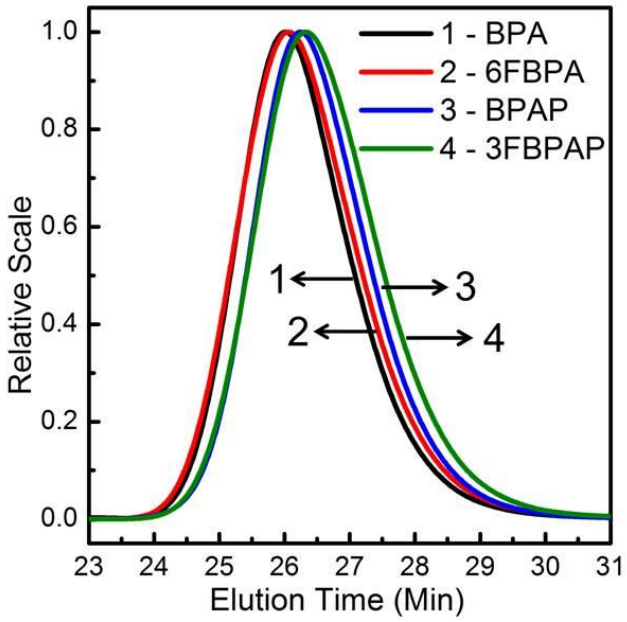

Figure 2. 3 Molecular weights by light scattering SEC

The DSC thermograms for the four polymers are shown in Fig. 2.4. The two symmetric polymers have Tg's near 160 °C while the two asymmetric polymers have Tg's near 180 °C. This increase is most likely caused by increased stiffness of the polymer backbone caused by introducing a phenyl substituent into the linking group in the bisphenol monomers. A stiffer backbone requires more energy to begin long-range segmental motion. Both of the fluorine-containing polymers have slightly higher Tg's than their nonfluorinated counterparts. The larger fluorine atom may cause more steric hindrance than the hydrogen, therefore leading to a stiffer polymer structure.

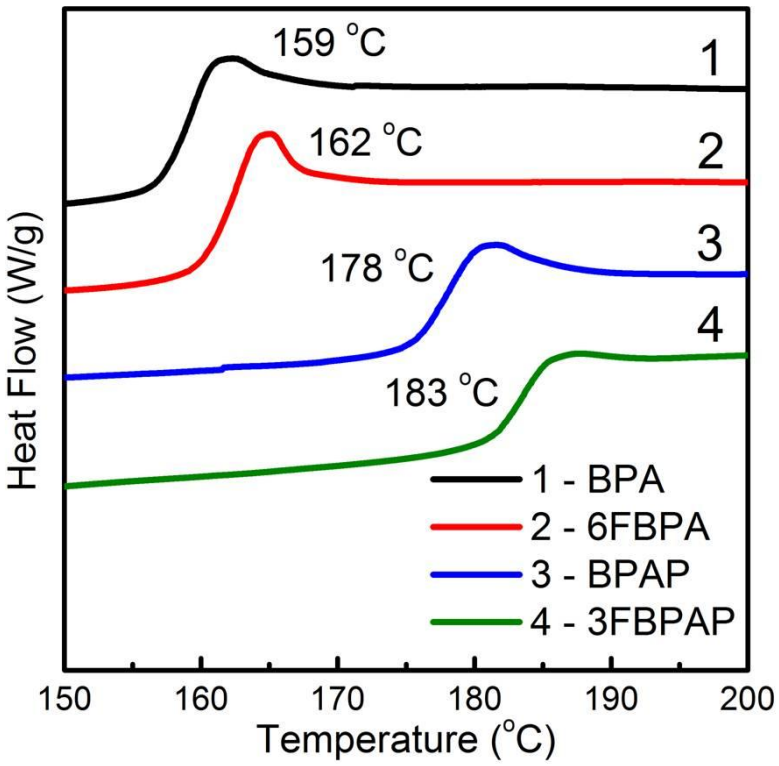

Figure 2. 4 DSC thermograms showing the glass transition temperatures

The calculated breakdown strengths of each of the materials as functions of temperature are listed in Table 2.2. At 25 °C, the trend is 3FBPAP > BPAP > 6FBPA > BPA with a difference of approximately 20 V between each. This can also likely be correlated to stiffness because breakdown strength has been shown to increase with Young's modulus[30, 31]. As the temperature is increased, the two asymmetric polymers maintain higher calculated breakdown strengths, most likely due to their higher Tg's and stiffer backbones. Even at 175 °C, the calculated breakdown strengths of the asymmetric polymers are greater than those of the symmetric polymers at 125 °C.

Table 2. 2 Calculated breakdown strengths measured via a needle-plane electrode method. The units of breakdown strength are volts/film thickness (kV/mm).

	25 °C	75 °C	125 °C	150 °C	175 °C
BPA PAEK	782±35	563±44	412±52	365±22	-
6FBPA PAEK	803±55	583±20	410±34	396±28	-
BPAP PAEK	821±45	753±33	651±50	615±27	511±36
3FBPAP PAEK	840±45	765±33	662±49	641±26	523±31

The relative permittivity (ε) was measured from 10^{-1} to 10^{4} Hz (Fig. 2.5). The trend in relative permittivity for the four polymers is BPAP > BPA > 3FBPAP > 6FBPA. The differences can be attributed to their fluorine content, introduction of a phenyl ring, and their symmetric versus asymmetric structures. Increased fluorine content in the polymer increases the fractional free volume, and an increase in fractional free volume decreases the amount of polarizable content per unit volume. With less material to be polarized, the relative permittivity will be lower [32]. Thus, it is reasonable to expect that 6FBPA and 3FBPAP would have lower relative permittivities than BPA and BPAP, respectively. Xie et al. made a series of poly(arylene ether ketone)s using 4,4'-difluorobenzophenone which showed comparable results to our own. Their nonfluorinated poly(arylene ether ketone) had an ε of 2.95 at 1 MHz where as our BPA-based poly(arylene ether ketone) had an ε of 2.94 at 0.1 MHz [33]. Further literature shows that the ε of both our fluorinated and non-fluorinated PAEK polymers are in the expected value range[34-36].

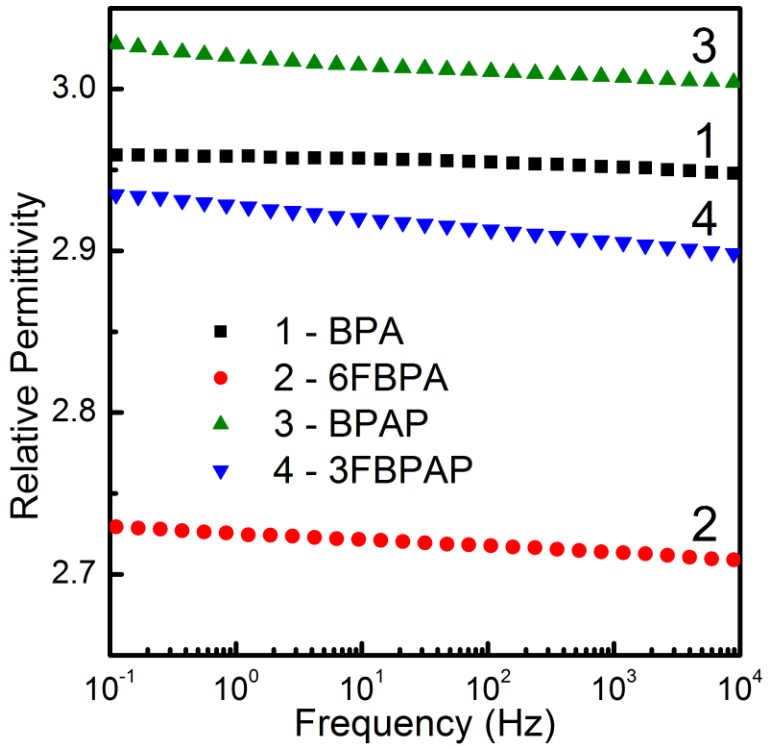

Figure 2. 5 The relative permittivity of each material over varying frequency at 25°C

Introduction of a phenyl ring in the bisphenol linking group increases the relative permittivity because its polarizability to weight contribution is higher than for the methyl or trifluoromethyl groups. This can be explained using the Vogel model polarization group contribution values[37]. The phenyl group has a polarization contribution of 123.5 and a MW of 77 to give a polarizability/ weight ratio of 1.604. In comparison, the methyl group has a polarization contribution of 17.66 and a MW of 15 to give a ratio of 1.177. The trifluoromethyl group has a polarization contribution of 86.4 and a MW of 69 to give a ratio of 1.252. The phenyl group contributes more polarization to the relative permittivity than the methyl or trifluoromethyl groups, and this can be correlated to its easily polarized aromaticity[32]. Other poly(ether ketone)s with highly aromatic structures

and ketones have high ε values, thus showing their structural importance to the polymer ε for dielectric films[10, 38, 39].

The higher performance of BPAP and 3FBPAP over their symmetric counterparts, BPA and 6FBPA, can be linked to their asymmetric methyl or trifluoromethyl groups. In the symmetric polymers the methyl or trifluoromethyl groups have an opposing group with the same composition so the dipole will be canceled. Without the opposing group, the asymmetric polymers have a net dipole and any group with a net dipole will contribute to orientation polarization (dipole polarization). Orientation polarization is one of the three main types of polarization that can contribute to the overall polarizability, which is one of the main factors in determining the relative permittivity. The three types are electronic, atomic, and orientation polarization[32].

In order to examine the contribution of incorporating fluorine in an asymmetric geometry, relative permittivities (ε) measured by dielectric spectroscopy were compared with the squares of the refractive indices, also known as the Maxwell ε. Equation (2.2) shows the relationship between the refractive index and relative permittivity. The difference between the measured and Maxwell ε provides some understanding of the contributions of orientation polarization to the permittivities in the polymer systems. This is because the Maxwell model represents the ε at high frequencies, which is dominated by electronic polarization. The measured ε by dielectric spectroscopy was at lower frequencies and has orientation polarization contributions. Therefore the difference gives an indication of the orientation contribution of the material.

$$\varepsilon_{maxwell} \propto n^2 \qquad (2.2)$$

In Fig. 2.6 the left graph compares the measured ε at 1 kHz to the Maxwell ε of the symmetric PAEK structures. The dashed line is included to make a better comparison between the two ε values. The measured ε and Maxwell comparison were extremely close since BPA and 6FBPA are both symmetric and therefore have no orientation polarization. The right graph makes the same comparison but with the two asymmetric structures. In this case there is a difference between the measured ε and the Maxwell comparison lines. This is expected since the orientation polarization due to the asymmetric trifluoromethyl group will be greater than for the asymmetric methyl. This is confirmed since the measured ε by dielectric spectroscopy has a less negative slope than the Maxwell comparison. This indicates that orientation polarization contributes more to the 3FBPAP measured ε than it contributes to the BPAP ε.

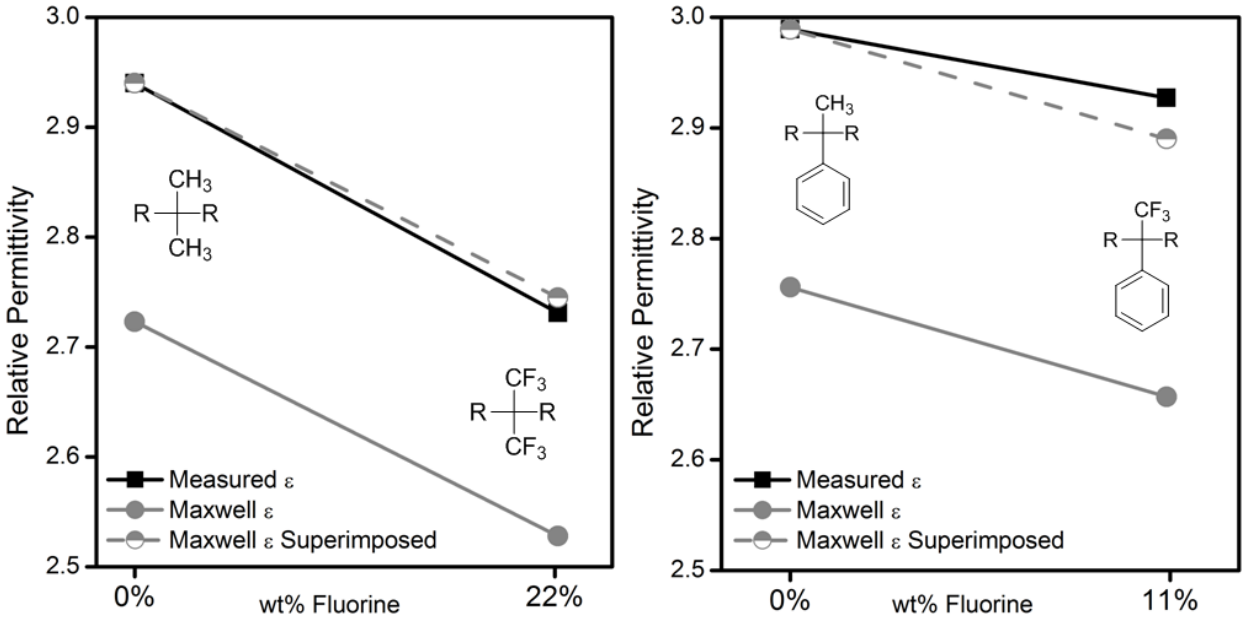

Figure 2. 6 Comparison of the measured relative permittivity by dielectric spectroscopy versus the squared refractive indices. The left graph is the comparison of the symmetric PAEK structures and the right graph is the comparison of the asymmetric structures. Relative permittivities were measured by dielectric spectroscopy at 1 kHz

2.4. Conclusions

In summary, we were able to make high molecular weight BPA, 6FBPA, BPAP, and 3FBPAP based poly(arylene ether ketone)s via nucleophilic aromatic substitution step growth polymerization. All four polymers displayed high Tg's with those of the asymmetric PAEK's approximately 20 °C higher than their symmetric counterparts, most likely due to increases in backbone stiffness. Consistent with the DSC results, the breakdown strengths of the asymmetric PAEK's were higher than for the symmetric polymers. The trend in ε was BPAP > BPA > 3FBPAP > 6FBPA and this was attributed to fluorine content, replacement of the methyl or trifluoromethyl in the bisphenol linking groups with the phenyl ring, and the asymmetric structure. Introduction of fluorine in place of hydrogen results in increased fractional free volume, and this reduces the polarizable content per unit volume. The phenyl ring has a superior polarizability to weight ratio. The asymmetric structure results in larger dipoles which contribute to orientation polarization. This was confirmed by comparing the relative permittivities measured at 1 kHz to the Maxwell model relative permittivities (squares of the refractive indices). This suggests that asymmetric structures with higher relative permittivities would be advantageous for multilayer capacitors with PVDF or its copolymers.

It is reasoned that energy storage density would be improved in multilayer films with increased interaction at the interface between the two materials. Thus, our approach has been to design engineering polymers that contain fluorinated groups so that they will interact positively with PVDF at the interfaces between the layers. The maximum energy storage density in an insulating material is proportional to the dielectric constant times the square of the breakdown strength. The breakdown strengths of these amorphous

poly(arylene ether ketone)s are higher than the aromatic polycarbonates that were studied previously. For example, at 125 °C, bisphenol A polycarbonate had a calculated breakdown strength of 540 kV/mm[12] while 3FBPAP PAEK has a calculated breakdown strength of 622 kV/mm. Moreover the Tg of bisphenol A polycarbonate is 150 °C whereas the Tg of 3FBPAP PAEK is 183 °C, and both have excellent mechanical properties. Thus, we believe that these poly(arylene ether ketone)s have potential for incorporation into multilayered (thin-film) capacitors with PVDF as a high dielectric constant layer. The processing parameters for making multilayered capacitors through forced assembly microlayer coextrusion and the dielectric properties of those materials with poly(arylene ether ketone)s and high dielectric constant fluorinated polymers will be a major focus of a forthcoming publication.

2.5. Supplemental Information

2.5.1. Experimental

Materials

In each multilayer system, one polymer has high breakdown strength and the other has high dielectric constant. PVDF homopolymer, Solef 6010 with a weight average molecular weight of 64,000 g/mol from Solvay Solexis, was chosen as the high dielectric constant material and was used in all three systems. PC, Calibre 200-6 with a number average molecular weight of 24,500 g/mol from Dow Chemical Company, was chosen as one of the high breakdown strength materials. PSF, Udel® P-3703 with a number-average molecular weight of 9,780 g/mol from Solvay Solexis, was another high breakdown strength material. The 6FBPA PAEK was the third material and the synthesis is reported in the section 2.2. The films were coextruded with sacrificial polyethylene

(PE) skin layers on both sides of the layered film in order to improve the film surface smoothness, handleability, and resistance to damage. This skin was peeled off before any measurements were carried out. A coextrusion temperature of 250 °C was chosen based on the rheological compatibility of the polymers. The polymer rheology was characterized using a melt flow indexer (MFI), on Kayeness Galaxy 1, at a shear rate that is similar to extrusion conditions (10 s^{-1}). Prior to processing the resin, it was dried in a oven under vacuum at 80 °C for 48 h.

Dielectric Hysteresis Measurements.

Electric displacement-electric field (D.E) hysteresis measurements were carried out on a Premiere II ferroelectric tester from Radiant Technologies, Inc. The applied voltage was a bipolar triangular waveform at 1 Hz. An electrostatic sandwich technique was used to apply electrodes, which were 5.8 μm metalized BOPP films, on both sides of the film. An 80-μm thick Kapton mask with a 1-cm diameter hole was used to control the area under high fields. In each sample, electric fields from 100 to 500 MV/m were applied to the sample in 50 MV/m increments. This electrostatic sandwich setup performed better without any insulating oils because the oil could prevent two metalized BOPP films from coming together and establishing a tight contact with the test film. To ensure safety, all high field measurements were remotely controlled with a computer.

2.5.2 Results and Discussion

Table 2. 3 Relative permittivity, Tg, Tm, and breakdown strength values for 6FBPA PAEK, PC, PSF, and PVDF.

	Relative Permittivity	Tg (°C)	Tm (°C)	Breakdown Strength at 125 °C	Breakdown Strength at 150 °C
6FBPA PEAK	2.7	165	-	410	396
Polycarbonate (PC)	2.8	147	-	540	190
Polysulfone (PSF)	3.1	185	-	580	530
PVDF	12	-35	177	365	-

The 6FBPA PAEK, PC and PSF were multilayered with PVDF into 32 layer films with a 50/50 composition. The overall thickness of the film was ~400 μm giving an individual layer thickness of 12 μm. The 6FBPA PAEK multilayered film was compared to multilayered films of PC and PSF. The T_g, ε, and breakdown strength of each individual polymer are shown in Table 2.3. The three engineering polymers have similar performance in all three areas but PC's low T_g produced poor breakdown strength at 150 °C.

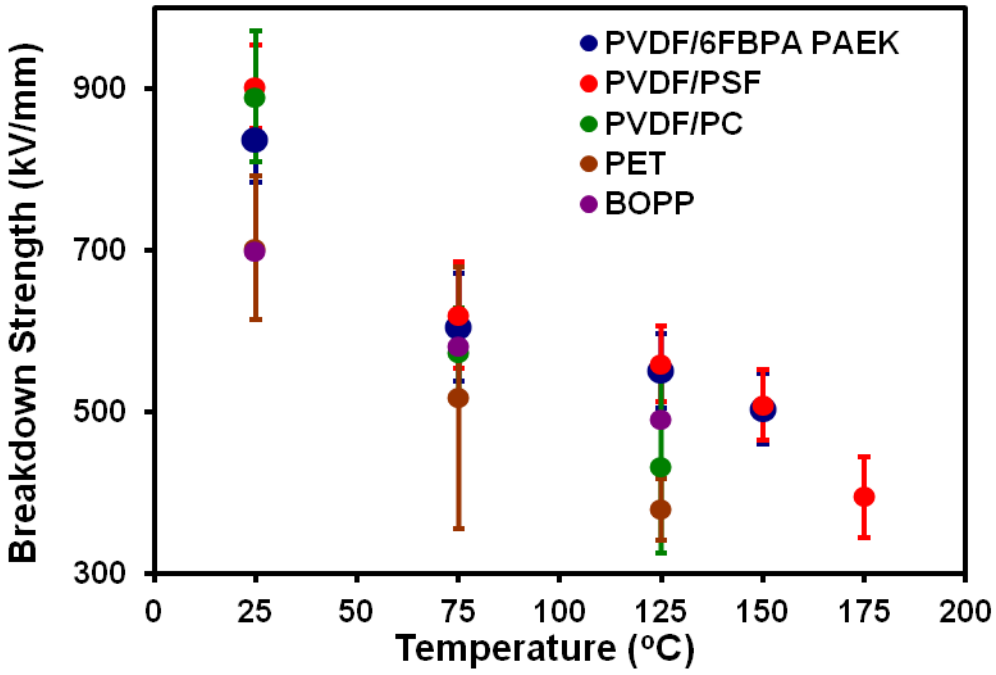

Figure 2. 7 Comparison of breakdown strength versus temperature of the microlayered films to commercial dielectric films.

The breakdown strengths of the multilayered films are shown in Figure 2.7. The system with the best performance in both temperature and dielectric strength was PVDF/PSF. The 6FBPA PAEK maintained similar performance up to 150 °C which correlates with its T_g, thus resulting in softening beginning at 165 °C. Both PSF and 6FBPA PAEK performed better than the commercial materials, poly(ethylene terephthalate) (PET) and biaxially oriented polypropylene (BOPP) at all temperatures.

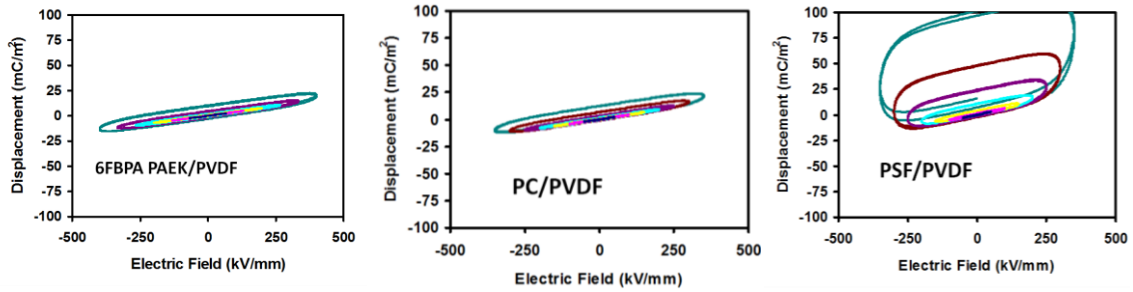

Figure 2. 8 Hysteresis loops of the three microlayered films.

The hysteresis results of the three multilayered systems are shown in Figure 2.8. The 6FBPA PAEK showed similar performance to the PC whereas the PSF showed significant hysteresis upon greater applied electric field. The main difference between PSF and the other two polymers is the sulfone linkage, indicating that it may be susceptible to permanent polarization or that it has an adverse effect on the PVDF crystallinity.

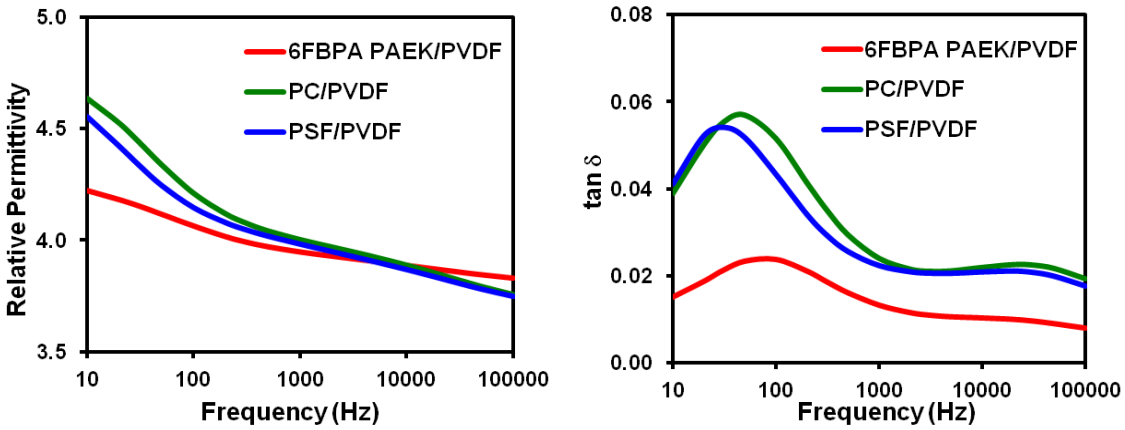

Figure 2. 9 The relative permittivity (left graph) and Tan δ data for the three multilayered systems.

The ε and tan δ were measured with DETA and the data is shown in Figure 2.9. The ε of the 6FBPA PAEK is lower at lower frequencies but higher at higher frequencies. The low frequency is dominated by ionic polarization which means that the 6FBPA

PAEK has lower ion or impurity content than PC or PSF. The higher ε at lower frequency is interesting because 6FBPA PAEK has a lower ε than PC or PSF. Therefore, the fluorine within the 6FBPA PAEK may positively interact with the fluorine in the PVDF to increase the ε.

The tan δ of the 6FBPA PAEK was reduced over the entire frequency range, indicating that there was a reduction in the loss of permittivity and therefore the 6FBPA PAEK was more efficient. The reduction at low frequencies can similarly be attributed to lower impurity content. At high frequencies, the reduction could also be attributed to the 6FBPA PAEK fluorine positively interacting with PVDF. Further investigation of this is needed and it would be possible to use FT-IR and X-ray diffraction to see if there is any change in the PVDF when layered with 6FBPA PAEK versus PC or PSF.

2.5.3. Conclusions

The 6FBPA PAEK was able to be processed with PVDF via forced assembly microlayer coextrusion. The breakdown strength of the PAEK was similar to PSF which was superior to PC. Hysteresis performance of the PAEK and PC was superior to PSF which is likely related to the sulfone linkage. The PAEK showed lower ε at lower frequencies but higher ε at higher frequencies which indicates the presence of fewer impurities and higher polarizability. Tan δ also confirmed the reduction of impurities and showed an increase in efficiency over a wide range of frequencies. Overall, 6FBPA PAEK multilayered with PVDF performed well in terms of hysteresis, breakdown strength, and relative permittivity. This could be attributed to the interaction between the fluorine in 6FBPA PAEK and PVDF. Further investigation of this is needed to see if there is any change in the PVDF when layered with 6FBPA PAEK versus PC or PSF.

References

1. Sarjeant, W. J.; Zirnheld, J.; MacDougall, F. W., *IEEE Trans. Plasma Sci.* **1998**, 26 (5), 1368-1392.

2. Zhu, L., *J Phys. Chem. Lett.* **2014**, 5 (21), 3677-3687.

3. MacDougall, F.; Ennis, J.; Xiao Hui, Y.; Cooper, R. A.; Gilbert, J. E.; Bates, J. F.; Naruo, C.; Schneider, M.; Keller, N.; Joshi, S.; Jow, T. R.; Ho, J.; Scozzie, C. J.; Yen, S. P. S., *IEEE Pulsed Power Conference in high energy density capacitors for pulsed power applications,* **2009**; pp 774-778.

4. Shihai, Z.; Zellers, B.; Henrish, J.; Rockey, S.; Anderson, D.; Chen, Z.; Qiming, Z. *In High energy density film capacitors, Pulsed Power Conference,* **2009**; pp 779-783.

5. Sarjeant, W. J.; Clelland, I. W.; Price, R. A., *Proceedings of the IEEE* **2001**, 89 (6), 846-855.

6. Venkat, N.; Dang, T. D.; Bai, Z.; McNier, V. K.; DeCerbo, J. N.; Tsao, B.-H.; Stricker, J. T., *Mater. Sci. Eng. B* **2010**, 168 (1–3), 16-21.

7. Nash, J. L., *Polym. Eng. Sci.* **1988**, 28 (13), 862-870.

8. J. Ho, R. Jow, Characterization of High Temperature Polymer Thin Films for Power Conditioning Capacitors, Army Research Lab, Sensors and Electronic Devices Directorate, Adelphi, MD, **2009**.

9. Zhu, L.; Wang, Q., *Macromolecules* **2012**, 45 (7), 2937-2954.

10. Tan, D.; Zhang, L.; Chen, Q.; Irwin, P., *J. Elec. Mater.* **2014**, 43 (12), 4569-4575.

11. Wolak, M. A.; Pan, M.-J.; Wan, A.; Shirk, J. S.; Mackey, M.; Hiltner, A.; Baer, E.; Flandin, L., *Appl. Phys. Lett.* **2008** 92 (11) 113301-113303.

12. Mackey, M.; Hiltner, A.; Baer, E.; Flandin, L.; Wolak, M. A.; Shirk, J. S., *J. Phys. D Appl. Phys.* **2009** 42 (17) 175304 (12 pp)

13. Zhou, Z.; Carr, J.; Mackey, M.; Yin, K.; Schuele, D.; Zhu, L.; Baer, E., *J. Polym. Sci. B Polym. Phys.* **2013**, 51 (12), 978-991.

14. Zhou, Z.; Mackey, M.; Carr, J.; Zhu, L.; Flandin, L.; Baer, E., *J Polym Sci B Polym Phys* **2012**, 50 (14), 993-1003.

15. Mackey, M.; Schuele, D. E.; Zhu, L.; Baer, E., *J. Appl. Phys.* **2012**, 111 (11), 113702-113702-9.

16. Mackey, M.; Schuele, D. E.; Zhu, L.; Flandin, L.; Wolak, M. A.; Shirk, J. S.; Hiltner, A.; Baer, E., *Macromolecules* **2012**, 45 (4), 1954-1962.

17. Wolak, M. A.; Wan, A. S.; Shirk, J. S.; Mackey, M.; Hiltner, A.; Baer, E., *J. Appl. Polym. Sci.* **2012**, 123 (4), 2548-2557.

18. Carr, J. M.; Mackey, M.; Flandin, L.; Schuele, D.; Zhu, L.; Baer, E., *J. Polym. Sci. B Polym. Phys.* **2013**, 51 (11), 882-896.

19. Tseng, J.-K.; Lewis, C.; Mackey, M.; Carr, J.; Baer, E.; Zhu, L., *PMSE Preprints* **2012**.

20. Ponting, M.; Hiltner, A.; Baer, E., *Macromolecular Symposia* **2010**, 294 (1), 19-32.

21. Hougham, G.; Tesoro, G.; Viehbeck, A.; Chapple-Sokol, J. D., *Macromolecules* **1994**, 27 (21), 5964-5971.

22. Vogelsang, R.; Farr, T.; Frohlich, K., *IEEE Trans. Dielectr. Electr. Insul.* **2006**, 13 (2), 373-382.

23. Hsiao, S.-H.; Chiang, H.-W., *Eur. Polym. J.* **2004**, 40 (8), 1691-1697.

24. Srinivasan, S. A.; McGrath, J. E., *High Perform. Polym.* **1993**, 5 (4), 259-274.

25. Bender, T. P.; Burt, R. A.; Hamer, G. K.; DeVisser, C.; Smith, P. F.; Saban, M., *Org. Process Res. Dev.* **2002**, 6 (5), 714-720.

26. Lyle, G. D.; Grubbs, H.; Tchatchoua, C.; McGrath, J. E., *Polym. Mater. Sci. Eng* **1993**, 69, 238-9.

27. Chen, Y.; Guo, R.; Lee, C. H.; Lee, M.; McGrath, J. E., *Int J Hydrogen Energ* **2012**, 37 (7), 6132-6139.

28. Lyle, G. D.; Senger, J. S.; Chen, D. H.; Kilic, S.; Wu, S. D.; Mohanty, D. K.; McGrath, J. E., *Polymer* **1989**, 30 (6), 978-985.

29. Metricon Operation Manual

30. Dissado, L. A.; Fothergill, J. C., Electrical Degradation and Breakdown in Polymers. P. Peregrinus: **1992**.

31. Kim, H. K.; Shi, F. G., *IEEE Trans. Dielectr. Electr. Insul.* **2001**, 8 (2), 248-252.

32. Zulkifli, A., Polymer Dielectric Materials in Dielectric Materials Silaghi, M. A. Ed., Intech, Rijeka, Croatia. 2012, 3 - 26.

33. Xie, J.; Peng, W.-Y.; Li, G.; Jiang, J.-M., *JFBI* **2010**, 3 (3), 142-147.

34. Treichel, H.; Ruhl, G.; Ansmann, P.; Würl, R.; Müller, C.; Dietlmeier, M., *Microelectronic Eng* **1998**, 40 (1), 1-19.

35. Mercer, F.; Goodman, T.; Wojtowicz, J.; Duff, D., *J Polym Sci A Polym Chem* **1992**, 30 (8), 1767-1770.

36. Frank, W. M.; David, W. D.; Timothy, D. G.; Janusz, B. W., Fluorinated Poly(arylene ethers) with Low Dielectric Constants. *In Polymers for Microelectronics, ACS:* **1993**; Vol. 537, pp 526-534.

37. van Krevelen, D. W.; te Nijenhuis, K., Properties of Polymers: Their Correlation with Chemical Structure; their Numerical Estimation and Prediction from Additive Group Contributions. Elsevier Science: 2009.

38. Pan, J.; Li, K.; Chuayprakong, S.; Hsu, T.; Wang, Q., *ACS Appl. Mater. Interfaces* **2010**, 2 (5), 1286-1289.

39. Pan, J.; Li, K.; Li, J.; Hsu, T.; Wang, Q., *Appl. Phys. Lett.* **2009**, 95 (2), 022902.

Chapter 3: Synthesis, Oxidation, and Crosslinking of Tetramethyl Bisphenol F (TMBPF)-Based Polymers for Oxygen/Nitrogen Gas Separations

Benjamin J. Sundell,[a] Andrew T. Shaver,[a] Qiang Liu,[b] Ali Nebipasagil,[a] Priya Pisipati,[a] Sue J. Mecham,[a] Judy S. Riffle,[a] Benny D. Freeman,[b] James E. McGrath[a]

[a]Macromolecules and Interfaces Institute, Virginia Polytechnic Institute and State University, Blacksburg, VA 24061, USA

[b]Department of Chemical Engineering, Center for Energy and Environmental Resources, The University of Texas at Austin, Austin, TX, 78758, USA

B. J. Sundell, A. T. Shaver, Q. Liu, A. Nebipasagil, P. Pisipati, S. J. Mecham, B. D. Freeman, J. S. Riffle, James E. McGrath, Synthesis, Polymer, 55(22), 5623-5634 (2014).

3.1. Abstract

Amorphous, high glass transition, crosslinkable poly(arylene ether)s for gas purification membranes have been synthesized. The polymers include a moiety capable of several oxidation reactions and UV crosslinking. Structural identification was confirmed by ^{1}H-NMR and IR spectroscopy and molecular weights were determined by size exclusion chromatography. The polymers were subjected to oxidation under two different conditions, one by chemical treatment using Oxone and KBr and one by elevated thermal treatment in air. Differential scanning calorimetrey and thermogravimetric analysis were used for thermal characterization, and thermogravimetric analysis, 1H-NMR and attenuated total reflectance fourier transform infrared spectroscopy revealed the progress of the thermal oxidation reactions. Both

polymers produced tough, ductile films and gas transport properties of the non-crosslinked linear polymers and crosslinked polymer are compared. The O_2 permeability of one exemplary non-crosslinked poly(arylene ether) was 2.8 Barrer, with an O_2/N_2 selectivity of 5.4. Following UV crosslinking, the O_2 permeability decreased to 1.8 Barrer, and the O_2/N_2 selectivity increased to 6.2.

3.2. Introduction

Polymeric membranes are important for the separation of gases in a variety of industrial applications.[1] Several excellent reviews have detailed industrial gas separations including the removal of carbon dioxide from natural gas,[2] nitrogen enrichment from air,[3] hydrogen recovery and a variety of smaller membrane markets.[1,4] These reviews also discuss some of the challenges associated with gas separation membranes such as achieving higher selectivity to provide higher purity products at high yield and making membranes more robust to harsh operating conditions and resistant to plasticization.

Transport of gases in dense polymeric membranes is based on the solution-diffusion model; the permeability of a gas across the membrane is the product of diffusion and solubility coefficients.[3,5] One measure of the ability of a membrane to separate a pair of gases is the ratio of the permeability coefficient of the more permeable gas to that of the less permeable gas, known as selectivity. The selectivity may be further separated into the product of solubility selectivity and diffusivity selectivity, the latter generally being the dominant factor controlling overall selectivity of glassy polymers.[6] Gas diffusion is very sensitive to the size of the diffusing gases and the availability of free volume within the polymer membrane.[7,8] A desirable gas separation membrane exhibits both high permeability and selectivity; however, an inherent trade-off

relationship between these two properties has been identified. Membranes with high gas permeability typically have lower selectivity, and vice-versa. This observation led to the development of the concept of the upper-bound by Robeson, which is typically represented as a log-log plot of selectivity versus permeability.[5] The upper-bound plots were revised upwards once9 based on the development of new classes of polymer membrane materials and have a mathematical and theoretical basis derived by Freeman.[6] Freeman, among others, noted that the most widely used approach to prepare materials with properties above the upper bound was to simultaneously increase polymer backbone stiffness and interrupt interchain packing to increase diffusivity.

Several families of glassy polymers have been investigated to explore the influence of polymer structure on gas transport properties. For example, one early effort studied the effect of tacticity on poly(methyl methacrylate).[10] Polyimides typically have good gas separation properties and are of significant interest in the field because of their chemical robustness and low chain mobility.[11,12] Another candidate for gas separation polymers are polysulfones due to their chemical stability and excellent mechanical properties, along with inherent rigidity due to in chain aromatic rings. The effect of variations in backbone chemical structure on permeability and selectivity of polysulfones has been studied.[13,14] For example, changes to the isopropylidene group, which influences bond rotation and intersegmental packing,[15] the effect of symmetry of phenylene linkages, and methyl group placement[16] all have significant influence on gas separation properties of polysulfones. Several specialty polyimides have exceeded the upper bound by undergoing a chemical transformation to form carbon membranes at very high temperatures, such as that induced via pyrolysis between 550-800 °C.[17] Additionally,

thermal rearrangement of *ortho*-positioned polyhydroxyimide precursors produce crosslinked polybenzoxazoles with much narrower pore size distributions than the precursor polyimides and, in some cases, gas separation properties beyond the upper bound.[18]

One intriguing approach for improving the properties of gas separation membranes is to crosslink them, which is a well-known method to decrease chain mobility. In the late 1980s, Hayes demonstrated that UV crosslinked aromatic polyimides had a significantly higher selectivity than their linear analogs.[19] The effect of UV crosslinking on gas separation properties of the polyimides has been studied,[20-23] and the effects of crosslinking have also been decoupled from thermal annealing.[24,25] These crosslinked membranes are especially effective in CO_2/CH_4 separations, because crosslinking greatly improves resistance to plasticization by CO_2[26] or in some cases interrupts polymer crystallization.[27]

In this paper, a poly(arylene ether sulfone) and poly(arylene ether ketone) have been synthesized from inexpensive reagents that contain moieties for UV crosslinking and an additional site for chemical oxidation. The materials considered in this study contain, in each repeat unit, a moiety derived from 4,4'-methylenebis(2,6-dimethylphenol), which has been used previously in polymers for forward osmosis[28] and as a self-cross-linked material for fuel cells.[29] This benzylic methylene group may be oxidized to a carbonyl by several routes and then UV crosslinked by benzylic hydrogen abstraction. This structure also provides the ability to UV crosslink a poly(arylene ether ketone) to increase backbone stiffness and interrupt chain packing by oxidizing the crosslinked polymeric backbone in the solid state. The synthesis and characterization of

these polymers are described, and investigations of several oxidation routes are discussed. Initial film casting, UV crosslinking, and gas transport properties are also discussed.

3.3. Experimental

Materials

2,6-Dimethylphenol (2,6-xylenol, 99+%), 37% formaldehyde in H_2O (formalin), phosphorous pentoxide (P_2O_5), lithium bromide (LiBr) and potassium bromide (KBr) were purchased from Sigma-Aldrich. *N*-Methyl-2-pyrrolidone (NMP), methanol (MeOH) and sulfuric acid were purchased from Spectrum Chemical. Chloroform ($CHCl_3$), *N*,*N*-dimethylacetamide (DMAc) and acetonitrile (CH_3CN) were purchased from Fisher. DMAc used as a reaction solvent was dried with calcium hydride (CaH_2), distilled under reduced pressure and stored over 3Å molecular sieves before use. Calcium hydride (90-95%) and potassium peroxymonosulfate (Oxone) were purchased from Alfa Aesar. 4,4'-Difluorobenzophenone (DFB) was purchased from TCI. 4,4'-Dichlorodiphenylsulfone (DCDPS) was kindly provided by Solvay and recrystallized from toluene before use.

Synthesis of 4,4'-methylenebis(2,6-dimethylphenol)

The synthesis of 4,4'-methylenebis(2,6-dimethylphenol), tetramethyl bisphenol F, hereafter referred to as TMBPF, was adapted from a traditional synthesis of a phenol-formaldehyde resin.[30] Excess 2,6-xylenol (415.83 mmol, 50.80 g) was added to a 250-mL three-necked flask equipped with a condenser, mechanical stirrer, and addition funnel. The 2,6-xylenol was heated in a thermocouple regulated oil bath to 90 °C and stirred as it began to melt. Sulfuric acid (0.5 g) was added very slowly via the addition funnel, which

changed the reaction solution to a dark pink color. The addition funnel was rinsed with DI water to ensure that all of the acid catalyst was transferred into the reaction flask. Formalin (37% by mass formaldehyde in H_2O, 15 mL) was added slowly via the addition funnel over the course of several hours; during this time, the reaction solution turned lighter in color and significantly more opaque. As more product continued to form, the reaction mixture transformed from a liquid to a solid. The crude product was removed from the flask and filtered using an aspirator and washed copiously with hot DI water. The crude product was dried at 70 °C in a convection oven and was recrystallized from MeOH to obtain a 90% yield. The melting point of the recrystallized solid was 177 °C.

Synthesis of bis-(2,6-xylenol)-F-DFB poly(arylene ether) ketone (TMBPF-DFB)

The TMBPF-DFB polymer was synthesized using a nucleophilic aromatic substitution procedure previously reported.[31] TMBPF (39.01 mmol, 10.0000 g), DFB (39.01 mmol, 8.5121 g) and DMAc (62 mL) were added to a 250-mL three necked flask. The reaction flask was equipped with a mechanical stirrer, nitrogen inlet, and Dean-Stark trap filled with toluene. A stirring, thermocouple regulated oil bath was heated to 155 °C. After a homogeneous solution was obtained and the oil bath was at 155 °C, K_2CO_3 (54.61 mmol, 7.5482 g) and toluene (31 mL) were added, which immediately turned the light yellow solution a deep violet color. The reaction was stirred at 155 °C for 3 h to azeotropically remove any water, and then the bath was heated to 175 °C. Toluene and water were drained from the Dean Stark trap, and the reaction was maintained at this final temperature overnight. After 16 h, the viscous solution was diluted with additional DMAc (62 mL) and filtered through celite using an aspirator. The polymer solution was precipitated into rapidly stirring DI water to produce a fibrous white solid, filtered using

an aspirator, and then boiled several times in DI water to remove any residual salt by-product. The solid polymer was finally dried at 150 °C in *vacuo*.

Synthesis of bis-(2,6-xylenol)-F-DCDPS poly(arylene ether) sulfone (TMBPF-DCDPS)

The TMBPF-DCDPS polymer was synthesized in the same manner as the TMBPF-DBF polymer, except DCDPS (39.01 mmol, 11.2023 g) was used instead of DFB, and more DMAc (71 mL) was used to obtain the same monomer concentration due to higher total monomer mass.

Oxidation of TMBPF-DCDPS polymer with Oxone/KBr

Oxidation of the TMBPF-DCDPS polymer was adapted from a literature procedure for the oxidation of small molecules with benzylic methylene linkages.[32] TMBPF-DCDPS polymer (1.0 g) was added to CH_3CN (26 mL) and DI water (2 mL) in a 100-mL round bottom flask. Oxone (4.675 mmol, 0.712 g) and KBr (1.063 mmol, 0.126 g) were added to the flask. The flask, under air, was sealed with septa and stirred in a thermocouple regulated water bath at 45 °C. After several hours, the temperature was raised to 60 °C, and the reaction was stirred overnight. The heterogeneous reaction was poured directly into stirring DI water (250 mL), stirred for several hours, filtered on an aspirator, and dried overnight at 70 °C in a convection oven.

Thermal oxidation of TMBPF polymers

The TMBPF polymers were thermally treated in air in a Lindberg/Blue M 1200 °C box furnace. Once the oven reached the specified temperature, the polymer inside of an open scintillation vial was placed into the oven. After a designated time, the vial was removed and sealed for analysis.

Structural Characterization

Proton nuclear magnetic resonance (^{1}H NMR) spectroscopy was performed on a Varian Inova spectrometer operating at 400 MHz. All spectra were obtained from 15% (w/v) 1 mL solutions in deuterated chloroform ($CDCl_3$). Fourier Transform Infrared Spectroscopy with attenuated total reflectance (FTIR-ATR) was applied to the polymers to observe the conversion of the methylene bridge to the carbonyl group as a result of oxidation. The FTIR-ATR spectra were recorded on an FTIR spectrometer (Varian 670 FTIR) equipped with an ATR attachment with a diamond crystal. The spectral resolution was 4 cm^{-1}, and 32 background scans were performed. A small amount of polymer was placed on the diamond crystal, and the FTIR spectrum was measured with 32 scans. The spectra were baseline corrected and normalized based on the initial C=O group stretch at ca. 1525 cm^{-1}. All measurements were performed at ambient temperature. Intrinsic viscosities (IV) and molecular weights of the polymers were obtained by size exclusion chromatography (SEC). The SEC system consisted of an isocratic pump (Agilent 1260 infinity, Agilent Technologies, Santa Clara, CA) with an online degasser (Agilent 1260, Agilent Technologies, Santa Clara, CA), autosampler and column oven used for mobile phase delivery and sample injection, and three Agilent PLgel 10μm Mixed B-LS columns 300 7.5 mm connected in series with a guard column as the stationary phase. A system of multiple detectors connected in series was used for the analysis. A multi-angle laser light scattering (MALS) detector (DAWN-HELEOS II, Wyatt Technology Corporation, Goleta, CA), operating at a wavelength of 658 nm, a viscometer detector (Viscostar, Wyatt Technology Corporation, Goleta, CA), and a refractive index detector operating at a wavelength of 658 nm (Optilab T-rEX, Wyatt Technology Corporation, Goleta, CA)

provided online results. The system was corrected for interdetector delay, band broadening, and the MALS signals were normalized using a 21,720 g/mol polystyrene standard obtained from Agilent Technologies or Varian. Data acquisition and analysis was conducted using Astra 6 software (Wyatt Technology Corporation, Goleta, CA). The mobile phase was NMP, which was vacuum distilled over P_2O_5 before use. The salt, 0.05M dried LiBr, was added and dissolved in the NMP before the solvent was degassed and filtered. The sample solutions were prepared in a concentration range of 2~3 mg/mL and were filtered to remove any dust or insoluble particles using 0.22-μm PTFE filters. Molecular weight values were measured using light scattering, and the intrinsic viscosity values were measured online. Specific refractive index increment (dn/dc) values were calculated for each backbone type based on 100 % mass recovery using the Astra 6 software.

Thermogravimetric analysis (TGA)

The thermal stability and oxidation of the polymers were investigated using a TA Instruments TGA Q5000. The polymers were first heated under a nitrogen atmosphere at a rate of 10 °C min^{-1} to 600 °C to test the thermal stability in an inert atmosphere. The thermal oxidation reaction and consequent weight gain were performed in air by heating at 10 °C min^{-1} to 220 °C, then 1 °C min^{-1} to 450 °C, and finally 10 °C min^{-1} to 700 °C.

Differential scanning calorimetry (DSC)

The glass transition temperatures (Tg) of the polymers were investigated with a TA Instruments DSC Q200. The polymers were heated under nitrogen at a rate of 10 °C min^{-1} to 350 °C, cooled to 50 °C, and heated again at a rate of 10 °C min^{-1} to 350 °C. The DSC thermograms shown are the second scan.

Film preparation

To prepare films, 0.8 g of polymer was added to 20 mL of chloroform ($CHCl_3$) in a scintillation vial, and the mixture was stirred until a homogeneous, transparent solution was obtained. The solution was syringe filtered through a 1.0 μm filter into a new vial. The vial was sonicated 3 times for 60 minutes each to remove dissolved gases. The solution was cast on a 10 x 15 cm clean, dry glass plate on a level casting surface and then dried in air at ambient conditions overnight. The following day the air dried film was removed, the edges were trimmed, and the film was dried at 120 °C under vacuum before gas transport experiments. TGA thermograms showed that these drying conditions were suitable for the complete removal of solvent.

UV Crosslinking

Crosslinking was performed by irradiating polymer films in air under a 100W high intensity, long-wave UV lamp equipped with a 365-nm light filter (Blak-Ray B-100, UVP). The film was placed about 3.5 cm from the UV lamp and irradiated for one hour on each side. At this distance, the UV intensity was measured to be 19.7 mW cm^{-2}.

Gel Fractions

Crosslinked films were dried at 120°C under vacuum overnight. Then 0.1-0.2 g of the crosslinked film was placed in a 20-mL scintillation vial filled with $CHCl_3$ and stirred overnight. The remaining solid was filtered, transferred to a pre-weighed vial, and dried at 120°C under vacuum overnight to the final weight. Gel Fractions were calculated by equation 1.

$$Gel\ Fraction\ (\%) = \frac{W_{final}}{W_{initial}} \text{ x } 100 \quad (3.1)$$

Density Measurements

Density was measured using a Mettler Toledo balance equipped with a density measurement kit. Ethanol was chosen as the reference liquid because the samples tested showed low ethanol uptake over the time scale of the density measurement.

Gas Permeation Measurements

Gas permeation properties were measured using a constant-volume/variable-pressure method.[33] The upstream portion of the system was constructed from commercially available Swagelok parts using Swagelok tube fittings. Welded joints and VCR connections were used in the downstream portion to minimize leaks. The membrane was housed in a stainless steel Millipore filter holder (Millipore, Billerica, MA, USA) with an included support. A Honeywell Super TJE 1500 psi (10.3 MPa) transducer (Honeywell Sensotec, Columbus, Ohio, USA) was used to track upstream pressure, and a MKS Baratron 626 transducer (MKS, Andover, MA, USA) was used to measure downstream pressure. The permeabilities of N_2 and O_2 were measured at 35 °C at 10 atm feed pressure.

3.4. Results and Discussion

Synthesis of Tetramethyl Bisphenol F monomer (TMBPF)

The TMBPF monomer is commercially available, and may be easily synthesized from inexpensive 2,6-xylenol and formalin via electrophilic aromatic substitution as shown in Figure 3.1.

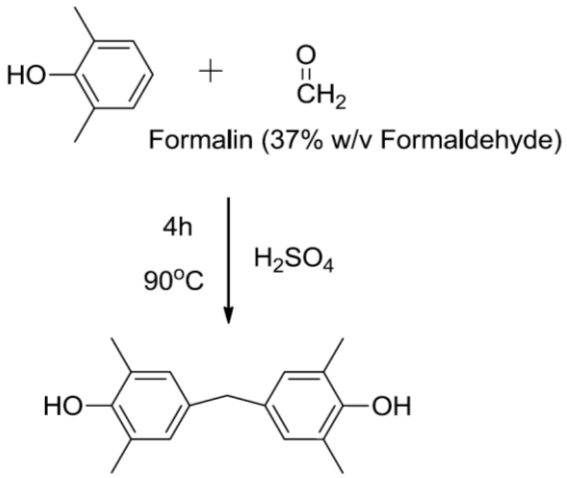

Figure 3. 1 Synthesis of TMBPF via electrophilic aromatic substitution

TMBPF is the key monomer in these polymers, because the benzylic methyl groups are necessary for UV crosslinking and the benzylic methylene group may undergo an oxidative chemical transformation.[32] A slight excess of 2,6-xylenol was used to drive the reaction to completion.[34] The reaction occurs very rapidly under the conditions utilized. A temperature of 90 °C was used to ensure that homogeneous stirring could occur. The 2,6-xylenol and sulfuric acid were charged to the flask and heated to 90 °C, then the formalin was added slowly. Upon formalin addition, the reaction shifted from a liquid to solid phase in addition to exhibiting a color change, which indicated the formation of product as TMBPF has a significantly higher melting point than 90 °C and is insoluble in water. Isolation of the monomer product was also very efficient. Washing with near boiling water was effective for removing residual acid and starting material. Upon drying, any residual 2,6-xylenol impurity in the crude product was assessed qualitatively by the presence of an orange/pink color, which is completely removed upon recrystallization from methanol to yield white crystals.

Characterization of TMBPF monomer

The ^{1}H-NMR spectrum of TMBPF is shown in Figure 3.2. All of the peaks integrate quantitatively with regard to the molecular structure. The ^{1}H-NMR spectrum did not show any organic side products or contaminants, including starting material. The melting point of the recrystallized product was 177 °C as measured via a melting point apparatus and this was in good agreement with reported values (177 °C).[35]

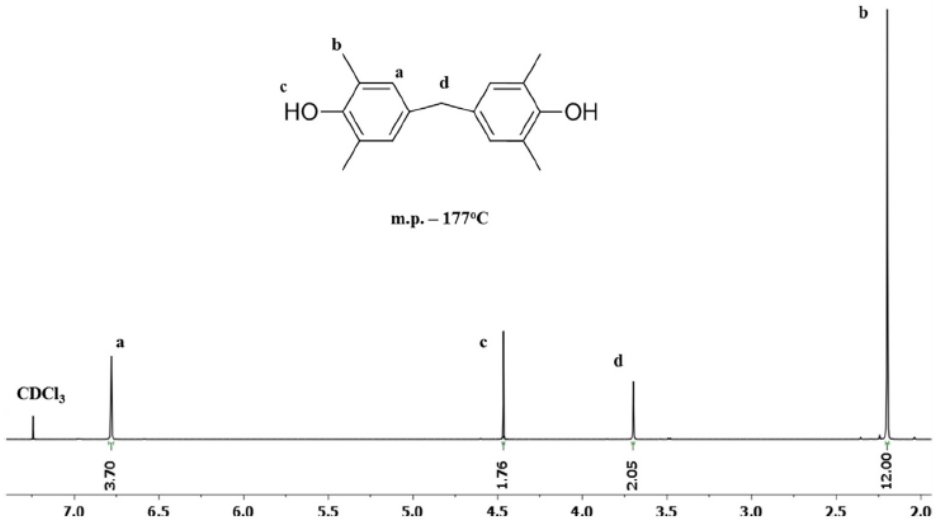

Figure 3. 2 ^{1}H-NMR spectrum of TMBPF monomer

Synthesis and NMR of TMBPF polymers

Poly(arylene ether)s are potentially important candidates for gas separation materials, and poly(arylene ether sulfone)s in particular have already found wide application in the field.[1,36] The success of poly(arylene ether)s as gas separation membranes has in part been due to their mechanical robustness and high chemical stability.[37,38]

The TMBPF containing poly(arylene ether ketone) (TMBPF-DFB) and poly(arylene ether sulfone) (TMBPF-DCDPS) in this study were synthesized by nucleophilic aromatic substitution with a weak base.[31,39] The syntheses of the poly(arylene ether sulfone) and poly(arylene ether ketone) are shown in Figures 3.3 and 3.4 respectively. Upon addition of toluene and K_2CO_3, both reaction solutions turned a deep violet color immediately, which persisted throughout the course of the reaction. In both reactions, toluene was used as an azeotropic solvent to remove water formed by the K_2CO_3 reaction with the bisphenol. Water could potentially react with the activated dihalide monomer at higher temperatures and upset the reaction stoichiometry, leading to low molecular weight polymers. It was important to use a heat gun to dry the joints on the three-necked flask during the azeotropic reflux, where water may have become trapped. After the water was removed from the reaction, toluene was drained, and the flask was brought to the final reaction temperature. Difluorobenzophenone is more reactive than dichlorodiphenyl sulfone, because the carbon-fluorine bond is more polarized than a carbon-chlorine bond, and therefore, it more efficiently stabilizes the Meisenheimer complex intermediate.[40] Thus, the final temperature of the poly(arylene ether ketone) reaction was 20 °C lower than that of the poly(arylene ether sulfone) reaction. Both reactions exhibited high viscosity after 16 hours and were stopped at this time.

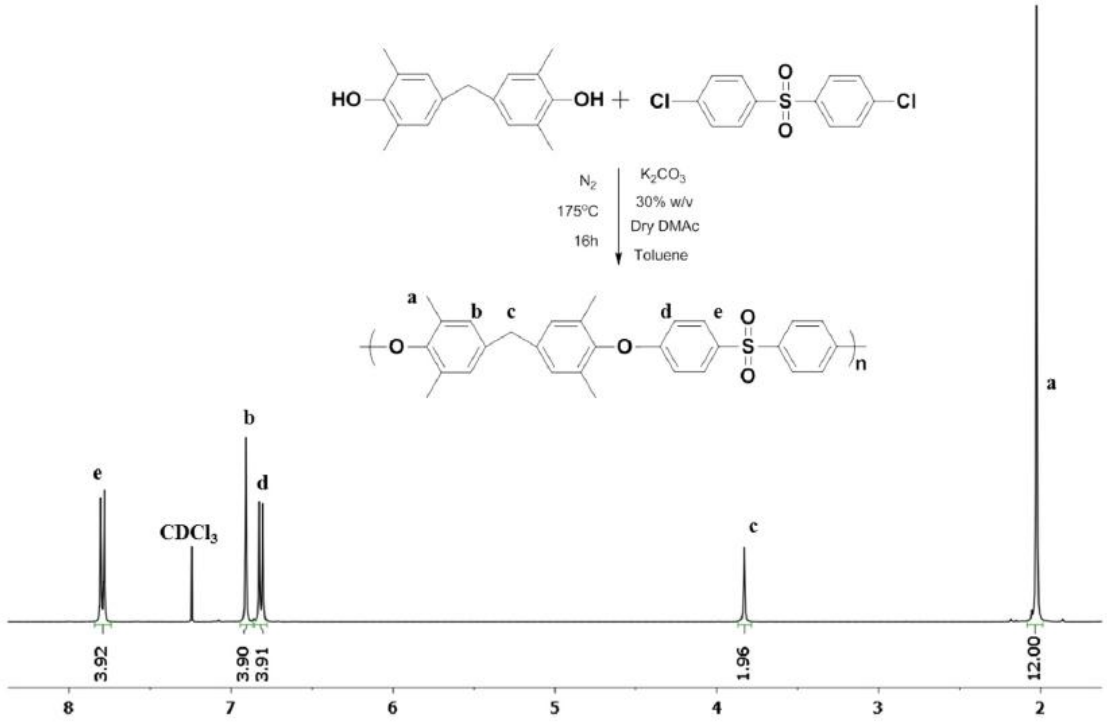

Figure 3. 3 Synthesis and ^{1}H NMR spectrum of the TMBPF-DCDPS polymer

After polymer isolation and drying, the TMBPF polymers were characterized by a variety of spectral and thermal methods. ^{1}H-NMR was performed to ensure polymer structural identification and removal of solvent. Figures 3.3 and 3.4 demonstrate that all of these objectives were achieved, as the integrations corresponded to the expected structures and no impurities or endgroups were observed in the spectra, an indication of high molecular weight.

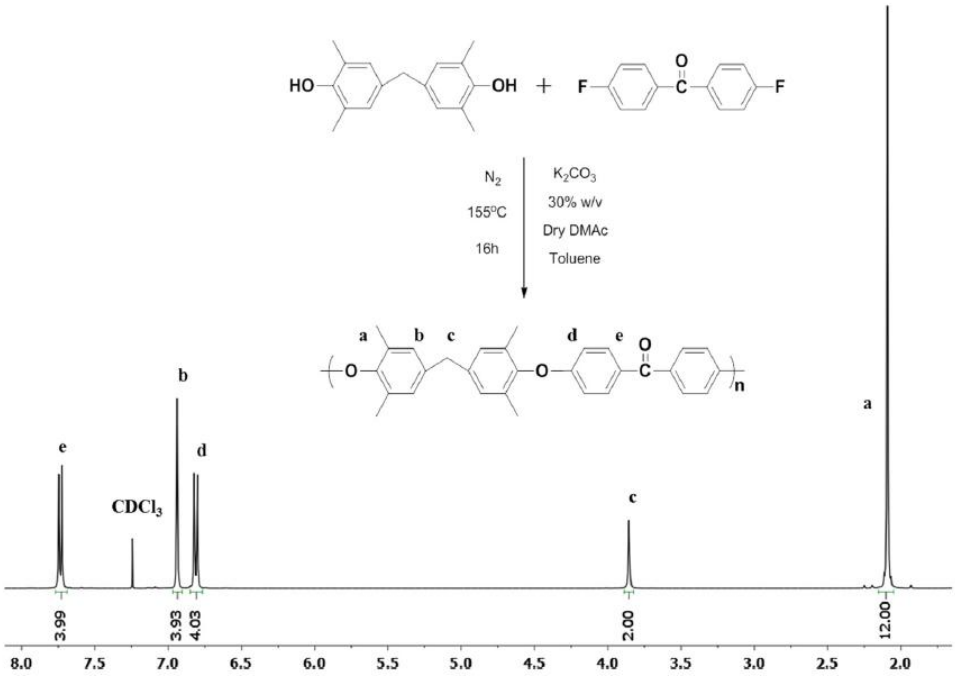

Figure 3. 4 Synthesis and ^{1}H NMR spectrum of TMBPF-DFB polymer

SEC of TMBPF polymers

The polymers were sufficiently high in molecular weight to form transparent, ductile films. SEC of the polymers quantitatively substantiated high molecular weight, and these results are shown in Figure 3.5 and Table 3.1. The polymers have a monomodal Gaussian distribution and polydispersity index (PDI) that one would expect from a step growth polymerization. The PDI should theoretically be 2. However, some lower molecular weight material is likely lost during polymer isolation, thereby decreasing the observed PDI.

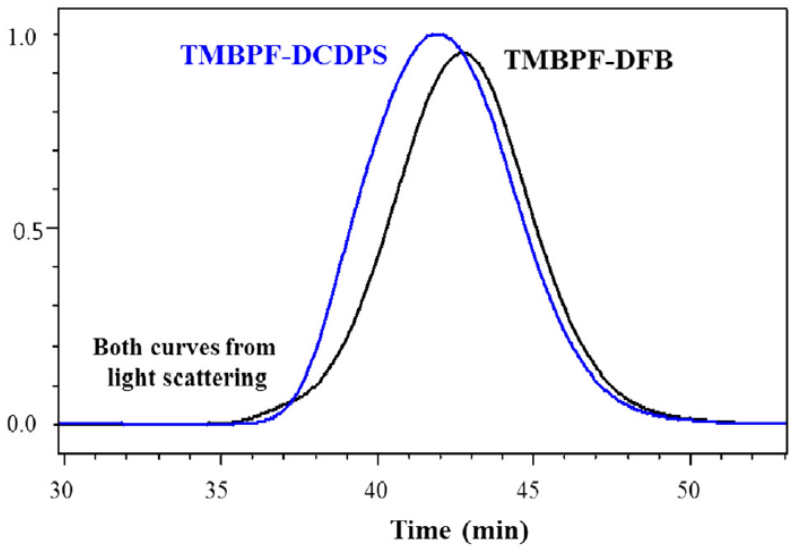

Figure 3. 5 SEC of TMBPF containing polymers

Table 3. 1 SEC of TMBPF containing polymers

Sample	Mn (kDa)	Mw (kDa)	PDI	[η] (dL/g)	dn/dc (mL/g)
TMBPF-DCDPS	66.2	127.5	1.9	0.61	0.14
TMBPF-DFB	51.7	92.7	1.8	0.54	0.15

Oxidation of TMBPF-DCDPS polymer with Oxone/KBr

UV crosslinking of these polymers requires the presence of aromatic carbonyl groups in the backbone and labile hydrogens such as those on the benzylic pendent methyl groups (or residual bridging methylene groups).[41] The methylene bridge of the TMBPF group in the backbone of the polymer can be converted to a carbonyl via oxidation.[42] Oxidation of the TMBPF containing poly(arylene ether sulfone) was initially attempted using potassium peroxymonosulfate (Oxone®) and KBr in a procedure adapted

from the oxidation of small molecules containing benzylic methylene linkages.[32] The poly(arylene ether sulfone) was initially studied in this reaction because the un-oxidized form does not contain carbonyl linkages, so the progress of this reaction could be followed by tracking the growth of the carbonyl ketone peak by FTIR spectroscopy.

The small-molecule procedure called for addition of Oxone and KBr in molar stoichiometries of 2.2 and 0.5 respectively. Because each repeat unit contained one benzylic methylene group capable of oxidation, the molecular weight of the repeat unit was used as the molar mass to determine 1 equivalent for stoichiometric considerations.

Addition of TMBPF-DCDPS polymer to water/acetonitrile (7/93 v/v) turned the liquid a light amber color, and addition of Oxone and KBr produced a slight red tint that quickly disappeared upon stirring. It was apparent that the polymer was insoluble in the solvent mixture, and gradual heating to 45 °C or 60 °C did not noticeably improve the solubility. The solvent system of aqueous acetonitrile was important for the success of oxidation in the small molecule reactions.[32] Water is the source of oxygen in the oxidized product, and changing the solvent to DMSO or DMF produced very low yields. One trial reaction for oxidizing the TMBPF-DCDPS was performed in chloroform, a good solvent for this polymer, but this also led to low levels of conversion with side reactions including crosslinking.

Spectral analysis of the oxidation reaction was done using ^{1}H NMR and FTIR-ATR spectroscopy. The ^{1}H NMR spectra of TMBPF-DCDPS and its partially oxidized analog are shown in Figure 3.6. Most notably, the benzylic methylene peak *c* decreased to about 80% of its initial value, indicating near 20% conversion to the oxidized product. The peaks corresponding to the pendent methyl groups (a) and the aromatic protons

adjacent to the benzylic methylene moiety, *b*, also decreased and new peaks, *a'* and *b'* appeared downfield relative to the initial control peaks. This downfield shift of the b' peak is also consistent with the electron withdrawing nature of the new carbonyl linkage compared to the original methylene group. Peaks *d* and *e* were less affected by this chemical transformation because of their distance from the methylene or carbonyl group, but a broadening of these peaks was observed. FTIR-ATR spectra of the TMBPF-DCDPS polymer and its partially oxidized analog are presented in Figure 3.7. Several signature peaks of the control polymer structure are highlighted, including the sulfone linkage and the benzylic methylene linkage. Most importantly, the partially oxidized polymer had a signature peak at 1656 cm^{-1}, indicating the appearance of a carbonyl group that was not observed in the control polymer.

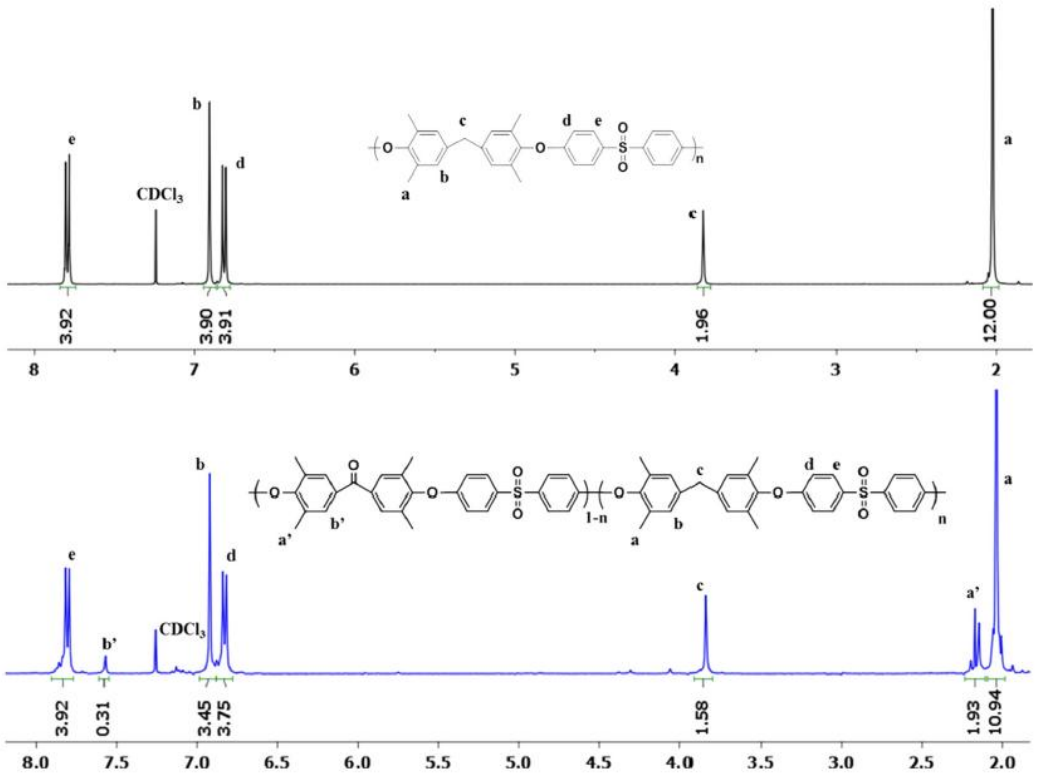

Figure 3. 6 ^{1}H NMR of TMBPF-DCDPS before and after oxidation with Oxone/KBr

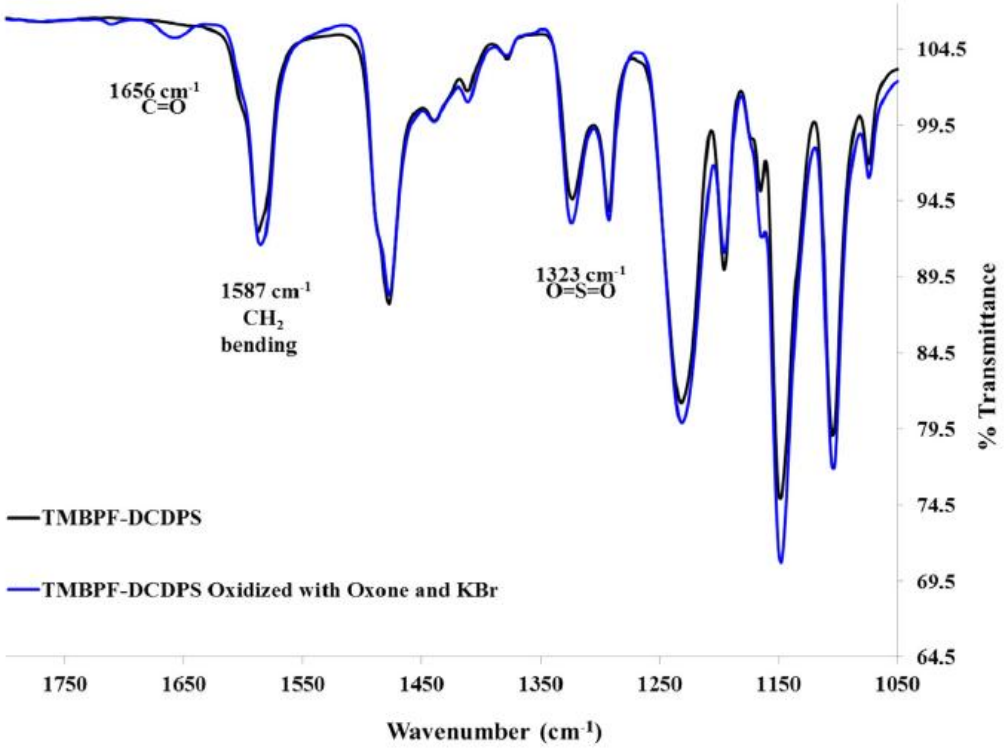

Figure 3. 7 IR of TMBPF-DCDPS before and after oxidation with Oxone/KBr

UV crosslinking of the oxidized TMBPF-DCDPS polymer

One important test on the partially oxidized TMBPF-DCDPS polymer was to determine whether it would crosslink upon exposure to UV radiation. The UV crosslinking mechanism involves excitement of the benzophenone ketone group to form a diradical followed by hydrogen abstraction from a benzylic position to form an OH, then radical-radical coupling..[43] The TMBPF-DCDPS control polymer without the benzophenone moiety was incapable of UV crosslinking under the conditions utilized. Two films were prepared to test the self-crosslinking reaction, one of the TMBPF-DCDPS control and one of the partially oxidized system. Both films were cast from chloroform, dried, and then exposed to UV light. After irradiation, both films were

weighed and extracted with chloroform. The TMBPF-DCDPS film quickly dissolved, indicating 0% gel fraction and no crosslinking. However, the partially oxidized TMBPF-DCDPS film was largely undissolved after one day and had a gel fraction of 80%, thus demonstrating a high level of network formation.

TGA of TMBPF polymers under N_2

In addition to chemical and mechanical stability, high thermal stability is also desired for some gas separation applications. Some hydrogen separations are performed near 100°C today, and there is discussion of performing separations at even higher temperatures, such as those involved in production of synthesis gas, which potentially require membrane stability above 300 °C,[1] and pre-combustion carbon capture, which may require membranes that are stable up to 150°C or higher.[44] The thermal stability of the TMBPF polymers was initially tested under pure nitrogen, as shown in Figure 3.8. Both polymers had very high thermal stabilities, showing no weight loss until 400 °C and a 10% weight loss above 450 °C.

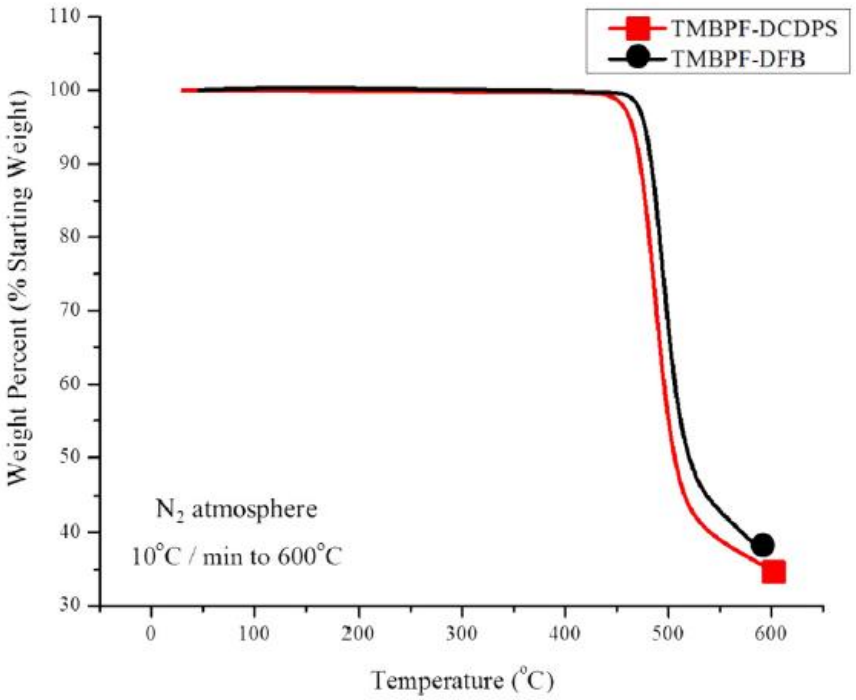

Figure 3. 8 TGA of unoxidized TMBPF containing polymers in N_2

TGA of TMBPF polymers in Air

Thermogravimetric analysis of the TMBPF polymers was also performed in air, and the results are presented in Figure 3.9. The polymers both showed a very interesting phenomenon, weight gain in the region of 250 to 325 °C. It became apparent that the benzylic methylene linkage could thermally oxidize at elevated temperatures in the presence of oxygen. The molecular mass difference between non-oxidized and oxidized polymer was calculated for the TMBPF containing poly(arylene ether ketone) and poly(arylene ether sulfone). The theoretical weight gain required to oxidize each methylene group to a carbonyl in the TMBPF-DFB polymer was 3.2%, and it was 3.0% for the TMBPF-DCDPS polymer. The theoretical weight percent increase was higher for the ketone system because of its lower molecular weight repeat unit. The actual weight

gains shown in Figure 3.9 were approximately 90% of the theoretically possible weight gains, suggesting a high level of oxidation. The temperature ramp above 220 °C was done at 1 °C /min, because incomplete oxidation was observed at higher heating rates (i.e., 10 °C /min).

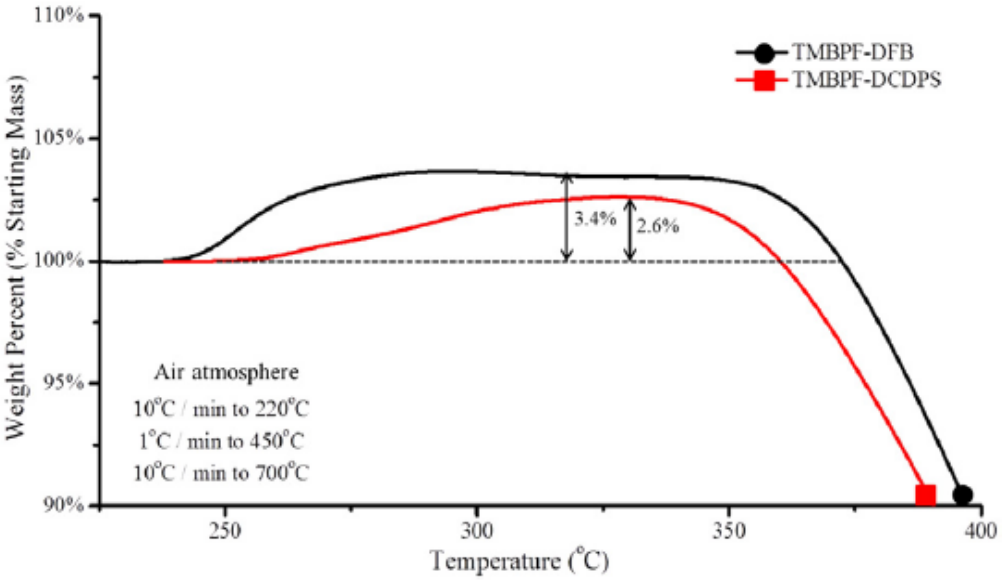

Figure 3. 9 TGA of TMBPF containing polymers in air

Thermal properties of TMBPF polymers under N_2

DSC was performed to identify the glass transition temperatures (Tg's) of the TMBPF polymers. The samples were heated to 350 °C to erase their thermal history, cooled, and then heated again to 350 °C to produce the thermograms in Figure 3.10. DSC was performed under an inert atmosphere to eliminate the possibility of thermal oxidation. Distinct endothermic transitions indicative of the Tg were found at 213 °C for TMBPF-DFB and 235 °C TMBPF-DCDPS. The Tg's were in the range expected for poly(arylene ethers); notably, the Tg of TMBPF-DCDPS was in excellent agreement with a prior study that investigated the effect of polysulfone backbone structure on Tg.[45] The

poly(arylene ether sulfone) had a Tg more than 20 °C higher than that of the poly(arylene ether ketone), likely due to increased restrictions to rotation about the sulfone linkage relative to the carbonyl linkage. Results indicated that thermal oxidation in air began at approximately 20 °C above the Tg of the polymers, as shown in Figure 3.9 by weight gain. These results seem to suggest that extensive chain motion is needed for the oxidation process.

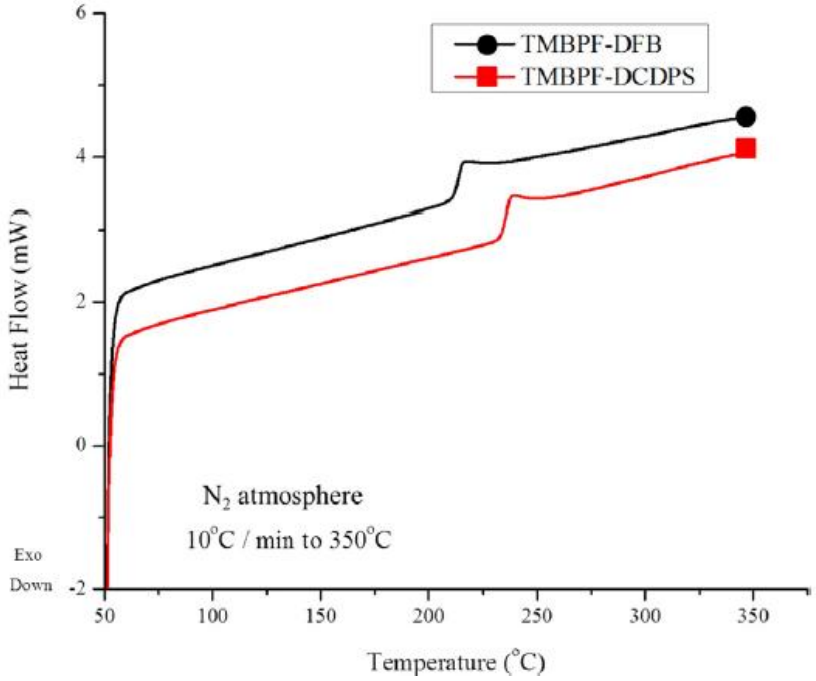

Figure 3. 10 DSC of TMBPF containing polymers in N_2

NMR of thermally oxidized TMBPF-DFB polymer

To investigate the thermal oxidation reactions, the TMBPF-DFB polymer was heated in air to 260 °C, well above Tg, and held for 10 min. The TMBPF-DCDPS polymer was heated to 280 °C in air, well above Tg, and held for 120 min. The TMBPF-DCDPS polymer was heated at a higher temperature and for a longer time to account for the slower oxidation rates observed via TGA. During these times, the polymers changed

from white to a light yellow color. The ^{1}H NMR spectrum of the soluble fraction of the thermally oxidized TMBPF-DFB is shown in Figure 3.11, and the spectrum for oxidized TMBPF-DCDPS is shown in Figure 3.12.

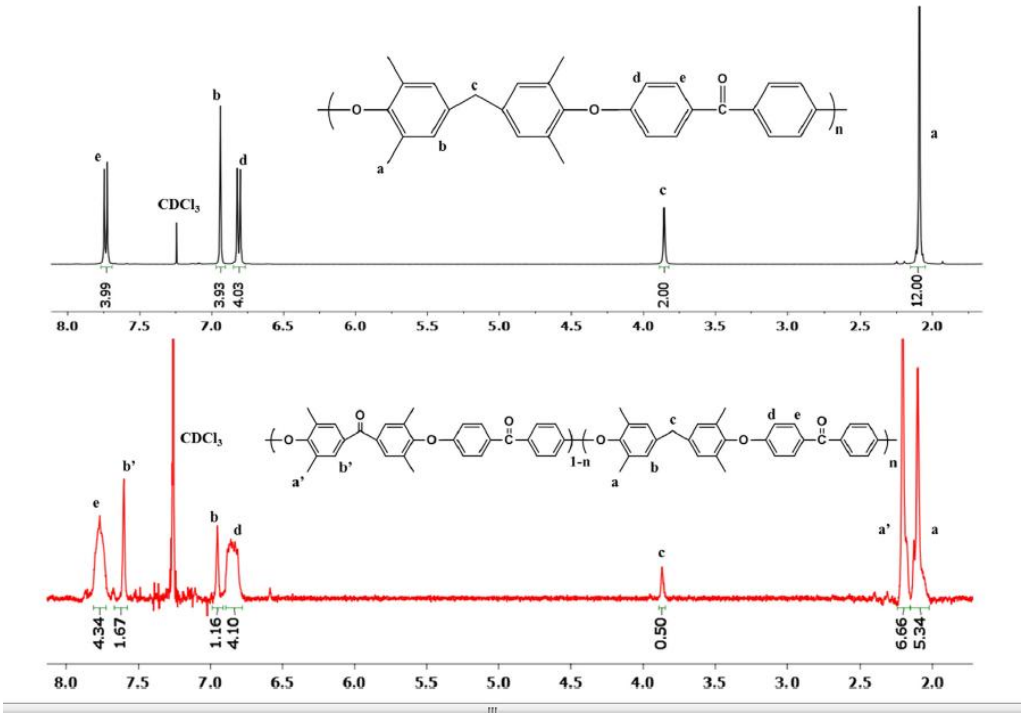

Figure 3. 11 ^{1}H-NMR of thermally oxidized TMBPF-DFB

Similar to the results obtained via partial Oxone/KBr oxidation, the thermal oxidation reactions were analyzed by ^{1}H NMR spectroscopy. The spectra show that the TMBPF-DFB polymer was oxidized to 75% conversion, and the TMBPF-DCDPS polymer was oxidized to 45% conversion, based on integration of the benzylic methylene peak (i.e., peak c in Figures 3.11 and 3.12) before and after thermal oxidation. The signal-to-noise ratio was lower in the thermal oxidation spectra compared to the Oxone/KBr oxidation because of poor solubility in the deuterated solvent, presumably as a result of thermal crosslinking concurrent with the ozone oxidation reaction. The growth

of several small peaks (Figures 3.11 and 3.12) may also indicate increased structural complexity as the polymers began to crosslink. The rates and temperatures of these thermal oxidation reactions and how they can be decoupled from crosslinking will require significantly more research.

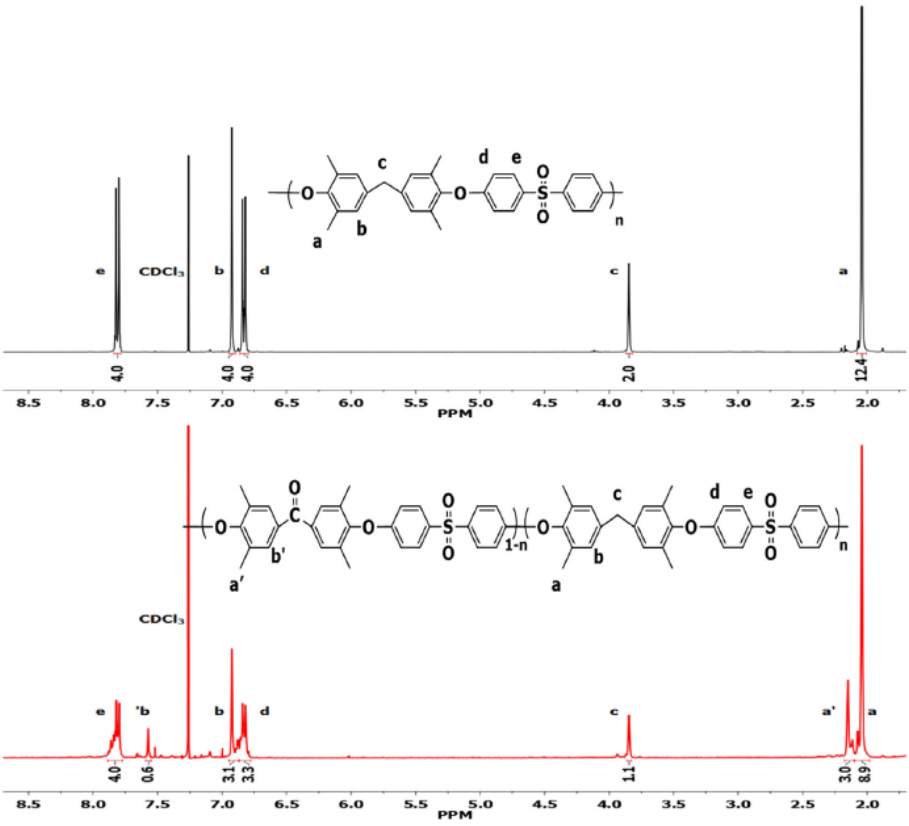

Figure 3. 12 ^{1}H-NMR of thermally oxidized TMBPF-DCDPS

FTIR of the thermally oxidized TMBPF-DCDPS polymer

Figure 3.13 shows the FTIR spectra of the thermally oxidized TMBPF-DCDPS compared to the untreated sample. In the thermally oxidized sample, a carbonyl peak appeared that was not present prior to oxidation.

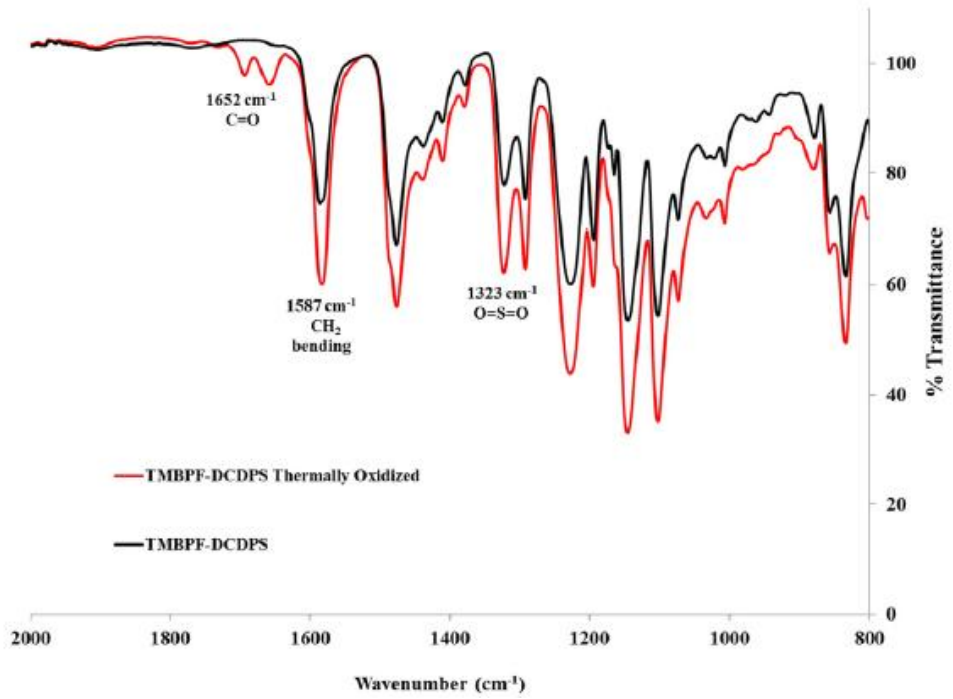

Figure 3. 13 IR of thermally oxidized TMBPF-DCDPS

Initial gas transport results

The effect of UV crosslinking on gas permeation properties was of interest for this research.. A control film was cast from the TMBPF-DFB polymer and then cut in half. Permeabilities and selectivities of five different gases were directly tested on one half. The other half was exposed to UV irradiation to induce photochemical crosslinking. The mechanism for this photochemical reaction is benzylic hydrogen abstraction by an excited state benzophenone moiety,[43,46] which has been shown to produce polyimides with high selectivity.[19] The gel fraction of this UV irradiated half was measured to be 100%, indicating that a highly crosslinked network was obtained. The density of the linear TMBPF-DFB polymer was 1.116 ± 0.003 g mL^{-1} and the density of the crosslinked TMBPF-DFB polymer was 1.146 ± 0.004 g mL^{-1}. The densification of the polymer membrane upon UV crosslinking was expected based on prior literature, and reflects a

decrease in interchain spacing.[47] The pure gas permeabilities and selectivities of these two films are shown in Tables 3.2 and 3.3, where they are compared with UDEL™ polysulfone. The TMBPF-DFB linear polymer was not oxidized or crosslinked, whereas the TMBPF-DFB crosslinked polymer was not oxidized, but it was crosslinked with UV irradiation to afford a 100% gel fraction. The transport properties of the TMBPF-DFB linear and TMBPF-DFB crosslinked polymers are also shown in Fig. 14, where they are graphed with a commercial polysulfone, polyimide (Matrimid), and the 1991 and 2008 upper bounds.

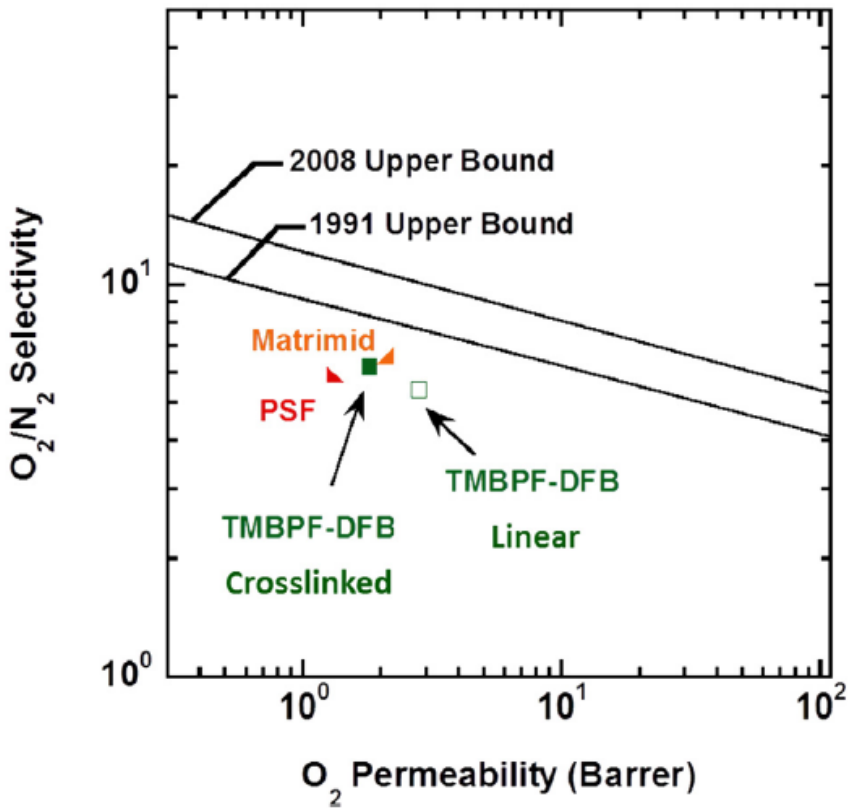

Figure 3. 14 Upper bound plot comparison of linear and crosslinked TMBPF-DFB [9]

Table 3. 2 Pure gas permeabilities of linear and crosslinked TMBPF-DFB

Polysulfone[16]: CO_2, CH_4 at 10 bar and 35 °C; O_2, N_2, H_2 at 1 bar and 35 °C

	Gas permeability (Barrer) at 10 atm & 35 °C				
	O_2	N_2	CO_2	CH_4	H_2
TMBPF-DFB linear	2.8	0.52	10	0.54	29
TMBPF-DFB crosslinked	1.8	0.29	7.1	0.25	23
Bisphenol A polysulfone[a]	1.4	0.25	5.6	0.25	14
Tetramethyl bisphenol A polysulfone[a]	5.6	1.06	21	0.95	32

Table 3. 3 Pure gas selectivities of linear and crosslinked TMBPF-DFB

Polysulfone[16]: CO_2, CH_4 at 10 bar and 35 °C; O_2, N_2, H_2 at 1 bar and 35 °C

	Gas selectivity at 10 atm & 35 °C				
	O_2/N_2	CO_2/CH_4	H_2/N_2	H_2/CH_4	CO_2/N_2
TMBPF-DFB linear	5.4	19	75	72	19
TMBPF-DFB crosslinked	6.2	28	79	92	24
Bisphenol A polysulfone[a]	5.6	22.4	56	56	22.4
Tetramethyl bisphenol A polysulfone[a]	5.3	22	30	34	19.8

The films demonstrate the expected relationship of crosslinking leading to decreased gas permeability and improved selectivity. An additional benefit of crosslinking of thin films is a reduction in physical aging.[46] The reduction of permeability after UV crosslinking has also been attributed to membrane densification.[48] Notably, the crosslinked TMBPF-DFB films had both higher permeability and selectivity compared to

UDEL polysulfone. One reason for the greatly enhanced gas permeability of the TMBPF systems is the presence of the numerous bulky methyl groups along the polymeric backbone. These two samples represent a minor set that was obtainable from these TMBPF polymer series. The pure gas permeability was measured at five different pressures, which is graphed in Figures 3.15 and 3.16.

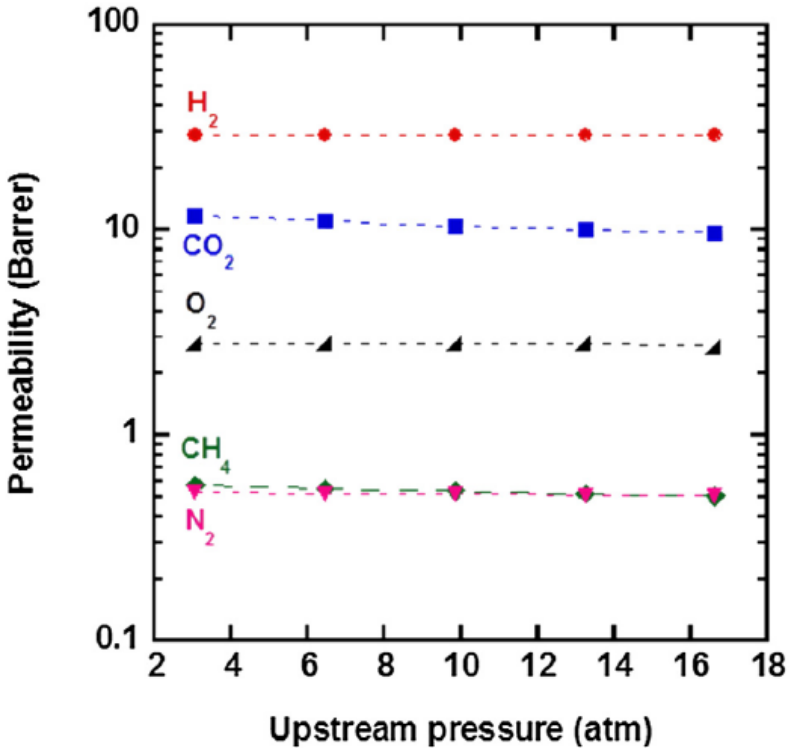

Figure 3. 15 Permeability as a function of feed pressure for linear TMBPF-DFB

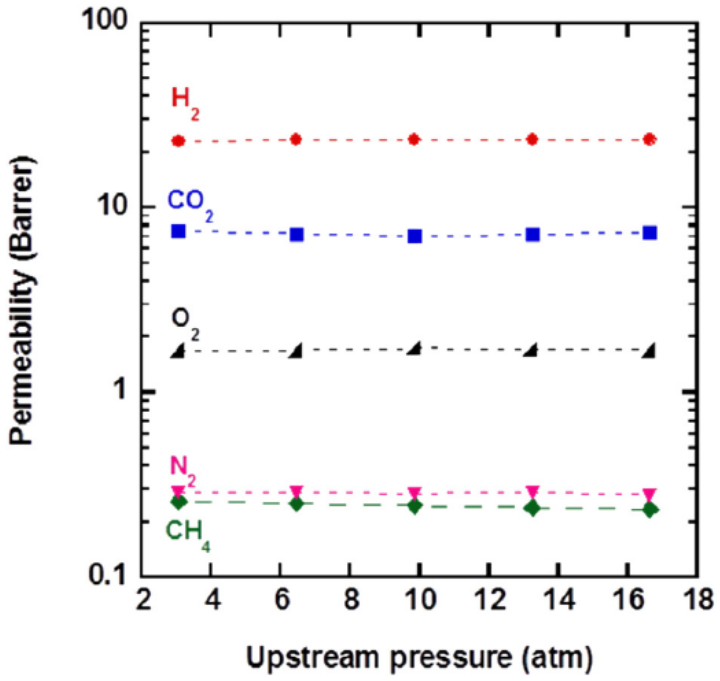

Figure 3. 16 Permeability as a function of feed pressure for UV-crosslinked TMBPF-DFB

In Figure 3.15, the permeability of CH_4 and CO_2 decreased slightly as upstream pressure was increased, because of their condensability.[49] The effect of decreasing permeability in glassy polymers as a function of upstream pressure has been attributed to the dual-sorption model.[50] An increase in upstream pressure effectively reduces the Langmuir term and thus reduces permeability. Interestingly this phenomenon was less pronounced in Figure 3.16 for the highly crosslinked TMBPF-DFB.

3.5. Conclusions

In this paper, an economical route was presented to synthesize the TMBPF monomer and two TMBPF containing poly(arylene ether) materials. High molecular weights were demonstrated quantitatively by SEC, and ductile films were obtained. The polymers were capable of backbone modifications that included thermal and chemical

oxidation and photochemical crosslinking. Thermal oxidation of the benzylic methylene groups somewhat above T_g was more successful than solution oxidation with ozone/KBr, in terms of conversion. Both polymers were capable of producing crosslinked films with high gel fractions through thermal crosslinking. ^{1}H NMR and FTIR spectroscopy were used for structural verification of the TMBPF monomer, TMBPF containing polymers, and conversion of the polymers to their oxidized forms. The thermal oxidation reaction was also studied by TGA, and quantitative proof of the oxidation was presented by demonstrating theoretical weight gains. Initial gas transport properties demonstrated that crosslinking these polymers produced more highly selective membranes at the cost of reduced gas permeability.

Acknowledgements

The authors gratefully acknowledge the financial support of Air Products, Inc. (212-153-P), and the National Science Foundation under contracts (NSF-AIR: IIP-1237857) and (NSF-MRI: DMR-1126534).

3.6. Supplemental Information

3.6.1. Results and Discussion

The TGA thermogram in Figure 3.17 compares the wt% gain of TMBPF-DFB discussed in Part 1 but at different isothermal temperatures. The four temperatures were 240, 250, 260 and 270 °C and these were chosen based on the onset of wt gain shown in Figure 3.9. The weight gain increased with increasing isotherm temperature. However, after the initial significant weight gain, the materials gained weight at the same rate regardless of the isotherm temperature. Therefore, the isotherm temperature mainly

affects the slope of the initial weight gain and the trend is that the higher the temperature, the steeper the slope.

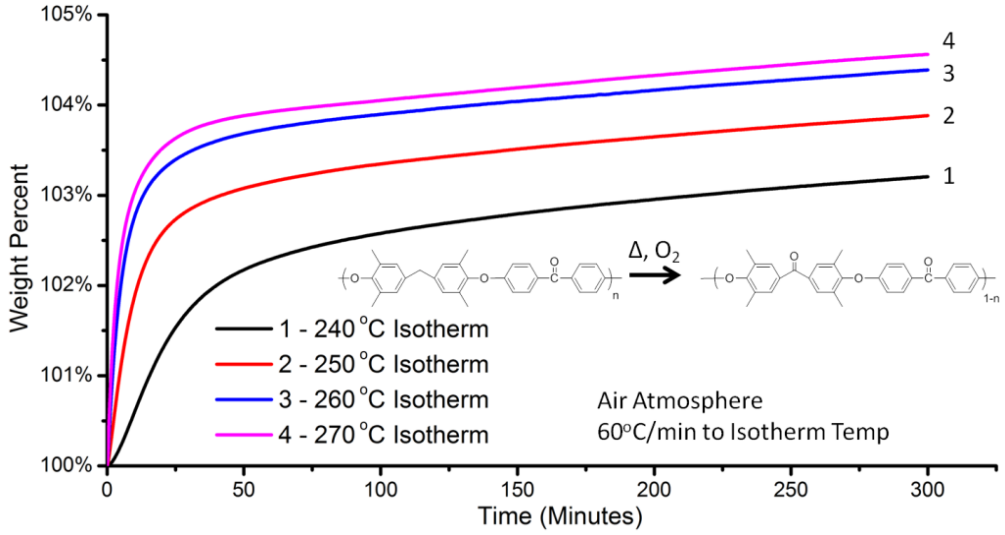

Figure 3. 17 Comparison of four isotherm temperatures under air of TMBPF-DFB

The TMBPF-DCDPS was tested using the same method and the results are shown in Figure 3.18. The three isotherm temperatures that TMBPF-DCDPS was tested at showed different slopes at the beginning and throughout the test. When compared to TMBPF-DFB at 260 °C, (Figure 3.19) the TMBPF-DCDPS did not undergo a significant early weight gain. This could be attributed to two factors. One reason is that the low Tg of the TMBPF-DFB allows for the oxidation to occur at lower temperatures and at higher rates. The Tg's were found at 213 °C for TMBPF-DFB and 235 °C TMBPF-DCDPS. The last possible reason is that the ketone linkage within the TMBPF-DFB initially accelerates the reaction and/or causes a second type of reaction to occur.

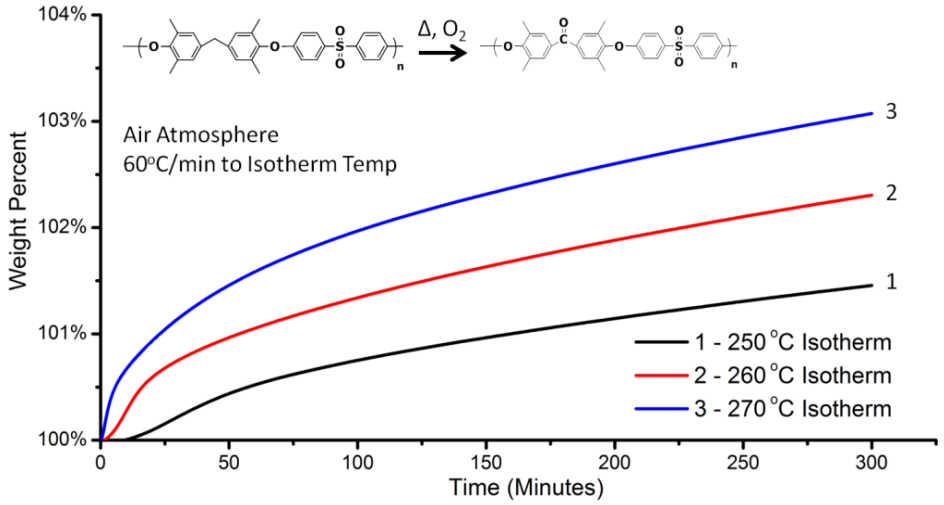

Figure 3. 18 Comparison of three isotherm temperatures under air of TMBPF-DCDPS

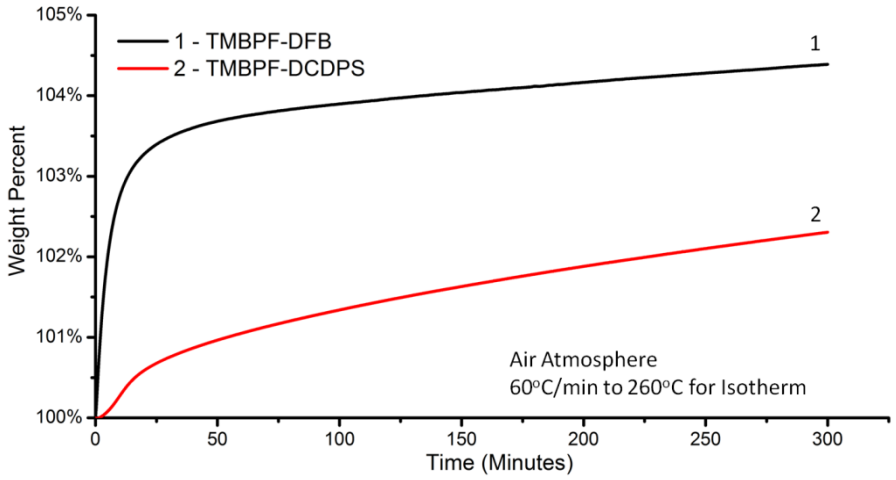

Figure 3. 19 Comparison of TMBPF-DFB and TMBPF-DCDPS under a 260 °C isotherm

After investigating the effect of temperature on the oxidation, the air flow rate was changed from 20 mL/min to 40 mL/min and 80 mL/min. In Figure 3.20 it is clear that the higher flow rate results in a greater weight gain rate. This is expected because the oxidation would occur at faster rates with more oxygen.

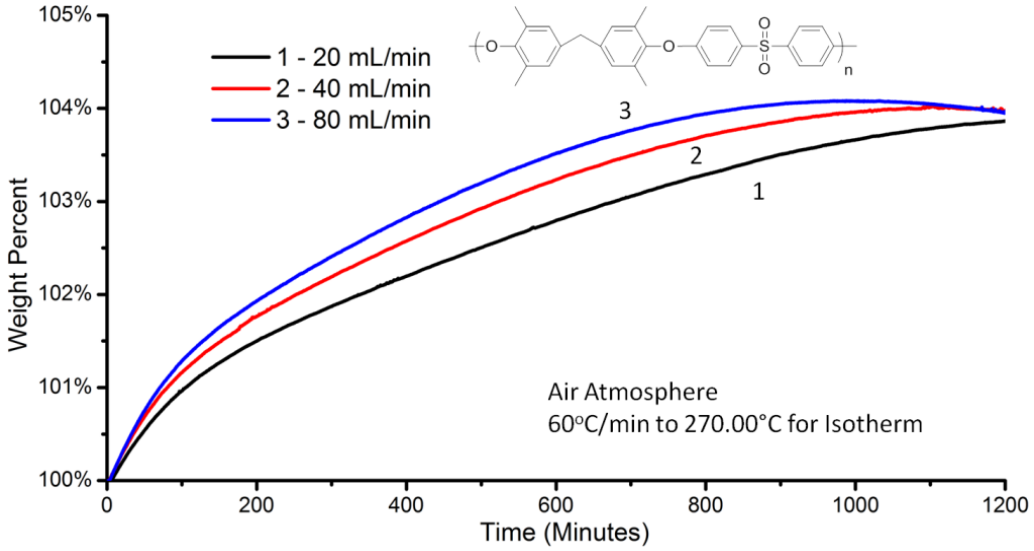

Figure 3. 20 Comparison of three flow rates on the weight gain of TMBPF-DCDPS under a 270 °C isotherm

Figure 3.21 shows comparisons of weight gains for TMBPF-DFB when heated for an extended period at two different temperatures. When held at 280 °C, the weight reached a maximum relatively quickly and then the sample began to lose weight. After 1800 minutes, the gain was almost half of the maximum gain that occurred at around 800 minutes, likely signifying polymer degradation. In the future, mass spec in conjunction with TGA could identify what is being lost. When heated at 260 °C for extended times, the material did not lose weight but did begin to plateau. Therefore, the oxidation is sensitive to the temperature and a lower temperature produces the greatest weight gain after a significant time frame. The same test was run on TMBPF-DCDPS and produced similar trends.

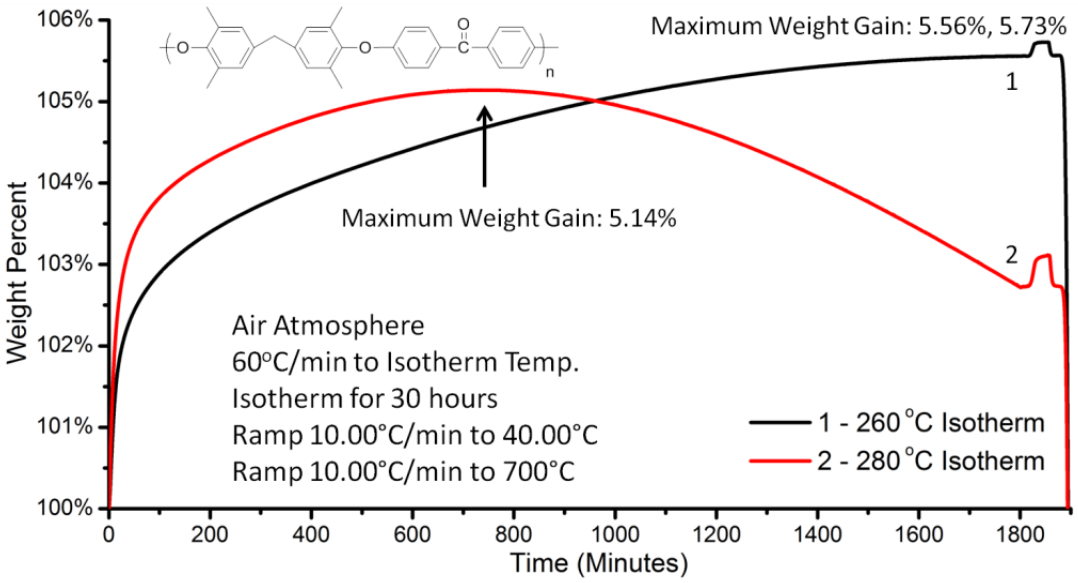

Figure 3. 21 Comparison of TMBPF-DFB under an extended isotherm at 260 °C and 280 °C

After oxidation at each of the temperatures, the TMBPF-DFB sample was brought back to 40 °C and this resulted in another small weight gain (see the small gains on the right of Figure 3.21). This, however, was quickly lost once the temperature was raised towards 700 °C. Other testing procedures were used to further explore this peak which will be termed the "room temperature peak" (RTP). All of these tests (Figure 3.22 to Figure 3.26) used TMBPF-DCDPS but the RTP also occurred in TMBPF-DFB. The first test was to determine if the RTP would continue to occur over time and multiple cycles. After oxidation at 280 °C for 10 hours, the temperature was cycled between 30 and 100 °C. Every time the temperature was decreased, the weight increased and then decreased again once the temperature was increased. The amount of increase and decrease did not change in any of the cycles which showed the RTP's reproducibility.

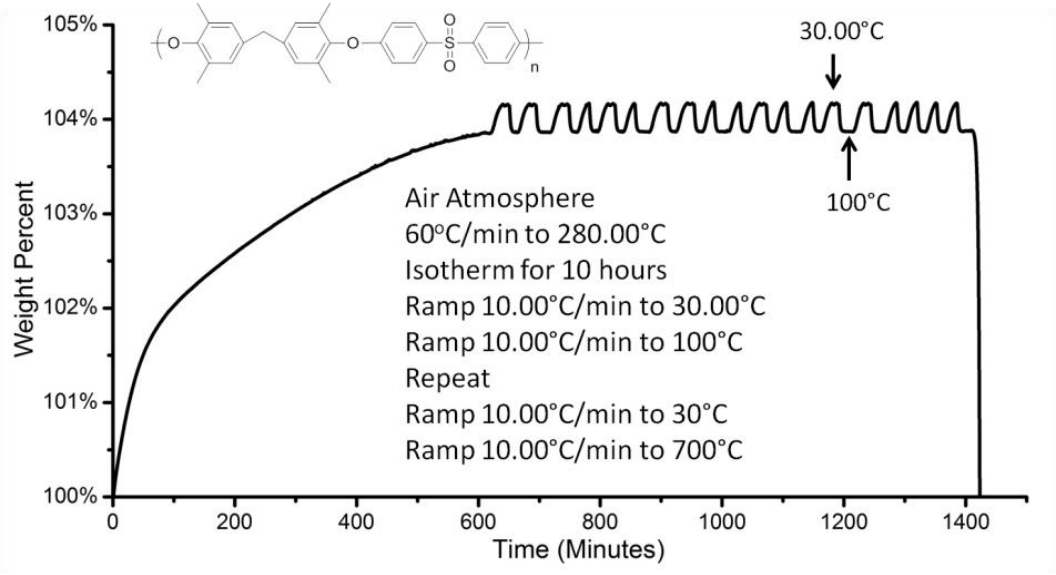

Figure 3. 22 Exploration of the RTP to determine repeatability

As shown In Figure 3.23, the polymer was oxidized for 24 hours in air and then the gas in the TGA was switched to nitrogen. The RTP still occured but was reduced in size. Figure 3.24 shows the RTP with the sample tested under nitrogen superimposed onto the RTP curve under air and the difference in weight gain is apparent. This indicates that this peak was related to the atmosphere which means that the polymer was absorbing either the gas itself or a small amount of water that was present. Water is very likely because when the temperature was cycled between 100 and 150 °C, no weight change was produced. If it was a gas (other than water vapor) being absorbed, it is reasoned that the peak should continue to occur when the sample is cycled between two temperatures above 100 °C. However, water would not be absorbed significantly above 100 °C due to its boiling point. Therefore, it is likely that the RTP is the rapid absorption of water upon cooling and removal of water upon heating. The high degree of hydrophilicity could be attributed to the high ketone content after oxidation of the methylene linkage.

To confirm that this does not occur in all polymers, Radel 5000 was subjected to the same heating protocol. Figure 3.25 compares the TMBPF-DCDPS to Radel 5000 and Figure 3.26 superimposes temperature cycling of the Radel 5000 with the TMBPF-DCDPS temperature cycling.

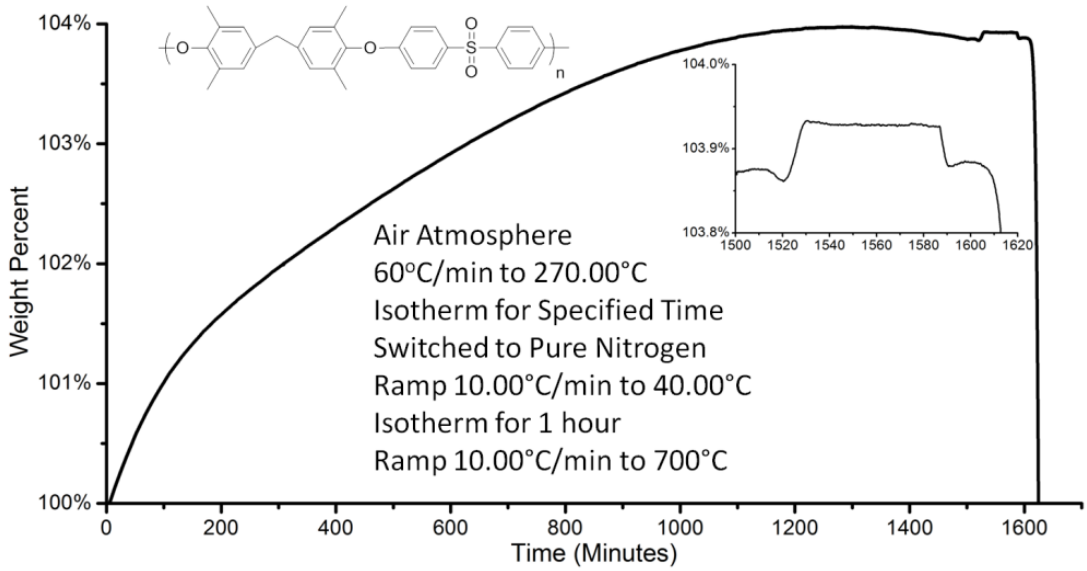

Figure 3. 23 Exploration of the RTP under a nitrogen atmosphere

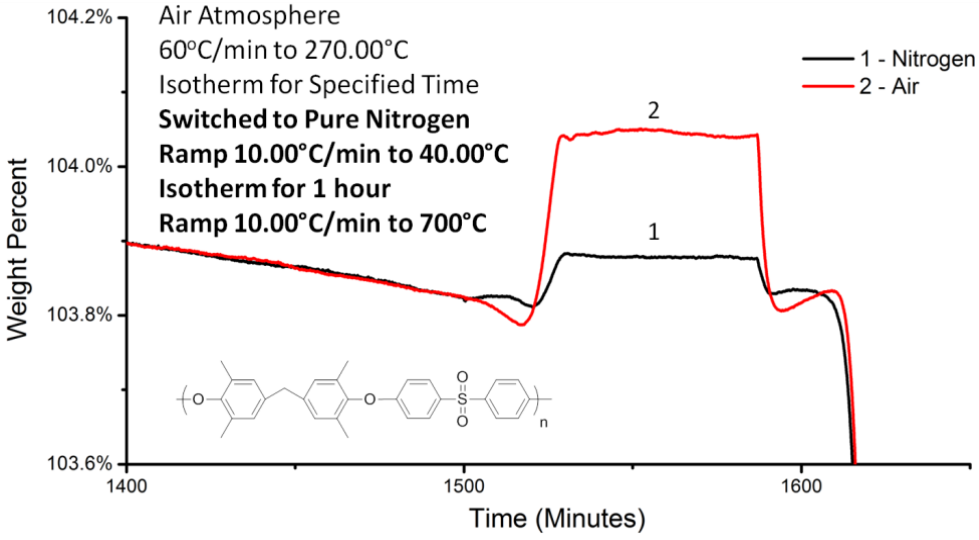

Figure 3. 24 Comparison of the RTP under both nitrogen and air atmosphere

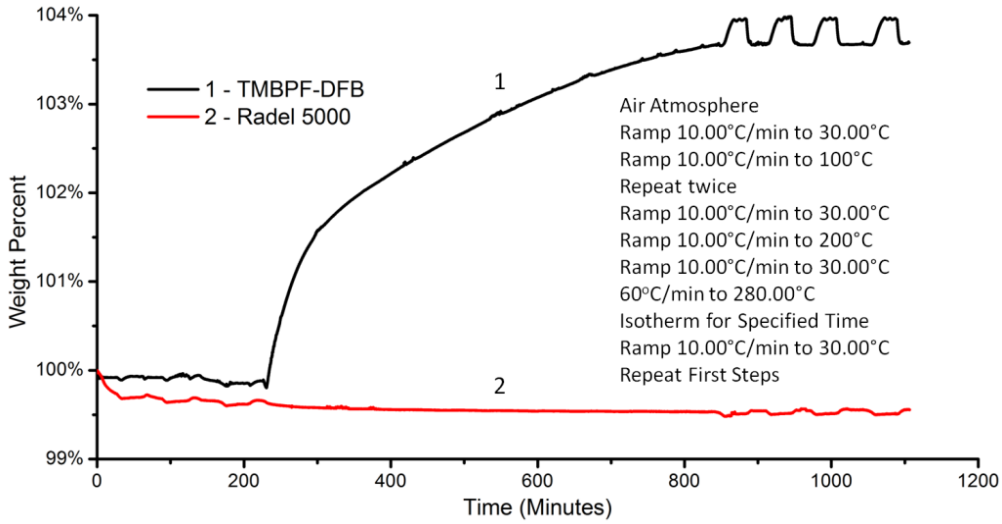

Figure 3. 25 Comparison of the TMBPF-DCDPS RTP against another sulfone material that does not oxidize

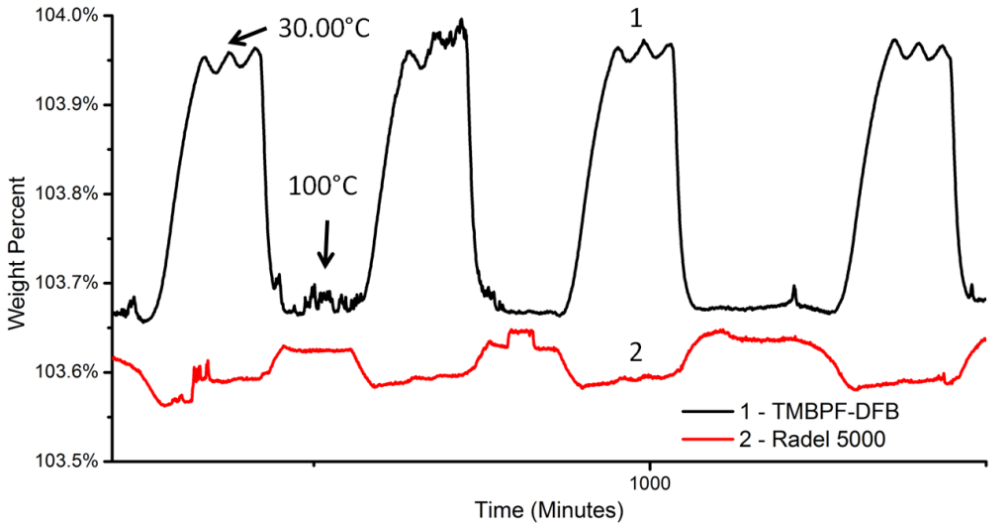

Figure 3. 26 RTP of TMBPF-DCDPS with Radel 5000 superimposed for a closer comparison

3.6.2. Conclusions

TGA was utilized to explore the oxidation of TMBPF-DFP and TMBPF-DCDPS. TMBPF-DFB produced a very rapid initial weight gain upon heating to elevated

temperatures, followed by a smaller, but steady gain. In contrast, TMBPF-DCDPS did not undergo a significant initial gain, but it increased in weight much more gradually throughout the entire isotherm. This can likely be attributed to less distance between it's Tg and the oxidation temperature. TMBPF-DFB was heated over an extended period at 260 and 280 °C. The isotherm at 280 °C showed a relatively rapid weight gain and reached a maximum at 800 minutes but began to lose weight following the maximum, likely corresponding to some polymer degradation. At 260 °C the gain was greater than at 280 °C and the sample did not lose weight, but this polymer required significantly more time to surpass the 280 °C maximum gain. The "room temperature peak" (RTP) that occurred after oxidation was investigated. Its reproducibility was confirmed and based on comparison with Radel 5000, the RTP does not occur in all polymers. The RTP size did change with the applied gas which indicates it was product of the exposure atmosphere. Therefore, the RTP was attributed to absorption of a gas or water vapor within the atmosphere. The peak size did not increase when the sample was cycled at temperatures above 100 °C, thus suggesting that the peak was likely attributable to water absorption.

References

1. Bernardo, P.; Drioli, E.; Golemme, G. Membrane Gas Separation: A Review/State of the Art. *Ind. Eng. Chem. Res.* **2009**, *48*, 4638.

2. Baker, R. W.; Lokhandwala, K. Natural Gas Processing with Membranes: An Overview. *Ind. Eng. Chem. Res.* **2008**, *47*, 2109.

3. Koros, W. J.; Fleming, G. K. Membrane-based gas separation. *J. Membr. Sci.* **1993**, *83*, 1.

4. Baker, R. W. Future Directions of Membrane Gas Separation Technology. *Ind. Eng. Chem. Res.* **2002**, *41*, 1393.

5. Robeson, L. M. Correlation of separation factor versus permeability for polymeric membranes. *J. Membr. Sci.* **1991**, *62*, 165.

6. Freeman, B. D. Basis of Permeability/Selectivity Tradeoff Relations in Polymeric Gas Separation Membranes. *Macromolecules* **1999**, *32*, 375.

7. Doolittle, A. K. Newtonian flow. II. The dependence of the viscosity of liquids on free space. *J. Appl. Phys.* **1951**, *22*, 1471.

8. Cohen, M. H.; Turnbull, D. Molecular transport in liquids and glasses. *J. Chem. Phys.* **1959**, *31*, 1164.

9. Robeson, L. M. The upper bound revisited. *J. of Membr. Sci.* **2008**, *320*, 390.

10. Min, K. E.; Paul, D. R. Effect of tacticity on permeation properties of poly(methyl methacrylate). *J. Polym. Sci., Part B: Polym. Phys.* **1988**, *26*, 1021.

11. Miyata, S.; Sato, S.; Nagai, K.; Nakagawa, T.; Kudo, K. Relationship between gas transport properties and fractional free volume determined from dielectric constant in polyimide films containing the hexafluoroisopropylidene group. *J. Appl. Polym. Sci.* **2008**, *107*, 3933.

12. Stern, S. A. Polymers for gas separations: the next decade. *J. Membr. Sci*. **1994**, *94*, 1.

13. McHattie, J. S.; Koros, W. J.; Paul, D. R. Gas transport properties of polysulfones. 1. Role of symmetry of methyl group placement on bisphenol. *Polymer* **1991**, *32*, 840.

14. Kim, I.-W.; Lee, K. J.; Jho, J. Y.; Park, H. C.; Won, J.; Kang, Y. S.; Guiver, M. D.; Robertson, G. P.; Dai, Y. Correlation between Structure and Gas Transport Properties of Silyl-Modified Polysulfones and Poly(phenyl sulfone)s. *Macromolecules* **2001**, *34*, 2908.

15. McHattie, J. S.; Koros, W. J.; Paul, D. R. Gas transport properties of polysulfones. 2. Effect of bisphenol connector groups. *Polymer* **1991**, *32*, 2618.

16. Aitken, C. L.; Koros, W. J.; Paul, D. R. Effect of structural symmetry on gas transport properties of polysulfones. *Macromolecules* **1992**, *25*, 3424.

17. Xiao, Y.; Chung, T.-S.; Chng, M. L.; Tamai, S.; Yamaguchi, A. Structure and Properties Relationships for Aromatic Polyimides and Their Derived Carbon Membranes: Experimental and Simulation Approaches. *J. Phys. Chem. B* **2005**, *109*, 18741.

18. Park, H. B.; Jung, C. H.; Lee, Y. M.; Hill, A. J.; Pas, S. J.; Mudie, S. T.; Van Wagner, E.; Freeman, B. D.; Cookson, D. J. Polymers with Cavities Tuned for Fast Selective Transport of Small Molecules and Ions. *Science* **2007**, *318*, 254.

19. Hayes, R. A. Polyimide gas-separation membranes. US4717393A,**1988**

20. Bennett, C. L.; Richards, R. E. Copolyimides for use as gas separation membranes. GB2244997A,**1991**

21. Kita, H.; Inada, T.; Tanaka, K.; Okamoto, K. Effect of photocrosslinking on permeability and permselectivity of gases through benzophenone-containing polyimide. *J. Membr. Sci.* **1994**, *87*, 139.

22. Ouyang, M.; Muisener, R. J.; Boulares, A.; Koberstein, J. T. UV-ozone induced growth of a SiOx surface layer on a cross-linked polysiloxane film: characterization and gas separation properties. *J. Membr. Sci.* **2000**, *177*, 177.

23. Kwisnek, L.; Heinz, S.; Wiggins, J. S.; Nazarenko, S. Multifunctional thiols as additives in UV-cured PEG-diacrylate membranes for CO2 separation. *J. Membr. Sci.* **2011**, *369*, 429.

24. Wind, J. D.; Paul, D. R.; Koros, W. J. Natural gas permeation in polyimide membranes. *J. Membr. Sci.* **2004**, *228*, 227.

25. Shao, L.; Samseth, J.; Hagg, M.-B. Crosslinking and stabilization of high fractional free volume polymers for gas separation. *Int. J. Greenhouse Gas Control* **2008**, *2*, 492.

26. Staudt-Bickel, C.; Koros, W. J. Improvement of CO2/CH4 separation characteristics of polyimides by chemical crosslinking. *J. Membr. Sci.* **1999**, *155*, 145.

27. Lin, H.; Van Wagner, E.; Freeman, B. D.; Toy, L. G.; Gupta, R. P. Plasticization-enhanced hydrogen purification using polymeric membranes. *Science* **2006**, *311*, 639.

28. Han, G.; Chung, T.-S.; Toriida, M.; Tamai, S. Thin-film composite forward osmosis membranes with novel hydrophilic supports for desalination. *J. Membr. Sci.* **2012**, *423- 424*, 543.

29. Sun, H.; Zhang, G.; Liu, Z.; Zhang, N.; Zhang, L.; Ma, W.; Zhao, C.; Qi, D.; Li, G.; Na, H. Self-crosslinked alkaline electrolyte membranes based on quaternary ammonium poly (ether sulfone) for high-performance alkaline fuel cells. *Int. J. Hydrogen Energy* **2012**, *37*, 9873.

30. *Macromolecular Synthesis*; John Wiley & Sons: New York, **1977**; Vol. 1.

31. Hedrick, J. L.; Mohanty, D. K.; Johnson, B. C.; Viswanathan, R.; Hinkley, J. A.; McGrath, J. E. Radiation resistant amorphous-all aromatic polyarylene ether sulfones: synthesis, characterization, and mechanical properties. *J. Polym. Sci., Part A: Polym. Chem.* **1986**, *24*, 287.

32. Yin, L.; Wu, J.; Xiao, J.; Cao, S. Oxidation of benzylic methylenes to ketones with Oxone– KBr in aqueous acetonitrile under transition metal free conditions. *Tetrahedron Letters* **2012**, *53*, 4418.

33. Lin, H., Freeman, B.D. In *Spring Handbook of Metrology and Testing*; 2nd Edition ed.; H. Czichos, T. S., L. Smith, Ed.; Springer: Berlin, **2011**, p 426.

34. Olah, G. A.; Kobayashi, S.; Nishimura, J. Aromatic Substitution. XXXI. Friedel-Crafts Sulfonylation of Benzene and Toluene with Alkyl- and Arylsulfonyl Halides and Anhydrides. *J. Amer. Chem. Soc.* **1973**, *95*, 564.

35. Bowman, P. J.; Brown, B. R.; Chapman, M. A.; Doyle, P. M. Synthesis and reactions of phenolic alkylbenzylnitrosamines. *J. Chem. Res., Synop.* **1984**, 72.

36. Sanders, D. F.; Smith, Z. P.; Guo, R.; Robeson, L. M.; McGrath, J. E.; Paul, D. R.; Freeman, B. D. Energy-efficient polymeric gas separation membranes for a sustainable future: A review. *Polymer* **2013**, *54*, 4729.

37. Robeson, L. M.; Farnham, A. G.; McGrath, J. E. Synthesis and dynamic mechanical characteristics of poly(aryl ethers). *Appl. Polym. Symp.* **1975**, *26*, 373.

38. Rose, J. B. Preparation and properties of poly(arylene ether sulphones). *Polymer* **1974**, *15*, 456.

39. Viswanathan, R.; Johnson, B. C.; McGrath*, J. E. In *Polymer* **1984**; Vol. 25, p 1827.

40. Bunnett, J. F. Mechanism and reactivity in aromatic nucleophilic substitution reactions. *Quarterly Reviews, Chemical Society* **1958**, *12*, 1.

41. Mohanty, D. K.; Sachdeva, Y.; Hedrick, J. L.; Wolfe, J. F.; McGrath, J. E. Synthesis and transformations of tetramethyl bis[phenol] A polyaryl ethers. *Polym. Prepr. (Am. Chem. Soc., Div. Polym. Chem.)* **1984**, *25*, 19.

42. Chen, M. S.; White, M. C. Combined Effects on Selectivity in Fe-Catalyzed Methylene Oxidation. *Science* **2010**, *327*, 566.

43. Wright, C. T.; Paul, D. R. Gas sorption and transport in UV-irradiated polyarylate copolymers based on tetramethylbisphenol-A and dihydroxybenzophenone. *J. Membr. Sci.* **1997**, *124*, 161.

44. Merkel, T. C.; Zhou, M.; Baker, R. W. Carbon dioxide capture with membranes at an IGCC power plant. *J. Membr. Sci.* **2012**, *389*, 441.

45. Aitken, C. L.; McHattie, J. S.; Paul, D. R. Dynamic mechanical behavior of polysulfones. *Macromolecules* **1992**, *25*, 2910.

46. McCaig, M. S.; Paul, D. R. Effect of UV crosslinking and physical aging on the gas permeability of thin glassy polyarylate films. *Polymer* **1999**, *40*, 7209.

47. Matsui, S.; Ishiguro, T.; Higuchi, A.; Nakagawa, T. Effect of ultraviolet light irradiation on gas permeability in polyimide membranes. 1. Irradiation with low pressure mercury lamp on photosensitive and non-photosensitive membranes. *J. Polym. Sci., Part B: Polym. Phys.* **1997**, *35*, 2259.

48. Matsui, S.; Sato, H.; Nakagawa, T. Effects of low molecular weight photosensitizer and UV irradiation on gas permeability and selectivity of polyimide membrane. *J. Membr. Sci.* **1998**, *141*, 31.

49. Sanders, D. F.; Smith, Z. P.; Ribeiro, C. P., Jr.; Guo, R.; McGrath, J. E.; Paul, D. R.; Freeman, B. D. Gas permeability, diffusivity, and free volume of thermally rearranged polymers based on 3,3'-dihydroxy-4,4'-diamino-biphenyl (HAB) and

2,2'-bis-(3,4- dicarboxyphenyl) hexafluoropropane dianhydride (6FDA). *J. Membr. Sci.* **2012**, *409-410*, 232.

50. Koros, W. J.; Chan, A. H.; Paul, D. R. Sorption and transport of various gases in polycarbonate. *J. Membr. Sci.* **1977**, *2*, 165.

Chapter 4: Poly(2,6-dimethyl-1,4-phenylene oxide) and Bisphenol A Poly(arylene ether ketone) Blends for Gas Separation Membranes

Andrew Shaver,[1] Josh Moon,[2] Donald Savacool,[1] Wenrui Zhang,[1] Gurtej Narang,[1] Gregory Miller,[1] Britannia Vondrasek,[1] J. J. Lesko,[1] Benny D. Freeman,[2] J. S. Riffle,[1*] James E. McGrath[1]

[1]Macromolecules and Interfaces Institute, Virginia Tech, Blacksburg, VA

[2]Dept of Chemical Engineering, University of Texas, Austin, TX

4.1. Introduction

Gas separations via membranes have grown over the past approximately 50 years due to reduced energy consumption, equipment size, and waste generation relative to cryogenic distillation and absorption processes.[1] Currently, membrane based gas separation is used to separate various gas pairs in applications including nitrogen enrichment, acid gas treatment, ammonia purge gas recovery, refinery gas purification, syngas ratio adjustment, and dehydration.[2] There are issues that need to be addressed within these areas such as gas purity, CO_2 and other condensable gas plasticization, physical aging, and chemical and thermal stability of the membranes.[2]

Major performance standards for non-porous membrane gas separation are permeability and selectivity. Permeability is the rate at which the gas moves through the material under a given pressure gradient and is a function of solubility and diffusivity. Solubility is a thermodynamic term that describes the sorption of molecules in a film. Diffusivity, which is usually the rate limiting step, is a kinetic term that describes the rate at which

molecules move through a film.[3, 4] Selectivity is the permeability ratio of two gases of interest, and this is usually expressed with the faster gas in the numerator. The best performance occurs when the permeability and selectivity of the membrane is high.[3, 4] However it is known that there is a tradeoff between permeability and selectivity which results in an upper bound. The first upper bound was reported by Robeson in 1991 and this has been theoretically explained by Freeman.[5-7]

Glassy polymers such as polyarylene ethers including polysulfones and poly(2,6-dimethyl-1,4-phenylene oxide), polycarbonates, polyimides, cellulose acetates, and aramids are all used as membrane materials and show great performance and processability for various applications. This paper will focus on poly(2,6-dimethyl-1,4-phenylene oxide) (PPO) as a membrane material. PPO was first commercialized over 50 years ago by General Electric Plastics, now Sabic Plastics.[8] It gained interest as a gas membrane material due to its aromatic ether chemical and conformational structure. The kinked ether linkages and benzylic methyl groups inhibit packing.[2] Its non-polar structure further assists in the non-packing nature and therefore PPO has a high fractional free volume.[2, 9] However, the high free volume leads to reduced selectivities when compared to other commercial materials and a significant amount of research has been attempted to solve this problem.[10, 11]

In this paper, a bisphenol A based poly(arylene ether ketone) (BPA PAEK) has been blended with PPO to produce a UV crosslinkable material with improved selectivity. Miscible and immiscible blends have been studied and modeled as gas separation membranes. Miscible blends show linear behavior between the permeability and selectivity of the control polymers with composition, similar to random copolymers.[12]

There can be negative deviation from linearity which has been modeled by Paul.[13] This deviation is due to densification which can be attributed to positive interactions between the two blended polymers.[13] Immiscible blends are more complex and will positively or negatively deviate from the linear behavior along the composition range depending on which phase is continuous.[12] The transport behavior at the extremes of composition can be described by a parallel or series model. If the more selective polymer is continuous throughout the blended film, it will follow the series model predictions. Counter to that, a blended film with a continuous permeable polymer will follow the parallel model predictions. A series polymer blend produces selectivity that is positive and permeability that is negative with respect to the linear behavior in a graph of volume fraction versus selectivity or permeability respectively. The parallel model for immiscible blends shows the opposite behavior and results in permeability that is positive and selectivity that is negative with respect to the linear behavior in a graph of volume fraction versus selectivity or permeability.[12] The intermediate compositions are much more difficult to predict and require more complex models, but they are outside of the scope of this paper.

Crosslinking is of great interest for dense-film gas separation membranes due to the potential to increase selectivity, decrease gas plasticization, and decrease the effect of aging.[2, 14] Selectivity can increase because crosslinking controllably reduces the free volume within the polymer, which improves the size sieving capability. Gas plasticization occurs when a sufficiently high concentration of a permeant gas builds up within the film and causes swelling which can decrease diffusion selectivity. Crosslinking inhibits this swelling and can reduce the overall effect of plasticization. Aging involves the gradual densification of a polymer over time and can decrease the permeation and

increase selectivity. By crosslinking the film, the aging rate may be reduced. This can be attributed to the fact that the crosslinked film has reduced free volume prior to aging. Both crosslinking and aging increase selectivity by reducing free volume, however literature has reported that crosslinking has a more pronounced effect for UV-irradiated polyarylates.[14, 15]

The focus of this study has been to UV crosslink PPO to enhance the transport properties. PPO was blended with BPA PAEK and the structures are shown in Figure 4.1. The key crosslinking groups within the polymers are the benzophenone in the BPA PAEK and the benzylic methyl groups in the PPO. UV light was used to excite a benzophenone moiety and abstract a hydrogen radical from a benzylic methyl group. This creates two free radicals which can then combine to form a covalent crosslinked bond. Qiang et al. has extensively described this crosslinking reaction and explored the effect of thickness, atmosphere, and aging.[15] Other systems have been studied utilizing this crosslinking reaction.[15, 16] However, in the previous work, the two key components were within the same polymer structure by polymerizing tetramethylbisphenol A or tetramethylbisphenol F with 4'4-difluorobenzophenone.

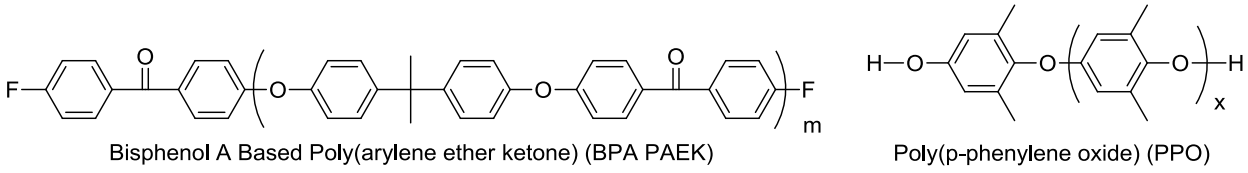

Bisphenol A Based Poly(arylene ether ketone) (BPA PAEK)

Poly(p-phenylene oxide) (PPO)

Figure 4. 1 Bisphenol A based poly(arylene ether ketone) and poly(2,6-dimethyl-1,4-phenylene oxide).

PPO is already used as a membrane material and the monomers used to make the BPA PAEK are both commercially available. In this study, blends were explored as a function

of the molecular weight of the PPO. Based on the data, a 22,000 M_n PPO was used to study the effect of PPO/BPA PAEK composition on the properties of the blended films. NMR, DSC, gel fractions, tensile and transport properties were used to characterize the films.

4.2. EXPERIMENTAL

Materials

N,N-Dimethylacetamide (DMAc), toluene, pyridine, and 2,6-dimethylphenol were purchased from Sigma Aldrich. DMAc was vacuum distilled from calcium hydride. Toluene, pyridine, and 2,6-dimethylphenol were used as received. 4,4'-Difluorobenzophenone and bisphenol A were kindly donated by Solvay and recrystallized from 2-propanol and toluene, respectively. Potassium carbonate was purchased from Fisher Scientific and dried at 150 °C under vacuum. Copper(I) chloride was purchased from Alfa Aesar and used as received. Hydrochloric acid and methanol were purchased from Spectrum Chemicals and used as received. Chloroform, purchased from Spectrum Chemicals, was stored over activated 3Å molecular sieves.

Synthesis of BPA PAEK

Synthesis of the BPA polymer was adapted from previous literature[17-21]. Bisphenol A (67.713 g, 296.6 mmol), 4,4'-difluorobenzophenone (65.643 g, 306.4 mmol), and DMAc (600 mL) were charged to a three-neck flask equipped with a N_2 inlet, mechanical stirrer, and Dean-Stark trap. Toluene (300 mL) and K_2CO_3 (48.352 g, 349.8 mmol) were added to the flask and the Dean Stark trap was filled with toluene. The apparatus was placed in a silicone oil bath that was heated to 155 °C to begin azeotropic removal of water. After 4 h the toluene and water were removed from the Dean-Stark

trap. The oil bath was maintained at 150 °C for 12 h, then the reaction was allowed to cool to room temperature. The polymer solution was filtered to remove any excess K_2CO_3 or by-product salts. The polymer solution was precipitated into deionized water, then the polymer was stirred in deionized water at 80 °C to further assist the removal of salts and solvents. The white polymer was filtered and dried at 110 °C under vacuum. Yield was 81%.

Synthesis of 4kK, 13k and 19k M_n poly(2,6-dimethyl-1,4-phenylene oxide)s

PPO synthesis was adapted from Hay et al. and the protocol for synthesizing the 6k M_n oligomer is provided. Procedures for the 17k and 22k M_n polymers are briefly described at the end of this section.[22] A 500-mL 4-neck round bottom flask equipped with an overhead stirrer, oxygen inlet tube, and condenser was charged with 250 mL of pyridine and 0.5 g (0.005 moles) of copper(I) chloride. Oxygen gas (0.1 SCFH) was passed through the vigorously stirred solution for 30 min and the solution became dark green. Then 10 g (0.082 mole) of 2,6-dimethylphenol was added. The reaction mixture became dark orange and the temperature was increased from 25 to 45°C. Oxygen flow was terminated after 1 h and the reaction was stirred for 2 h. The solution became viscous and the color of the solution returned to dark green. The reaction mixture was cooled to room temperature and slowly added into 500 mL of methanol to precipitate the polymer, then the polymer was filtered and washed thoroughly with methanol containing a small amount of hydrochloric acid. The product was dissolved in chloroform, filtered and reprecipitated into methanol. After filtration, the faint yellow powder was dried at 110 °C for 24 h in vacuo. The product (7.1 g, yield 71%) was obtained. The structure was confirmed by ^{1}H-NMR.

For the 17k M_n poly(2,6-dimethyl-1,4-phenylene oxide), a 1 L 4-neck round bottom flask was used and 800 mL of pyridine, 2.0 g (0.02 moles) of copper(I) chloride, and 30 g (0.246 mole) of 2,6-dimethylphenol were added. The product (23.4 g, yield 78%) was obtained and the structure was confirmed by ^{1}H-NMR. For the 22k M_n poly(2,6-dimethyl-1,4-phenylene oxide), a 500-mL 4-neck round bottom flask was used and 250 mL of pyridine, 1.0 g (0.01 mole) of copper(I) chloride and 10 g (0.082 mole) of 2,6-dimethylphenol were added. The product (8.0 g, yield 80%) was obtained and the structure was confirmed by ^{1}H-NMR.

Size Exclusion Chromatography (SEC)

SEC was conducted to measure molecular weights and distributions. The eluent was $CHCl_3$. The column set consisted of two Shodex KF-801 columns connected in series with a guard column having the same stationary phase. The columns and detectors were maintained at 35 °C. An isocratic pump (Water 515 HPLC Pump, Waters Technologies), and 717 Waters autosampler were used for mobile phase delivery and sample injection. A system of multiple detectors connected in series was used for the analyses. A multi-angle laser light scattering detector (mini-DAWN, Wyatt Technology Corp.), operating at a wavelength of 658 nm, and a refractive index detector operating at a wavelength of 880 nm (Waters 410, Waters Technology) were employed. Calibrations were performed using a set of nine Shodex polystyrene standards spanning the entire column molecular weight range.

Film-casting

The polymer or polymers (0.6 g) were weighed into a small glass vial with a magnetic stir bar at the desired wt/wt ratio. Chloroform (20 mL) was added to the vial to

obtain a 2 wt% solution. The solution was filtered using a 0.45 μm syringe filter into a clean glass vial. A 6" x 6" glass plate with the corners cut off (34 in2 area) was placed in a base bath for 30 min to clean the surface. The glass plate was rinsed and dried, then placed on a level surface for casting. The solution was poured onto the plate and the solution was spread to the edges of the plate until it covered the whole glass plate. A glass dome with 2 outlets was used to cover the plate. One outlet was fitted with a syringe filter and the other was connected to the house air stream running at 2 SCFH. The plate was left undisturbed for a minimum of 30 min, then transferred to an oven at 110 °C for an additional 30 min. Once removed from the oven, the film was secured to the glass plate with clips and placed into a DI water bath for 1 min to assist with film removal. The free-standing films were then placed in a vacuum oven set at 110 °C for 2 h without vacuum and then for 10 h with vacuum. The resulting films were between 20 and 30 μm thick.

Proton nuclear magnetic resonance (NMR) spectroscopy

The composition of PPO to BPA PAEK was determined via NMR. 1H NMR analysis was performed on a Varian Inova spectrometer operating at 400 MHz. All spectra were obtained from 15% (w/v) 1-mL solutions in chloroform-d. The two peaks used in the calculation were from the three hydrogens on each benzylic methyl group (PPO) and from the four benzene hydrogens nearest the ketone linkage (BPA PAEK).

Thermogravimetric analysis (TGA)

Thermal stabilities of the polymers were investigated using a TA Instruments TGA Q5000 under a N_2 atmosphere with the N_2 running at 25 mL/min. The heating rate was 10 °C/min from room temperature to 700 °C.

Differential scanning calorimetry (DSC)

The thermal properties were investigated with a TA Instruments DSC Q2000. The polymers were heated under N_2 at 60 mL/min to ensure an inert atmosphere. The heating rate was 10 ^{o}C/min to 350 °C, then the sample was cooled to 0 °C at 10 °C/min. It was heated once more to 350 °C at 10 °C/min and the reported DSC thermograms are from the second scans.

UV Spectroscopy

The UV spectra of the bulk polymers and the blends were collected using a Shimazdu Corp. UV – 1601 UV analyzer. Solutions (0.05 mg/mL) of the samples in chloroform were analyzed in quartz cuvettes placed in the sample cell with chloroform in a similar cuvette in the reference cell. A 50 W Tungsten bulb (from 1100 nm to 340.8 nm) and a Deuterium bulb (340.8 nm to 190 nm) were used as the light sources. Scans were conducted in 'Spectrum Mode' sweeping wavelengths from 700 to 190 nm.

UV Crosslinking

The polymer membranes were placed between an upper quartz and a lower glass plate. The setup was then passed under a Heraeus UV Fusion "H+" bulb via a conveyor belt set at 6 ft/min. This procedure was repeated until the film was exposed to the desired amount of radiation. A UV Power Puck was used to measure the amount of energy that the sample was exposed to, and this was multiplied by the number of passes.

Gel Fraction Measurement

Crosslinked films were dried at 120°C under vacuum overnight. Then 0.1-0.2 g of the crosslinked film was placed in a 20-mL scintillation vial filled with chloroform and stirred overnight. The remaining solid was filtered through a pre-weighed Buchner funnel

filter paper and dried at 120°C under vacuum overnight and weighed once more to obtain the final weight. Gel fractions were calculated by equation 4.1.

$$Gel\ Fraction\ (\%) = \frac{W_{final}}{W_{initial}} \text{ x } 100 \tag{4.1}$$

Pure Gas Permeability Measurements

The pure gas permeabilities for a series of light gases (H_2, CH_4, N_2, O_2, CO_2) were measured at 35 °C in one of two constant-volume, variable-pressure apparatus as described elsewhere.[1-2] The membrane sample, after being epoxied to a brass support disk, was loaded into a stainless steel Millipore filter holder (Millipore, Billerica, MA, USA) inside a temperature-regulated water bath. The downstream pressure was measured with a MKS Baratron 626B transducer (MKS, Andover, MA, USA) with a max pressure of 10 Torr, and the pressure in the upstream was measured using a Honeywell Super TJE transducer (Honeywell Sensotec, Columbus, Ohio, USA) with a max pressure of 1500 psig. The feed pressure of each gas was varied between 3 and 17 atm, and both the upstream and downstream pressures were recorded in a custom Python application using National Instruments. Each sample was degassed overnight prior to measuring transport of the gas, and the stainless steel upstream line connected to the feed gas cylinder was flushed and degassed for a minimum of 45 min prior to each test to prevent contamination from other gases.

Tensile Properties

Tensile samples were cut from the solvent cast films using a Cricut Explore One™ computer controlled cutting machine. The resulting samples were consistent with sample Type V described in ASTM D638-14. The nine samples produced by the cutter

were then inspected for any visible flaws, defects, or inclusions that arose during the casting process. The six highest quality samples were selected for testing. The sample thickness was measured at both ends of the narrow section using a Mitutoyo digimatic micrometer model MDC-1"SXF. Uniaxial load tests were performed using an Instron ElectroPuls E1000 testing machine equipped with a 250N Dynacell load cell. The crosshead displacement rate was 5 mm/min and the initial grip separation was 25 mm. Nominal strain was calculated by dividing the change in grip separation by the initial grip separation. Tensile strength was calculated by dividing the load by the average cross-sectional area of the narrow section, which was based on the average of the two sample thickness measurements and a sample width of 3.18 mm.

4.3. Results and Discussion

NMR and SEC were used to characterize the PPO and BPA PAEK molecular weights and the results are shown in Table 4.1 and Figure 4.2. The PPO nomenclature is based on the SEC M_n's. A series of molecular weights were produced to investigate structure-property behavior as a function of the molecular weights of the PPO component.

Table 4. 1 Molecular weights in chloroform at 35 °C

	M_n (kDa) NMR	**M_n (kDa) SEC**	**M_w (kDa) SEC**	**PDI SEC**
BPA PAEK	-	52	78	1.5
2k PPO	1.0	2	3.2	1.7
6k PPO	4.0	6	11.8	2.0
17k PPO	13	17	50.2	3.0
19k PPO	33	19	55.8	2.9
22k PPO	19	22	109	5.0

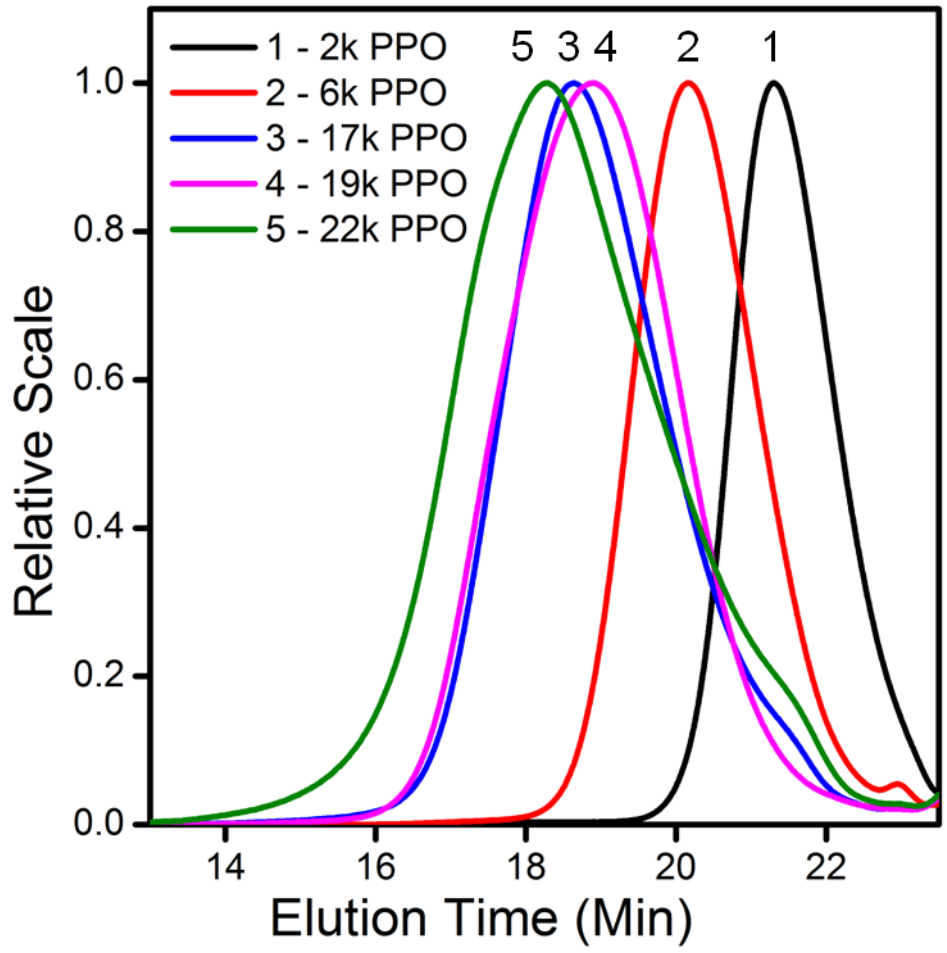

Figure 4. 2 Molecular weights of the PPO oligomers by SEC

The DSC thermograms of the films are shown in Figure 4.3. Figure 4.3A compares two blended films with different PPO molecular weights of 2k and 22k at a wt/wt composition of 33/67 PPO/BPA-PAEK relative to their controls. Thermogram 2 shows the 2k PPO/BPB-PAEK blend and its T_g is 149 ^oC. This T_g is located between the two control T_g's, curves 1 and 3, which suggests that the 2k PPO is miscible with BPA-PAEK. Curve 4 shows the thermogram of a high molecular weight 22k PPO/BPA-PAEK blend that produced two T_g's, one at 152 and another at 213 ^oC. These two T_g's correspond with the control T_g's in curves 3 and 5 which indicates that the 22k PPO produced an immiscible blend with BPA-PAEK. The T_g's of the blend are slightly

reduced in comparison to the respective control polymers T_g's. A definite reason for this behavior is unclear but it does occur consistently. This can be observed in Figure 4.3B with the lower Tg's corresponding to the PBA-PAEK in blends with the 6, 17, 19, and 22k PPO.

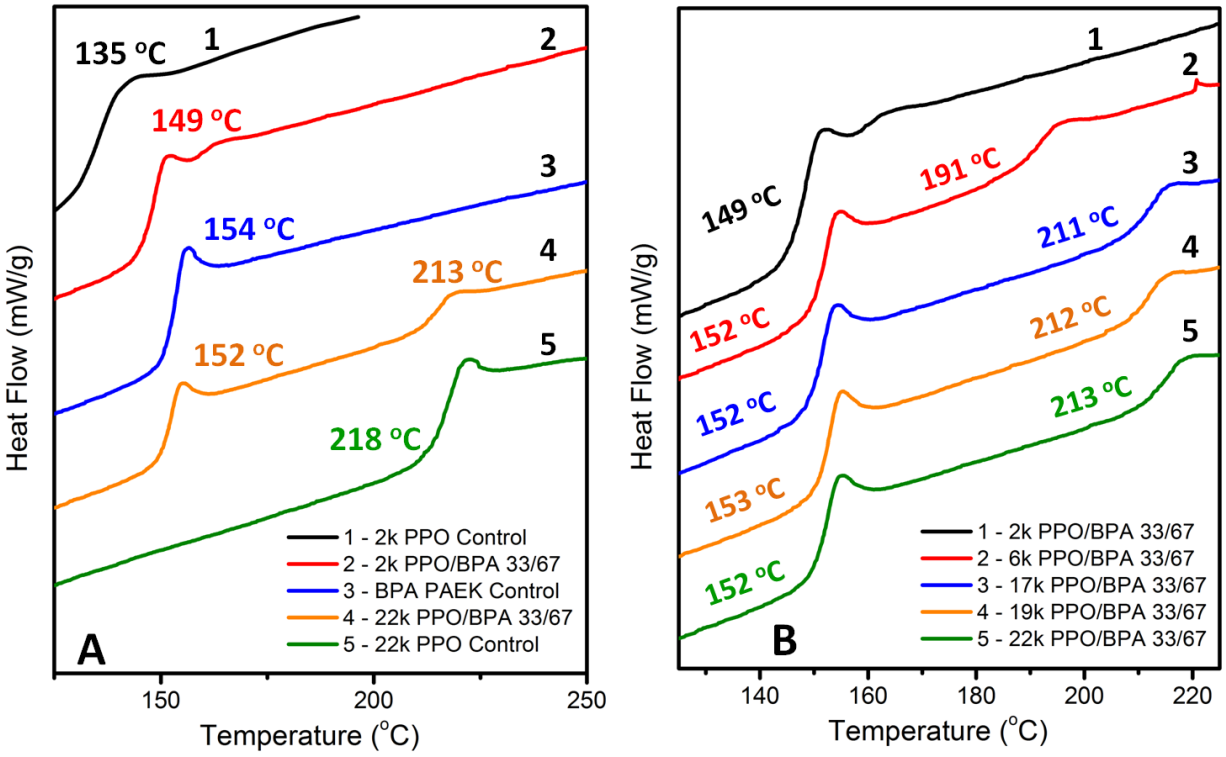

Figure 4. 3 Figure 4.3A shows DSC thermograms of the 2k PPO/BPA-PAEK 33/67 and the 22k PPO/BPA-PAEK 33/67 wt/wt composition blends with their respective controls. Figure 4.3B compares all of the PPO molecular weights blended with BPA PAEK at the 33/67 wt/wt composition of PPO/BPA PAEK.

Figure 4.3B compares blends with the five PPO polymers with different molecular weights with 67 wt% of BPA PAEK. Thermogram 1 shows the single Tg for the 2k PPO/BPA-PAEK blend. Once the molecular weight of the PPO in the blends was increased to 6k M_n, two clear T_g's emerged and this was also true as the molecular weight

was increased further, thus indicating the presence of two phases. The upper T_g in the 5k PPO/BPA-PAEK blend, which correlates to the PPO phase, is lower than the 17, 19, and 22k upper PPO T_g's in the blends. This is expected since T_g is a function of molecular weight. In Figure 4.4, the 6k PPO uncrosslinked blend (curve 2) is compared to its BPA PAEK control (curve 1), the 6k PPO control (curve 4), and the crosslinked blend (curve 3). The PPO T_g in the uncrosslinked blend correlates with the control 6k PPO T_g. Once crosslinked, at least the upper T_g was slightly raised and this was attributed to reduced mobility, particularly of the PPO chains.

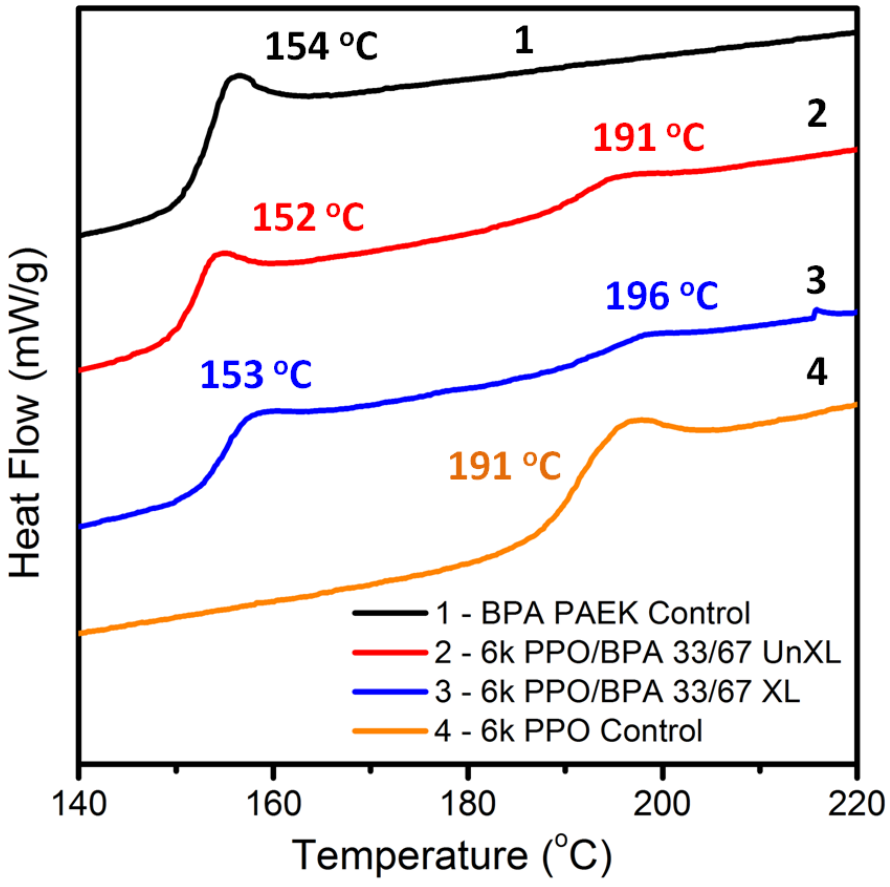

Figure 4. 4 DSC thermograms of 6k PPO/BPA PAEK 33/67 wt/wt uncrosslinked and crosslinked blends with the controls.

The crosslinking mechanism discussed in the introduction is activated via UV light and is a reaction between the ketone and benzylic methyl groups. Figure 4.5 shows the solution UV absorbance spectra of the six control polymers. PPO has significantly less absorbance than BPA PAEK. The significant absorbance of the BPA PAEK can be attributed to the ketone excitation from the nonbonding state to the antibonding state. Therefore, in later discussions regarding the gel fractions as a function of PPO weight composition, it will be important to remember that a greater PPO content will not absorb as much light as blends with higher compositions of the PBA-PAEK. This is beneficial because the UV light will penetrate further into the film to crosslink more polymer chains.

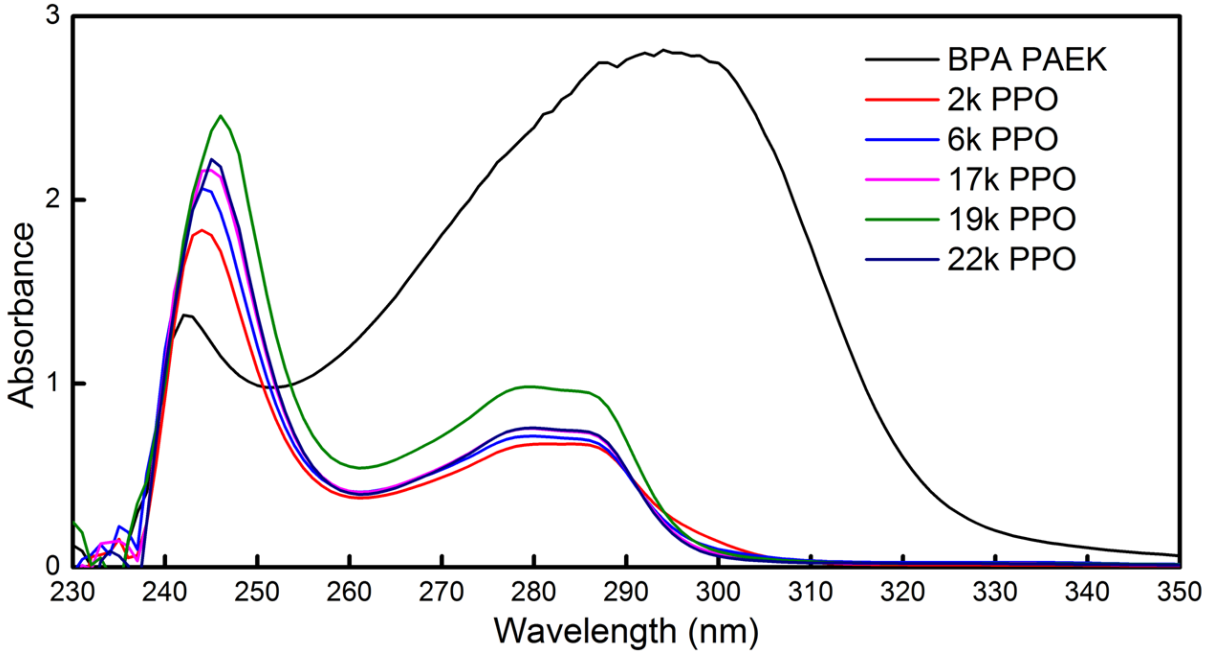

Figure 4. 5 Solution UV absorption data of the PPO and BPA PAEK.

The extent of crosslinking was explored by measuring gel fractions. The set of gel fractions shown in Figure 4.6 compares the five PPO molecular weights blended with BPA-PAEK along with those for the 19k PPO homopolymer. The films were exposed to

11, 23, or 34 J/cm^2 of energy in efforts to optimize the UV exposure. The higher exposure resulted in increased gel fractions in the blended films but not in the PPO homopolymer control. The control PPO film did not undergo significant crosslinking which showed the importance of the ketone group to the crosslinking reaction. The 2k PPO/BPA 33/67 wt/wt blend only reached gel fractions a little above 20 %, and this was much lower as compared to the gel fractions obtained with blends having higher PPO molecular weights. This was attributed to the fact that higher molecular weight PPO contains more benzylic crosslinkable methyl groups per mole, and thus requires fewer crosslinks to reach gelation.

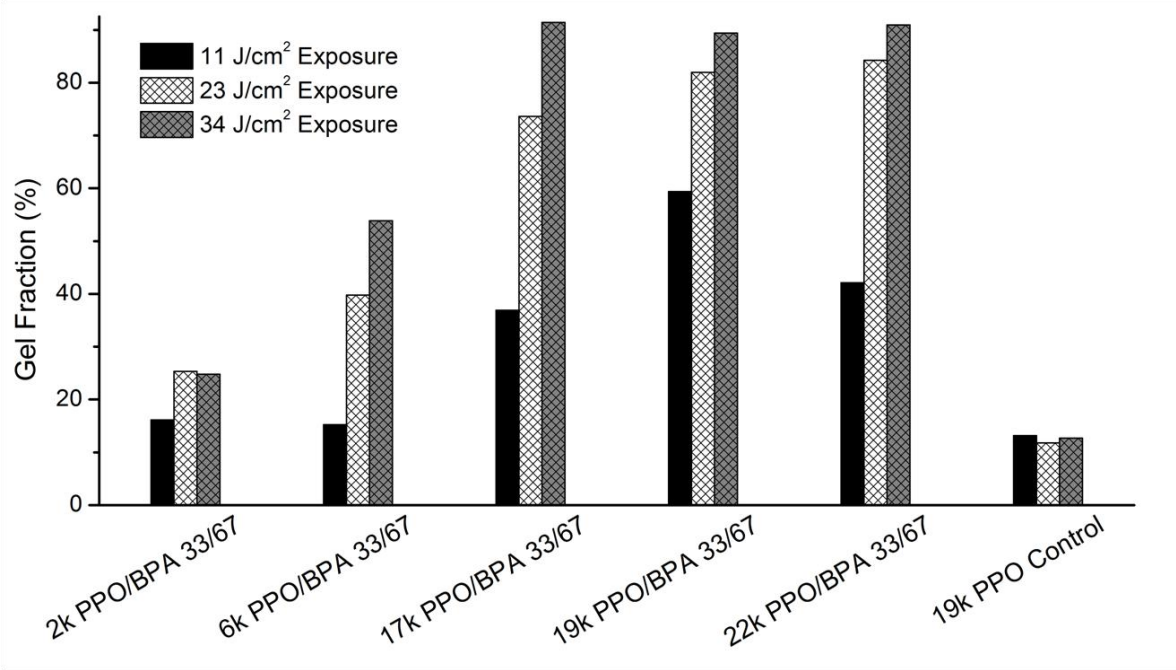

Figure 4. 6 Gel fractions after UV crosslinking of PPO/BPA-PAEK blends over a range of PPO molecular weights

The 22k M_n PPO was used to explore gel fractions and gas separation properties in these blends as a function of PPO composition. Figure 4.7 compares the gel fractions of four blend compositions. Unexpectedly, there was not a significant change in gel

fraction as a function of composition. This is likely a result of several competing factors. One is that the amount of crosslinks may have decreased with less BPA-PAEK content simply because fewer ketone groups that participate in the crosslinking reaction are present. Secondly, the UV light should penetrate more deeply into the film with increasing PPO content since the PPO absorbs less of the light relative to the PBA-PAEK. These factors are counter to each other which may cause the insignificant change observed in Figure 4.7.

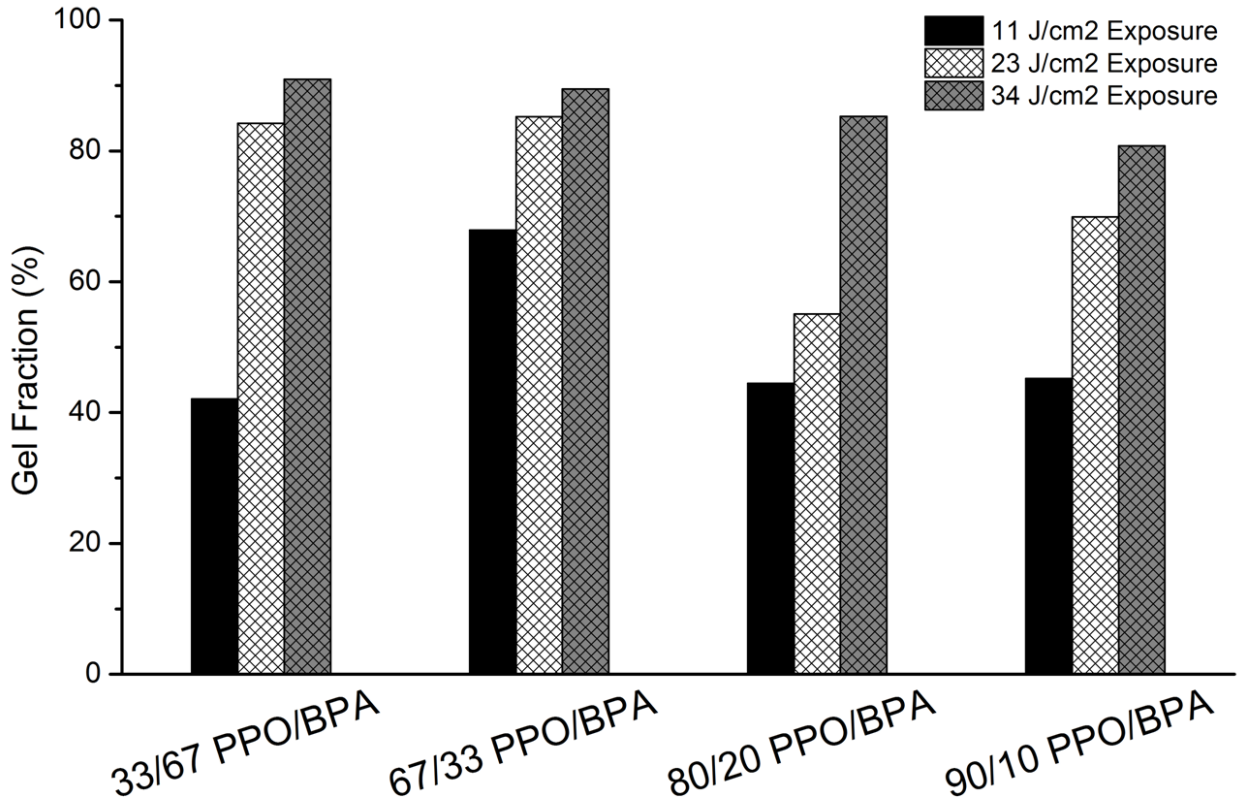

Figure 4. 7 Gel fractions after UV crosslinking of blends of 22k M_n PPO with BPA-PAEK over a range of compositions

It is expected that the phase structure of the blends is also a contributing factor. The DSC thermograms in Figures 4.3-4 show two T_g's for all of the PPO molecular

weights except for the very low 2000 M_n polymer, thus strongly suggesting that two phases are present. However, high gel fractions were obtained after crosslinking blends of the 22k PPO/BPA PAEK, and it is postulated that this can only occur when the benzylic methyl groups are in the same phase as the ketone groups. This indicates some level of miscibility within the system. It is believed that there are two phases within the blends and that each contain both PPO and BPA PAEK. The morphology of the blends was not explored in this study but would provide regarding the unique behavior of this system.

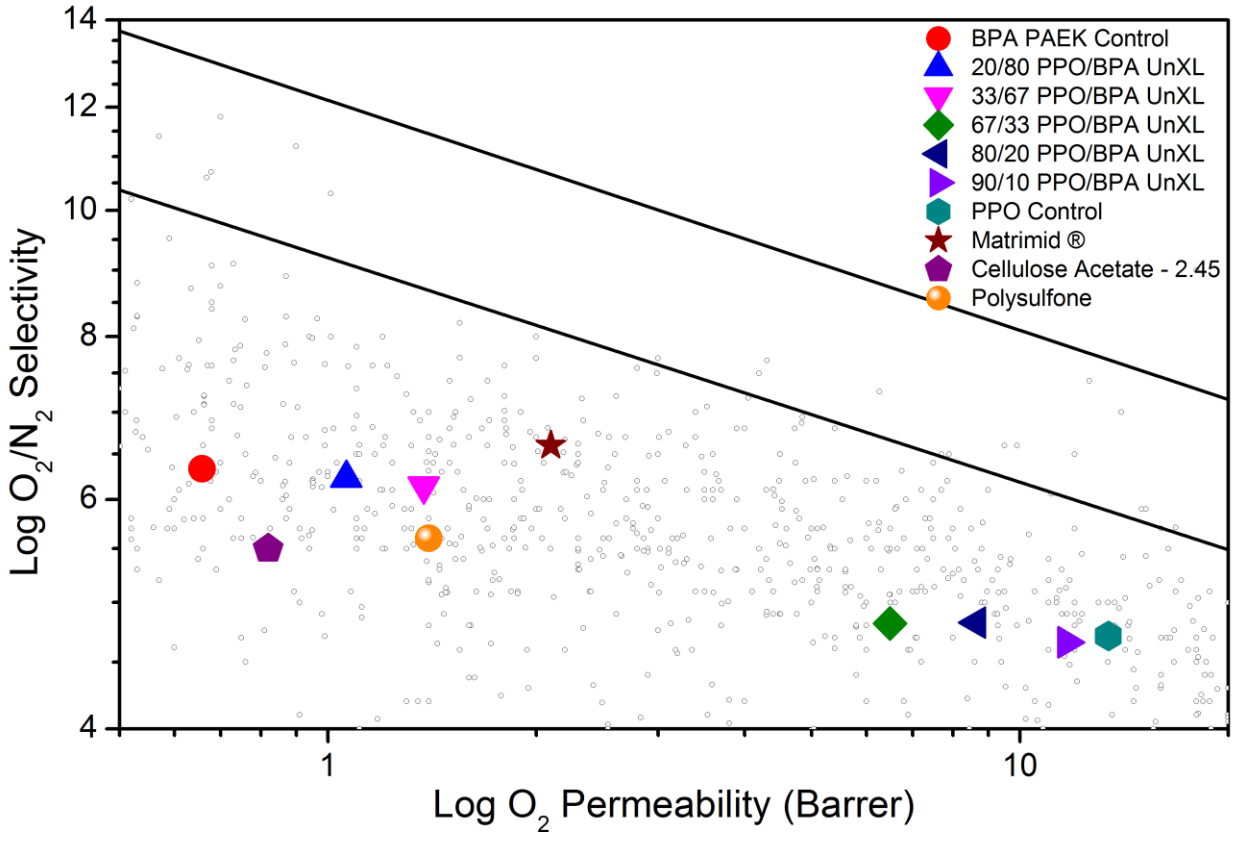

Figure 4. 8 Comparison of oxygen and nitrogen transport in 22k M_n PPO/BPA PAEK blends at different compositions and the controls. The dashed line represents the linear behavior.

The permeabilities and ideal selectivities for oxygen versus nitrogen gases through 22k PPO/BPA PAEK films with different compositions are shown in Figure 4.8

on an upper bound graph, and the values are provided in Table 4.2. The linear dashed line in Figure 4.8 represents the expected transport properties of miscible blends. In these multiphase blends, as would be expected, the membranes with high compositions of PPO have higher permeabilities and lower selectivities and this is attributed to the high free volume of PPO. When the high-selectivity polymer, BPA-PAEK, comprises a large volume fraction of the continuous phase, the membranes exhibit transport properties similar to a series model. On the other hand, when the high-permeability polymer, 22k M_n PPO, occupies a large volume fraction of the continuous phase, the films have transport properties similar to a parallel model. The commercial polymers were included in Figure 4.8 and the blended materials showed better performance polysulfone and cellulose acetate. Matrimid® performs slightly better than the 33/67 22k PPO/BPA PAEK but crosslinking has the potential to close that performance gap.

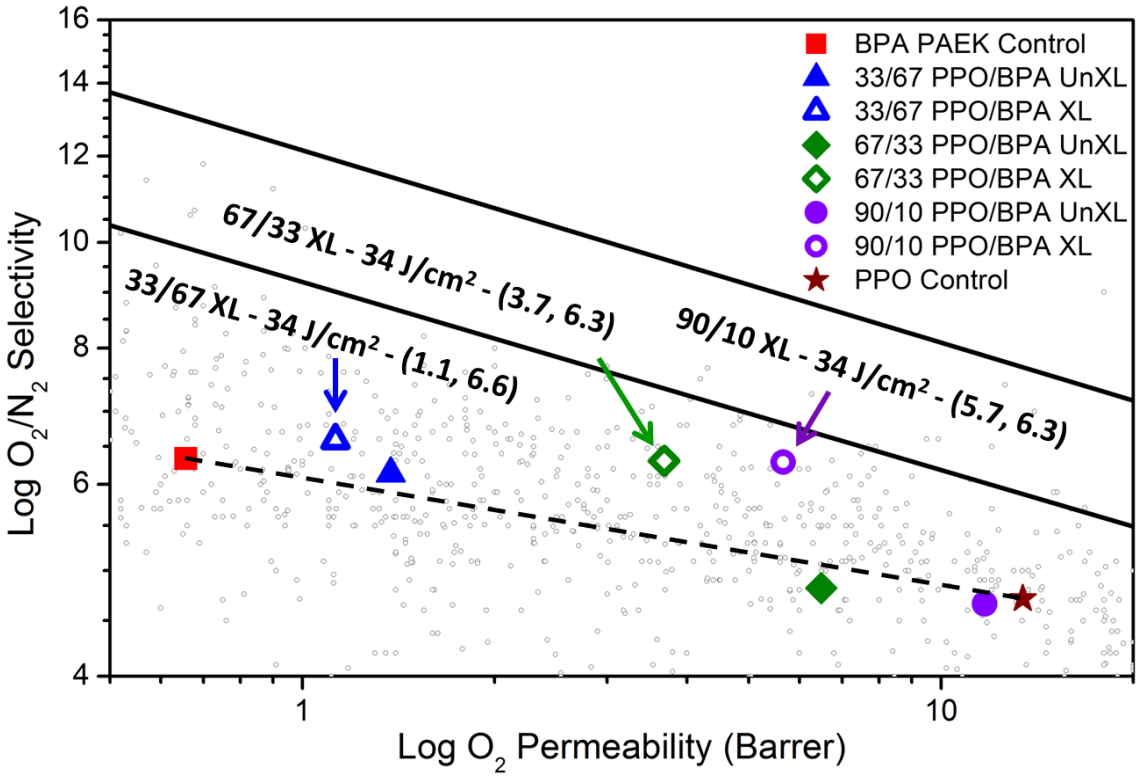

Figure 4. 9 Comparison plot of 22k PPO/BPA PAEK linear and crosslinked blends at different compositions and the controls. The dashed line represents the linear behavior and the numbers on the graph are permeability and selectivity values with the format (x,y).

The 33/67, 67/33, and 90/10 22k PPO/BPA PAEK films were crosslinked via exposure to UV radiation and the results are provided in Figure 4.9 along with the bulk and uncrosslinked controls. The 90/10 22k PPO/BPA PAEK crosslinked membrane yielded quite interesting transport results in that good selectivity and permeability were obtained for oxygen/nitrogen separation in a film that was comprised largely of a readily available commercial polymer. As discussed previously, the UV light was able to penetrate further into this film to crosslink more polymer and therefore increase the selectivity substantially. Secondly, the UV exposure created a gradient of crosslinked material through the thickness of the film. Therefore, the highly crosslinked surface likely

contributed to the high selectivity while the lightly crosslinked center of the film likely contributed to the high permeability.[15]

Table 4. 2 Transport properties of bisphenol A based poly(arylene ether ketone) blends with poly(2,6-dimethyl-1,4-phenylene oxide)

*** Values are from Sanders et al.**

	O_2 (Barrer)	N_2 (Barrer)	O_2/N_2	H_2 (Barrer)	CH_4 (Barrer)	CO_2 (Barrer)
BPA PAEK Control	0.66	0.10	6.3	8.2	0.12	2.7
20/80 22k PPO/BPA UnXL	1.1	0.17	6.2	13	0.19	4.5
33/67 22k PPO/BPA UnXL	1.4	0.22	6.1	16	0.24	5.8
33/67 22k PPO/BPA XL	1.1	0.17	6.6	16	0.15	4.5
67/33 22k PPO/BPA UnXL	6.5	1.4	4.8	54	1.6	28
67/33 22k PPO/BPA XL	3.7	0.59	6.3	45	0.47	14
80/20 22k PPO/BPA UnXL	8.7	1.8	4.8	70	2.1	36
90/10 22k PPO/BPA UnXL	12	2.5	4.7	90	2.9	50
90/10 22k PPO/BPA XL	5.7	0.90	6.3	68	0.71	22
22k PPO Control	13	2.9	4.7	105	3.3	57
Matrimid® *	2.1	0.32	6.6	18	0.28	10
Cellulose Acetate - 2.45 *	0.82	0.15	5.5	12	0.15	4.8
Polysulfone *	1.4	0.25	5.6	14	0.25	5.6

The tensile properties of the uncrosslinked blends at all blend ratios presented above were compared with those of pure 22k PPO, as it has suitable mechanical properties for gas separation membrane applications. Based on the data obtained from thin film samples (Table 3), there is no statistical difference between the mechanical properties of the blends and 22k PPO. It should be noted that BPA-PAEK tends to show

significant strain-hardening behavior at high elongations, which led to very high strength and strain at break values for some PAEK-rich blend samples. All polymer samples in this analysis displayed a non-uniform yield and draw behavior and no direct strain measurement technique was employed during testing, therefore the strain at break values presented here should serve for comparison purposes only.

Table 4. 3 Mechanical properties of uncrosslinked BPA-PAEK blends with 22k M_n PPO compared to neat 22k M_n PPO

	Blend range	PPO Range
Tensile strength at break	52 – 134 MPa	61 – 76 MPa
Tensile strength at yield	62 – 85 MPa	71 – 82 MPa
Nominal strain at break	0.34– 1.84	0.14 – 0.62
Nominal strain at yield	0.04 – 0.06	0.05 – 0.07
Young's modulus	1810 – 2370 MPa	1860 – 2290 MPa

Blends containing 67 wt% BPA-PAEK and 33 wt% PPO of varying molecular weights were also tested in tension. Despite the higher fraction of BPA-PAEK, the molecular weight of the PPO had a significant impact on the mechanics of the films. Films containing the 2k and 6k PPO exhibited a brittle failure mechanism with little to no yielding while films containing higher molecular weight PPO displayed similar yielding and drawing behavior.

4.4 Conclusion

In conclusion, we were able to blend PPO and BPA-PAEK to make membranes that were phase separated except for the samples with the very low M_n PPO. The DSC results showed that the 5k, 17k, 19k, and 22k blended films have two T_g's that closely

correlated with the corresponding homopolymers T_g which indicates immiscibility. Despite the immiscibility of these films, the gel fraction results showed significant insolubility after UV exposure. Gel fraction as a function of 22k PPO composition was explored and did not show any significant change. This is likely a result of several competing factors. One trend is that as the PPO composition is increased, there will be a lower ketone content which begins the crosslinking reaction. Counter to that is that with increased PPO content, the UV light will be able to penetrate further into the film and crosslink more chains. This is because PPO absorbs significantly less UV light than the BPA PAEK which was shown via solution UV absorbance spectra.

The gas permeability and selectivity was measured for the linear blend films and the results followed the modeled behavior with the BPA PAEK continuous films having series model behavior and 22k PPO continuous films having parallel model behavior. With respect to the linear behavior between the two control polymers, the 33/67 PPO/BPA PAEK has the best performance due to its increased permeability with little decrease in selectivity. However, with respect to the upper bound, the 90/10 PPO/BPA PAEK is has the best performance due to PPO's high free volume. Between the three crosslinked blended films, the 90/10 PPO/BPA PAEK gained the most selectivity and maintained a larger amount of its permeability. This can be attributed to a greater degree of UV light penetration into the film to crosslink more polymer chains due to PPO's lower absorbance. Another reason is that the UV exposure created a gradient of crosslinked material which created a selective surface and a permeable center.

Overall, we were able to blend a small amount of BPA PAEK with the commercially used PPO to create a mechanically robust crosslinkable polymer film. In

comparison to commercial gas separation polymers, the 33/67 22k PPO/BPA PAEK blend was able to outperform polysulfone and cellulose acetate - 2.45 without any crosslinking. Matrimid® was able to outperform the uncrosslinked blended films with regards to gas separation but crosslinking has the potential to close that gap. In terms of expense, Matrimid® has been known to be an expensive polymer whereas PPO is more economical.[2] Further, Matrimid® suffers from plasticization whereas our crosslinked blends would be less likely to suffer from that issue.[2] In the future, the system might be able to utilize even less of the ketone containing polymer and still maintain crosslinkability. Additionally, PPO can be blended with other materials to focus on other gas pairs and applications.

References

1. Bernardo, P.; Drioli, E.; Golemme, G., *Ind. Eng. Chem. Res.* **2009**, 48 (10), 4638-4663.

2. Sanders, D. F.; Smith, Z. P.; Guo, R.; Robeson, L. M.; McGrath, J. E.; Paul, D. R.; Freeman, B. D., *Polymer* **2013**, 54 (18), 4729-4761.

3. Yampolskii, Y., *Macromolecules* **2012**, 45 (8), 3298-3311.

4. Freeman, B. D.; Pinnau, I., Polymeric Materials for Gas Separations. *ACS Polymer Membranes for Gas and Vapor Separation*, **1999**; 733, 1-27.

5. Robeson, L. M., *J. Membr. Sci.* **1991**, 62 (2), 165-185.

6. Robeson, L. M., *J. Membr. Sci.* **2008**, 320 (1–2), 390-400.

7. Freeman, B. D., *Macromolecules* **1999**, 32 (2), 375-380.

8. Hay, A. S., Oxidation of phenols and resulting products. US3306875 **1967**.

9. Aguilar-Vega, M.; Paul, D. R., *J. Polym. Sci. B Polym. Phys.* **1993**, 31 (11), 1599-1610.

10. Ghosal, K.; Chern, R. T., *J. Membr. Sci.* **1992**, 72 (1), 91-97.

11. Sridhar, S.; Smitha, B.; Ramakrishna, M.; Aminabhavi, T. M., *J. Membr. Sci.* **2006**, 280 (1–2), 202-209.

12. Robeson, L. M., *Ind. Eng. Chem. Res.* **2010**, 49 (23), 11859-11865.

13. Paul, D. R., *J. Membr. Sci.***1984**, 18, 75-86.

14. McCaig, M. S.; Paul, D. R., *Polymer* **1999**, 40 (26), 7209-7225.

15. Liu, Q.; Shaver, A. T.; Chen, Y.; Miller, G.; Paul, D. R.; Riffle, J. S.; McGrath, J. E.; Freeman, B. D., *Polymer* **2016**, 87, 202-214

16. Sundell, B. J.; Shaver, A. T.; Liu, Q.; Nebipasagil, A.; Pisipati, P.; Mecham, S. J.; Riffle, J. S.; Freeman, B. D.; McGrath, J. E., *Polymer* **2014**, 55 (22), 5623-5634.

17. Srinivasan, S. A.; McGrath, J. E., *High Perform. Polym.***1993**, 5 (4), 259-274.

18. Bender, T. P.; Burt, R. A.; Hamer, G. K.; DeVisser, C.; Smith, P. F.; Saban, M., *Org. Process Res. Dev.* **2002**, 6 (5), 714-720.

19. Lyle, G. D.; Grubbs, H.; Tchatchoua, C.; McGrath, J. E., *Polym. Mater. Sci. Eng.* **1993**, 69, 238-9.

20. Chen, Y.; Guo, R.; Lee, C. H.; Lee, M.; McGrath, J. E., *Int. J. Hydrogen Energ.* **2012**, 37 (7), 6132-6139.

21. Lyle, G. D.; Senger, J. S.; Chen, D. H.; Kilic, S.; Wu, S. D.; Mohanty, D. K.; McGrath, J. E., *Polymer* **1989**, 30 (6), 978-985.

22. Hay, A. S., *J. Poly Sci* **1962**, 58 (166), 581-591.

Chapter 5: Recommended Future Research

5.1 Fluorinated Poly(Arylene Ether Ketone)s for High Temperature Dielectrics – Bulk and Multilayered Films

The multilayered 6FBPA-PAEK showed good performance in breakdown strength, hysteresis, relative permittivity, and Tan δ. However, isolating the effect of the fluorine in the 6FBPA PAEK on PVDF was not explored. This would be possible if BPA PAEK was also microlayered with PVDF and the differences between BPA PAEK and 6FBPA PAEK could be compared.

One way to study the differences it to utilize the "pulse" process which is how small batches of polymer are microlayer coextruded. In the case of this study, we have undersized batches because the polymer is synthesized in lab. In the process, a material that is available in large quantities (secondary polymer) is processed first to achieve a steady flow. Once the flow is achieved, the polymer of interest (primary polymer) is added to the hopper and is processed. The secondary polymer is then added again to maintain flow. The final film will have an area with the primary polymer and PVDF along with a transition section on both sides where there is a mixture of the primary and secondary polymers. An example film depiction is in Figure 5.1.

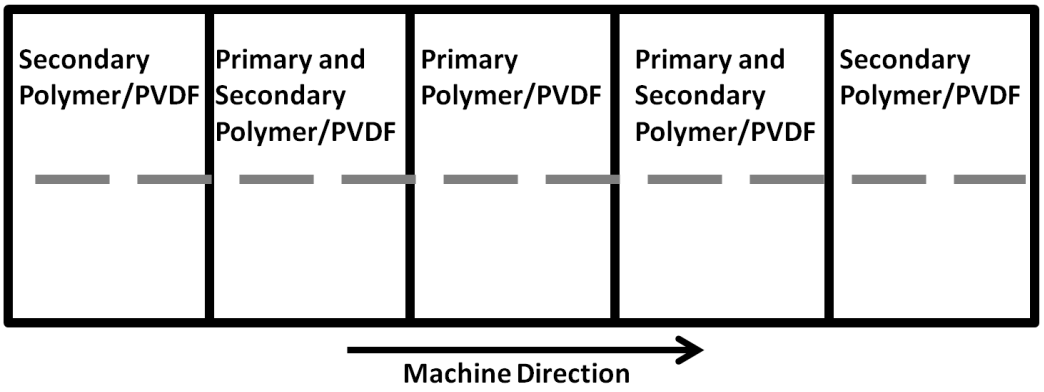

Figure 5. 1 Figure 5.1 Depiction of a film processed via the "pulse" microlayer coextrusion process.

The first step would be to confirm the integrity and composition of the primary polymer/PVDF region to verify the expected system. This could be done using FT-IR or NMR by confirming the peaks of the primary polymer and absence of secondary polymer peaks. Once confirmed, small samples along the machine direction could be cut that span through the secondary polymer/PVDF, the primary-secondary/PVDF, and primary polymer/PVDF sections as represented by the grey dashed line in Figure 5.1. The breakdown strength, hysteresis, relative permittivity, and Tan δ properties could then be tested and compared along the machine direction. Further, these samples would be analyzed via FT-IR and X-ray diffraction to see if there are any changes in the PVDF crystallinity or structure as the material is transitioned from the secondary polymer to the primary polymer. The FT-IR and X-ray diffraction testing would be similar to the testing seen in Mackey et al.[1] These measurements would be most effective if 6FBPA PAEK was the primary polymer and BPA PAEK was the secondary polymer. Another option would be to use polycarbonate and then process the BPA PAEK and then 6FBPA PAEK.

5.2 Synthesis, Oxidation, Crosslinking and Characterization of Tetramethyl Bisphenol F (TMBPF)-Based Polymers for Oxygen/Nitrogen Gas Separation

TMBPF-DFB and TMBPF-DCDPS were able to be thermally oxidized but required temperatures above the T_g's. Therefore, it would have limited use as a gas separation membrane because commercial membranes are made into hollow fibers with a dense outer layer and porous substrate.[2] If the hollow fibers were subjected to the thermal treatment, the porous substrate would collapse, rendering it useless. A possible solution to this problem is to incorporate the benzylic methylene group into a polymer with a significantly higher Tg such as a polyimide. If it is possible to oxidize the polymer below T_g, this method of crosslinking would become more commercially viable.

5.3 Poly(2,6-dimethyl-1,4-phenylene oxide) and Bisphenol A Poly(arylene ether ketone) Blends for Gas Separation Membranes

The most significant future recommendation would be to conduct a thin film study similar to the one done by Qiang et al. using this blended system.[3] The films used in Chapter 4 were between 25 to 30 μm and UV light is unable to completely penetrate the film which means that there will be a gradient of crosslinked polymer. Further complications occur when the composition of PPO is changed which causes the UV absorption of the material to change. These two factors make it difficult to make any definitive comparisons between the different crosslinked blends or even other materials.

Further exploration into this system's morphology would be beneficial and might able to answer many questions. DMA testing would be able to confirm or give a better

look at why both Tg's decrease rather than moving towards the center which is the expected behavior of partially miscible polymers.[4] Light scattering measurements might be beneficial because there is a noticeable difference in the transparencies of the films depending on the molecular weight. However, this might have issues if the refractive indices similar. Further techniques to characterize blends can be found in Robeson's "Polymer Blends: A Comprehensive Review" such as solid state NMR, IR, and UV-visible spectroscopy.[4]

References

1. Mackey, M.; Schuele, D. E.; Zhu, L.; Flandin, L.; Wolak, M. A.; Shirk, J. S.; Hiltner, A.; Baer, E., *Macromolecules* **2012,** *45* (4), 1954-1962.

2. Sanders, D. F.; Smith, Z. P.; Guo, R.; Robeson, L. M.; McGrath, J. E.; Paul, D. R.; Freeman, B. D., *Polymer* **2013,** *54* (18), 4729-4761.

3. Liu, Q.; Shaver, A. T.; Chen, Y.; Miller, G.; Paul, D. R.; Riffle, J. S.; McGrath, J. E.; Freeman, B. D., *Polymer* **2016,** *87*, 202-214.

4. Robeson, L. M., Polymer Blends: A Comprehensive Review. Hanser: **2007**.